UNIVERSITY
OF TASMANIA

Farming macroalgae to mitigate coastal nutrification from finfish aquaculture: a modelling study

By

Scott Alistair Hadley

BSc. (Hons) Grad Dip. App. Comp. MSc.

Quantitative Marine Sciences,
Institute of Marine and Antarctic Sciences (IMAS)

Submitted in fulfillment of the requirements for the degree of
Doctor of Philosophy in Biogeochemical Modelling,
University of Tasmania April, 2015.

STATEMENTS AND DECLARATIONS

Declaration of Originality

This thesis contains no material which has been accepted for a degree or diploma by the University or any other institution, except by way of background information and duly acknowledged in the thesis, and to the best of my knowledge and belief no material previously published or written by another person except where due acknowledgement is made in the text of the thesis, nor does the thesis contain any material that infringes copyright.

Authority of Access

This thesis may be made available for loan and limited copying and communication in accordance with the Copyright Act 1968.

The publisher of the papers in chapters 2 and 4 holds the copyright for that content, and access to the material should be sought from the journal. Chapters 3 and 5 have been submitted for publication and upon acceptance access to the material contained within similarly should be obtained from the respective journals. The remaining non-published content of the thesis may be made available for loan and limited copying and communication in accordance with the Copyright Act 1968.

Statement of Ethical Conduct (where applicable)

The research associated with this thesis abides by the international and Australian codes on human and animal experimentation, the guidelines by the Australian Government's Office of the Gene Technology Regulator and the rulings of the Safety, Ethics and Institutional Biosafety Committees of the University.

Signed Date 29th October 2015

Scott Hadley

Statement of Co-authorship

The following people and institutions contributed to the publication of work undertaken as part of this thesis:

Scott Hadley IMAS QMS = **Candidate**

Craig Johnson, IMAS, University of Tasmania = **Author 1**

Catriona Macleod, IMAS, University of Tasmania = **Author 2**

Karen Wild-Allen, CSIRO = **Author 3**

Emlyn Jones, CSIRO = **Author 4**

Author details and their roles:

Paper 1 **Modelling macroalgae growth and nutrient dynamics for Integrated Multitrophic Aquaculture:**

Located in chapter 2

Candidate was the primary author and largely contributed to the idea, its formalisation and development. Author 1, author 2 and author 3 contributed to the idea, its formalisation and development and in an editorial capacity.

Paper 2 **A Bayesian approach to data assimilation in a macroalgae base Integrated Multitrophic Aquaculture:**

Located in chapter 3

Candidate was the primary author and largely contributed to the idea, its formalisation and development. Author 4 was responsible for expert advice and guidance on applying the model with the LibBI framework. Author 1, author 2, author 3 and author 4 contributed to the idea, its formalisation and development and in an editorial capacity.

Paper 3 **Quantification of the impacts of finfish aquaculture and bioremediation capacity of Integrated Multitrophic Aquaculture using a 3D estuary model:**

Located in chapter 4

Candidate was the primary author and largely contributed to the idea, its formalisation and development. Author 1, author 2 and author 3 contributed to the idea, its formalisation and development and in an editorial capacity

Paper 4 **Investigation of broad scale implementation of IMTA in a temperate estuary using a 3D model**

Located in chapter 5

Candidate was the primary author and largely contributed to the idea, its formalisation and development. Author 1, author 2 and author 3 contributed to the idea, its formalisation and development and in an editorial capacity.

We the undersigned agree with the above stated for each of the above published (or submitted) peer-reviewed manuscripts contributing to this thesis:

Signed: _____ _____

Craig Johnson
Supervisor
Head, Ecology & Biodiversity Centre
IMAS
University of Tasmania

Nathan Bindoff
Head, Oceans & Cryosphere Centre
IMAS
University of Tasmania

Date: 29th October 2015

ACKNOWLEDGEMENTS

I would like to thank the Fisheries Research and Development Council (FRDC) whose funding made this project possible. I would also like to thank Catriona Macleod in particular for securing this funding. The research was also made possible through the support of the Institute of Marine and Antarctic Studies (IMAS), University of Tasmania (Quantitative Marine Sciences Scholarship) and the CSIRO. I would also like to acknowledge the support given by TASSAL in allowing me conduct research at one of their farms.

I would like to thank the Coastal Environmental Modelling Team at CSIRO whose generous support enabled me to become a biogeochemical modeller. In particular I would like to acknowledge Mark Baird for his insights into the modelling process. I would also like to thank Emlyn Jones for his assistance with the Bayesian statistical analysis performed in chapter 3. Without LibBI chapter 3 would not have been possible.

I am extremely grateful to my supervisors for helping me through this process. I would like to say thank you to Karen Wild-Allen for her generous support and for sharing her knowledge of modelling with me, Craig Johnson for his generous support and insights into the problem at hand, and Catriona Macleod for her generous support and her focus on the important details.

Finally I would like to thank my family. To my wife Kristin for her love and support, my mother Maureen who made it possible, and my son Fergus for showing me the myriad of solutions possible if you remove logic from the equation.

GENERAL ABSTRACT

Aquaculture is an increasingly expanding industry driven both by economic opportunity and necessity, as countries seek contemporary solutions to food security. However there are risks with unchecked or poorly managed expansion, including the potential to harm natural ecosystems in the vicinity of aquaculture farms. It is unknown exactly how sensitive estuarine biogeochemistry is to a major input of dissolved inorganic nitrogen (DIN) from finfish aquaculture. DIN is the limiting nutrient in autotrophic growth in temperate Australian estuaries, and increase in DIN loading has the potential to greatly increase primary phytoplankton production with possible consequences ranging from general decrease in water quality to harmful algal blooms and a trophic shift to eutrophication.

The present work investigates the impact of salmon farming on the marine environment and key ecological processes in the D'Entrecasteaux Channel and Huon Estuary in Tasmania. This study uses purpose built ecosystem models to assess the increase of nutrients in the region due to the nutrient input from fish farms. The results indicate a need to develop strategies to deal with nutrient loading from salmon aquaculture, particularly if the industry were to increase production beyond current levels. One method gaining increasing interest worldwide is Integrated Multitrophic Aquaculture (IMTA) in which species that utilize the waste products from the primary species are farmed alongside the focus species. Here I construct an IMTA process model to identify the most suitable macroalgae, from a set of potential species for this region, and present a thorough uncertainty analysis of the model. The model is then used within larger estuary models to quantify the potential benefits of IMTA at the system level. The thesis comprises separate chapters for the General Introduction, General Conclusion and four standalone chapters that focus on quantifying the potential of using macroalgae as an agent for IMTA in conjunction with finfish aquaculture in southeast Tasmania.

In Chapter 2 the aim was to identify a suitable species of macroalgae for IMTA in the D'Entrecasteaux Channel and Huon Estuary. To achieve this aim, a macroalgae growth model was developed and then applied in a simulation of IMTA in a near field experiment, whereby macroalgae are grown close to a point source of nutrients. The model was used to compare the capacity of three species of macroalgae (*Macrocystis pyrifera*, *Ulva lactuca* and *Porphyra umbilicalis*) to remove 'waste' DIN under a range of scenarios. The species were selected based on certain assumptions about their intrinsic worth; *M. pyrifera* is a species that has largely disappeared from the region and so has environmental and conservation value, *P. umbilicalis* has high economic value in the seafood industry, while *U. lactuca* has the highest absolute growth rate of these three rapidly-growing algae and so is an obvious candidate as a potential 'nutrient pump'. The model distinguishes between

the species based on parameters representing sub-processes that control growth. An allometric growth term was developed to allow *M. pyrifera* to vary its height and thus exploit its ability to occupy the water column. The results show that *M. pyrifera* vastly out-performs the other two species in terms of its ability to remove the DIN output from the finfish cages in the near field case, largely as a result of its size advantage over the other species. Quantifying the potential optimization of IMTA considering cultivation depth, site selection and harvesting, suggests that varying cultivation depth up to a maximum of 5m impacts *M. pyrifera* production but has no effect on the other two species; DIN removal varied with flow rate (for all 3 species) and the appropriate harvesting scheme can improve bioremediation by a factor of 15 compared to non-harvested crops.

In Chapter 3 a thorough uncertainty analysis of the model was conducted and a method to incorporate empirical data to improve model performance was also developed. A Bayesian inference method was used to quantify uncertainty in the IMTA model with *M. pyrifera* used as the extractive species. The deterministic model was reformulated into a stochastic form through the representation of sub-processes (e.g. mortality and maximal growth rate) as time varying, using first order auto-regressive processes. Parameter uncertainty was accounted for using prior distributions. We used data from three empirical growth experiments to test the effect of seeding density on ropes supporting *M. pyrifera* grown around salmon pens. The data were assimilated into the model using a Sequential Monte Carlo method. Through conditioning the state variables on the parameter priors alone we obtained a comprehensive uncertainty analysis of the model, and were able to constrain the model output to observed values. The results showed learning in a subset of model parameters, and overall the data assimilation method resulted in a 90% reduction in model uncertainty in both the state and parameters. These results will assist in future applications of the model by providing a more realistic parameter set. We were also able to show that low to medium density as an initial seeding of *M. pyrifera* resulted in best uptake of DIN. This approach offers a method by which empirical data from IMTA experiments can be used to improve IMTA process models.

The next two chapters incorporate the model into a three-dimensional coupled hydrodynamic, sediment and biogeochemical model. The 3D model, which was used in the original study that prompted this work, has been developed through numerous case studies to offer a realistic simulation of estuarine dynamics. In chapter 4 an idealized 'test' estuary was created as the setting of finfish aquaculture. Firstly, through incremental increases in DIN output from finfish aquaculture a relationship between nutrient loading rates and water quality as determined by chlorophyll concentration, was obtained. Through the simulation of IMTA farms adjacent to the finfish sites, the capacity of *M. pyrifera* to remediate the estuary was then established. The results showed that *M. pyrifera* could effectively bioremediate the output from the finfish aquaculture as loading increased. This ensured a classification of 'good' water quality based on chlorophyll concentrations, was

retained within the estuary. The hydrodynamic conditions was determined to be the primary driver of both the distribution of chlorophyll and successful IMTA. Farms in the southern section of the estuary achieved the highest biomass of macroalgae, but had little impact on the reduction of primary production due to this area being well flushed from strong river flow; which limited phytoplankton growth in this area. A region of freshwater influence was responsible for the high productivity observed in the northern region of the estuary, and IMTA in this section was solely responsible for reducing chlorophyll concentration.

The last phase of the study (Chapter 5) focused on a more realistic simulation of macroalgae-based IMTA by incorporating the stylized model into a model of the D'Entrecasteaux Channel and Huon Estuary - a region of intensive salmon aquaculture in southeast Tasmania. In this chapter the aim was to estimate phytoplankton production in this region stimulated from 'waste' DIN from finfish aquaculture, and investigate the effectiveness of IMTA in remediating any increase in production. We identify the spatial pattern and magnitude of phytoplankton production in the region under a range of outputs from finfish aquaculture. Scenario analysis showed that the most productive area to grow *M. pyrifera* is in the immediate vicinity of the salmon farms, and that growing giant kelp in this way can mitigate undesirable effects on chlorophyll concentration of DIN loading from the farms if activity expands beyond current levels. However, mitigation using IMTA is non-linear and there are limits to the magnitude of salmon aquaculture activity beyond which significant declines in water quality seem inevitable, even if *M. pyrifera* is grown extensively around farms.

This study provides a thorough investigation of the potential of macroalgae-based IMTA to prevent the potentially damaging waste DIN output from finfish aquaculture from adversely affecting water quality (as assessed by chlorophyll concentration). It provides important baseline information that will help both management and future studies into IMTA by: (i) identifying vertical distribution as the most important feature for potential macroalgae culture species in near field IMTA; (ii) showing the impact of farm arrangement on DIN uptake by macroalgae for a range of potential IMTA species; (iii) describing a method for data assimilation to improve the validity of model results and reduce uncertainty, and (iv) providing a general guide to considerations for the successful implementation of macroalgae-based IMTA to mitigate reduction in water quality resulting from the addition of anthropogenic nutrification in estuaries.

TABLE OF CONTENTS

LIST OF FIGURES

LIST OF TABLES

CHAPTER 1
GENERAL INTRODUCTION, OVERVIEW AND THESIS STRUCTURE

1.1 Background

Global aquaculture production reached 66 million tonnes in 2012, which was 43% of the world's total fish supply, increasing from 25% in 2000 (FAO 2014). Whilst capture fisheries have maintained steady production since the 1980s, the growth in aquaculture production for the past 20 years has been 6.9% per annum (FAO 2011). Global fish production is projected to increase to 181 million tonnes by 2022 with the major driver being the increase in aquaculture production (Lem et al. 2014). Australian aquaculture currently produces 80 thousand tonnes and the aim is to reach 100 thousand tonnes by 2015 (FRDC 2015). Farmed salmonids (salmon and trout) accounted for 34% of the total volume of aquaculture production by volume in (2007-08) Australia (FRDC 2015). Globally, annual production of Atlantic salmon reached 1.5 million tonnes in 2008, up 11.2% on the 10-year mean with prices up 23% on the 10-year mean (Lem et al. 2014).

The rapid growth in the production of carnivorous species such as salmon is due to favorable economics of larger scale intensive farming (Bostock et al. 2010). However, most aquaculture systems rely on uncosted environmental goods and services like waste removal (Bostock et al. 2010). Currently for coastal finfish aquaculture, cages are cost effective as they support expansion and are easily assembled. The cages allow water flow through and thus promote oxygenation and flushing of waste products, minimising production costs. It follows that if regulations were set on environmental impact and companies made to bear this cost, then the economics of production would be strongly affected. However, problems can arise from imposing regulations where, for example, only one potential impact is costed. If technologies that reduce that particular impact are promoted to facilitate an increase in overall production, the ultimate result may be even greater impacts later on. Thus a critical question is how issues such as nutrient cycling, disturbance regulation, biological control and recreational and cultural services are brought into company accounts. If they aren't, then increased competition for natural resources will force governments to either allocate these vital resources strategically or adopt a policy which leaves the market to determine their use depending on activities that can extract the highest value. However the marine environment also has an intrinsic economic value, fifty percent of which is ascribed to the coastal region (chapter 8, Holmer et al. 2008) which is vulnerable to disturbance by anthropogenic influence.

The aquaculture industry needs to address its environmental impacts in order to both obtain a social license to operate and to optimise production, as finfish aquaculture requires high water quality. Poor water quality can result in reduced biomass of fish produced (Staurnes et al. 1995) or enhance the impact of disease or health issues (Forrest et al. 2007) In addition, there are also water quality

requirements which must be maintained for a coastal body of water to be considered healthy. In Australia and New Zealand the ANZECC (2000) guidelines provide a regulatory framework for water quality in coastal areas. Coastal waters are a shared resource and adverse public opinion, as a result of real or perceived environmental impacts, may be damaging for an aquaculture company and their products in a world where consumers are increasingly making more informed choices regarding environmental sustainability of their food. Increasingly, aquaculture products need to provide certification that they meet certain standards as insurance against negative consumer sentiment (FAO 2011.) The protection of the environment remains a key issue in aquaculture, tightly linked to productivity and ultimately success.

1.2 Impacts of aquaculture

Carnivorous species of finfish, such as salmon, require a high protein diet. Consequently salmon aquaculture can modify the environment through the release of nutrient enriched waste into the surrounding water (Figure 1-1). This results in concentrating a considerable amount of feed and/or fish faeces into relatively small areas within an ecosystem. Dissolved inorganic nitrogen (DIN), mainly in the form of ammonium, can represent a significant proportion of the excreted waste, and this can be readily taken up by phytoplankton (Wang et al. 2012). The amount of waste released depends on the type of feed used and feeding procedures. Total salmon feed for aquaculture is predicted to reach 4 million tonnes by 2020 (Bostock et al. 2020). Models for waste output of DIN associated with fish farming (Islam et al. 2005; Wang et al. 2012) have estimated that as much as 85% of total feed nitrogen is released back into the water. Wild-Allen et al. (2010) suggested that 65% of feed nitrogen is release back into the environment from salmon farms in southeast Tasmania, with 85% of this in dissolved form. All of these estimates are based on feed conversion ratios provided by the fish farmers, which provide an estimate of the amount of feed required to produce a given biomass of farmed fish and, knowing the amount of nitrogen in the feed and in the farmed product, this in turn can be used to calculate how much nitrogen is needed to produce each kilogram of salmon, with any remaining proportion of feed/ nitrogen assumed to be lost to the environment.

As management practices and feeding procedures improve, feed conversions have become more efficient. However, given the use of cages in open waters an amount of waste nitrogen will always be lost to the environment. Enrichment of benthic regions from waste has the potential to change both sediment chemistry and the flora and fauna composition (Keeley et al. 2013; Keeley et al. 2014; Macleod et al. 2004). Dissolved nutrients can cause problems in areas with extensive aquaculture production or with otherwise oligotrophic or mesotrophic environments (Bostock et al. 2010). In general, increasing inputs of DIN can potentially modify phytoplankton community composition (Buschmann et al. 2009; Bonsdorff et al. 1997), increase algal biomass in general and, in worst cases, result in eutrophication

(Anderson et al. 2002; Carmona et al. 2006). Wild-Allen et al. (2010) modeled the effect of salmon aquaculture on a southeast Tasmanian estuary, with the results suggesting the potential for a shift in trophic status from oligotrophic to mesotrophic for 12% of the estuary, and predicting that this could extend to 53% of the estuary under a proposed 3-fold increase in farm leases. Importantly, whilst aquaculture production and the efficiency of production is increasing as a result of improved knowledge, the science around impacts is not as readily funded. Buschmann et al. (2009) highlight the lack of scientific evaluation of the impact of coastal salmon aquaculture in Chile particularly given that the impact of inorganic and organic waste on the benthic and pelagic communities is well documented.

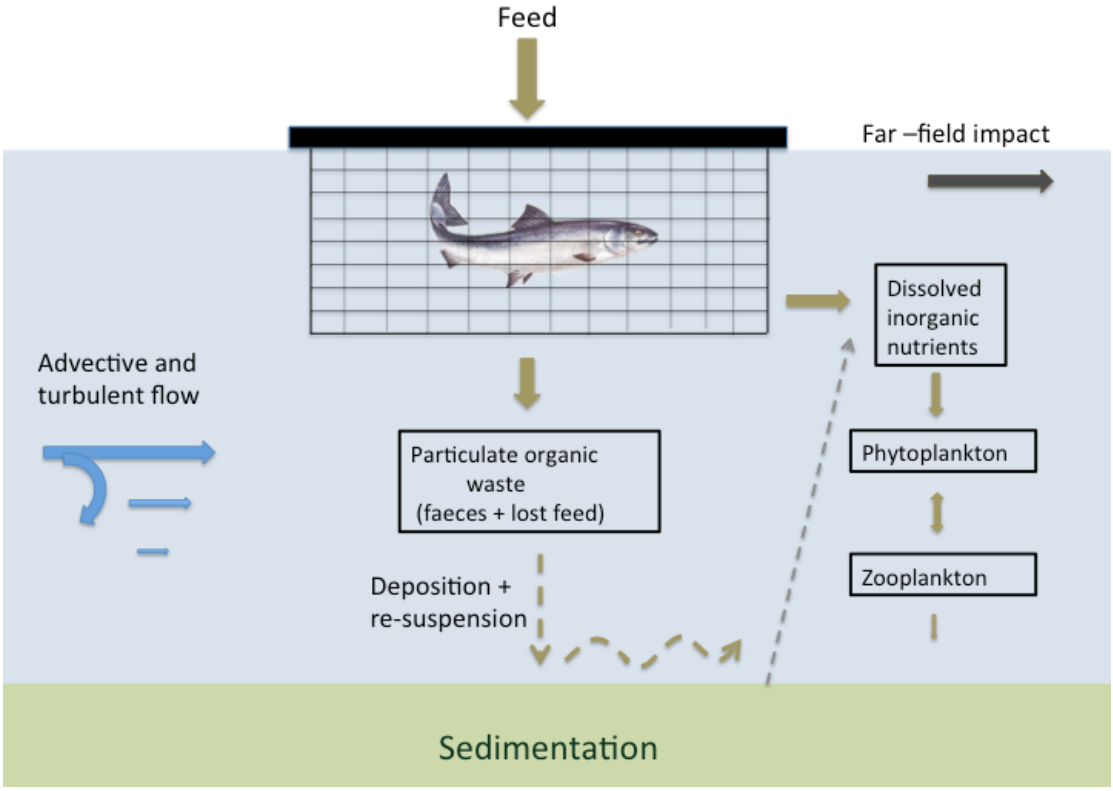

Figure 1-1: Schematic of the effect salmon aquaculture has on the nutrient cycle in a coastal ecosystem.

Estuaries tend to be subject to high nutrient input rates from both natural and, increasingly, anthropogenic sources. Hydrodynamic conditions set by bathymetry, tidal currents and river flow determine whether the estuary is well-mixed or stratified and the flushing rates, which in turn determines both the production cycles and rate of conversion of nutrients to algal biomass within the estuary (Mann & Lazier 1991; Cloern 2001). A major review of ecosystems in estuaries and other water bodies influenced by a connection to land, showed annual phytoplankton primary production can vary up to 10-fold spatially and 5-fold from year to year depending on sinking, advection, growth and mortality processes

(Cloern 2014). Understanding the mechanism(s) by which exogenous nutrient output from finfish aquaculture affect estuarine primary production is of global interest but is not a straightforward task given the pronounced natural variability between and within estuaries. Ultimately the carrying capacity of an estuary will be determined through sources and sinks, flushing rates, biogeochemical processes and an appropriate definition of water quality.

1.3 Integrated Multitrophic Aquaculture

Integrated multitrophic aquaculture (IMTA) involves the farming of species from different trophic levels within the same system whereby extractive species, such as macroalgae or filter feeders, are farmed alongside species that require feeding, such as finfish. The concept is not new, and cultivating multiple species simultaneously in this way is well established in Asia particularly. What has received more attention recently is the idea of using IMTA for bioremediation of excessive nutrient input from intensive aquaculture (Troell et al. 2009; Buschmann et al. 2008; Carmona et al. 2006). Macroalgal culture is particularly attractive not only with respect to removing farm waste, but also because it potentially provides capacity for a new market to offset costs. Consequently, algal species with high growth rates, particularly in summer when natural production is high, and which are easily cultivated and have economic potential are especially attractive (Troell et al. 2009). The use of local species is generally encouraged because these are suited to the conditions (Carmona et al. 2006) and would not have the issues that would be associated with introduction of non-native species. With the emphasis in IMTA placed on farm implementation (FAO 2009), much of the research has focused on matching the ratio of extractive to fed species in order to optimise IMTA (Ren et al. 2012; Broch et al. 2013). However given the range of macroalgal species and possible farm implementation schemas, and the environmental variability that may exist between IMTA sites within an estuary, optimization in that sense needs more qualification.

The success of macroalgal based IMTA is dependent on the individual species used and local conditions. Buschmann et al. (2008) in a comparison of 2 species found that both benefitted from farm effluent (increased growth rates) but at different cultivation depths. Sanderson et al. (2010) similarly found enhanced algal growth rates using an IMTA approach but concluded that knowledge of the hydrodynamic flow around finfish cages is necessary to take full advantage of the plumes of nutrients emanating from them. There have been many trials and pilot studies into the potential of IMTA for sustainable aquaculture at ‘experimental’ scales (Abreu et al 2009; Westermeier et al. 2011; Buschmann et al. 2008; Carmona et al. 2006) but the results from small scale experiments do not necessarily extrapolate to full-scale operations due to inherent non-linear feedbacks. For this reason a modeling approach should be considered by researchers when exploring a range of potential scenarios possible in an IMTA approach (Ren et al 2014; Broch et

al 2013). Modeling provides a means to extrapolateresults from small-scale field based IMTA studies to greater scales. Furthermore, this type of approach enables investigation of a range of species and IMTA scenarios that are beyond the reach of field-based studies or at a much lower cost than a full scale farming operation.

1.4 General approach and structure of thesis

A Previous study by CSIRO quantified the impact of finfish farming on the D'Entrecasteaux Channel and Huon Estuary (DHD) in southeast Tasmania (Wild-Allen et al. 2010). This connected system (Figure 1-2) is characterized as a micro-tidal estuary that is highly seasonally variable. It is used for water sports, recreational fishing and supports a low population base as well as a salmon industry (Butler et al. 2006). Using a coupled hydrodynamic, sediment and biogeochemical (BGC) model of the region, the CSIRO study predicted a shift in trophic status from oligotrophic to mesotrophic for 53% of the region based on mean annual chlorophyll concentration under a proposed 3-fold increase in the number of salmon farm leases.

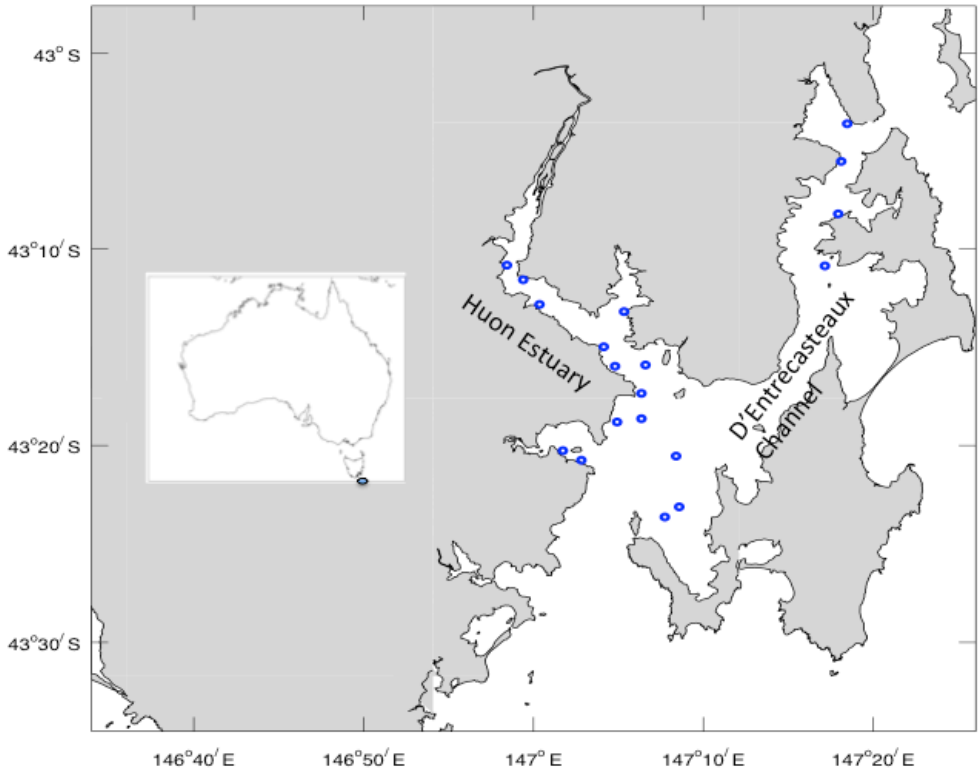

Figure 1-2: The D'Entrecasteaux Channel and Huon Estuary form a connected system, which is the site of salmon aquaculture (blue circles are salmon leases) in southeast Tasmania.

The overarching goal of this thesis is to quantify the capacity of macroalgal-based IMTA to remediate the DIN input into the D'Entrecasteaux Channel and Huon

Estuary by salmon aquaculture under current and projected future potential stocking regimes. The CSIRO have developed a fully coupled 3D hydrodynamic, biogeochemical and sediment model for this region, which was used to provide the initial assessment of the impacts of salmon aquaculture. The aim of the present research is to construct and apply an additional model component within CSIRO's existing model to quantify IMTA within the region. Models require validation and this is often achieved through comparison with existing observations or the collection of specific data. Fortunately, CSIRO, the University of Tasmania and a range of environmental managers both in state government and industry regularly monitor this estuarine system, providing reliable data for calibration and validation purposes. There are four chapters devoted to developing an IMTA model and implementing it within the 3D estuary model. They comprise novel research, and relate to specific questions as follows:

Chapter 2, details the development and implementation of a generic IMTA model based on the growth of macroalgae from DIN output from finfish cages. This model incorporates data relating to the key components of macroalgal growth. It is used to compare and contrast the performance of three macroalgal species and provides an assessment of the most suitable candidate for near-field IMTA in the southeast Tasmanian region. All three species are fast growing 'local' macroalgae, and each has individual characteristics that make them preferable for cultivation under particular circumstances, i.e. for either economic, environmental or bioremediation potential. The model is used to explore where differences in the farming approach (e.g. cultivation depth and harvesting protocols) and/ or site location (i.e. affecting flow rate and water clarity) might provide different outcomes to identify optimal farming practices.

A vital component in a modeling approach is validation of the results. For the model results to be accepted there must be assessment of how well they match observation and fulfill other validation criteria (Rykiel 1999). Furthermore, most models currently used to represent biogeochemical processes are highly parameterized and there is often a degree of uncertainty around the true value of these parameters. Chapter 3 outlines a specific method for using empirical data to inform the underlying model parameterization and thereby ensure greater confidence in the model results. The inference method proposed also makes it possible to fully quantify the models uncertainty based on an improved understanding of the uncertainty in the underlying parameters and process. In relation to improving understanding of IMTA specifically, this chapter analyses the underlying model interactions and looks at the effect of initial stocking density (for macroalgae sporelings) on the model results. This work offers a way of combining empirical data with IMTA process models in a way that both improves model performance and better defines the envelope of confidence in the outputs (IMTA results) for management.

Chapter 4 provides a tool for improved spatial resolution of IMTA in an impacted estuary. In this approach we incorporate the IMTA model within a 3D model of an idealised estuary (created using CSIRO's environmental modelling suite [EMS] platform). Through an incremental increase in the output of DIN from finfish aquaculture the general interactions between hydrodynamics, biogeochemistry, finfish aquaculture, macro-/ microalgae production and water quality (as defined by ANZECC guidelines for chlorophyll concentration) are assessed. Factors such at site specificity and finfish farming intensity are manipulated to analyse spatial patterns of phytoplankton production based on aquaculture loads. Through a subsequent simulation of macroalgae farms within the system the effectiveness of IMTA in remediating the water quality is examined. Differences associated with spatial positioning of farmed macroalgae were also assessed, and related to the determining hydrodynamic and biogeochemical factors within the estuary. In the idealised estuary it is possible to control environmental variability which, while it may not be realistic for a particular real estuary, enables the process interactions to be constrained and better defined, and therefore facilitates a more accurate interpretation of the observed spatial variability.

In chapter 5 the IMTA model is modularised within the estuary model of the D'Entrecasteaux Channel and Huon Estuary (DHD), which is nested within intermediate and regional scale hydrodynamic models to provide boundary conditions. The DHD model includes forcing for salmon aquaculture, with details provided by industry to ensure an accurate and realistic representation. This realistic simulation is used to quantify the effectiveness of macroalgae based IMTA to remediate DIN waste output from salmon farms in the D'Entrecasteaux Channel and Huon estuary regions in SE Tasmania. The impact of finfish aquaculture is defined in terms of chlorophyll concentration based on ANZECC guidelines. A series of scenarios look at the impact of finfish aquaculture on the DHD model with and without IMTA present. Scenarios examining the effect of different farming practices and farm arrangements offer a fully quantitative approach.

Overall, this study provides important information to environmental and aquaculture managers regarding the potential of the IMTA approach in general, and its specific application in the D'Entrecasteaux Channel and Huon estuary. The modeling tools developed and their application is innovative and offer a way to assess the potential for IMTA for species of macroalgae in any specific situation. There is also a method of incorporating empirical results from field-based experiments to improve model performance and provide greater confidence in the results. The study develops from the general model to offer a specific quantification of the effectiveness of IMTA if it were to be used in D'Entrecasteaux Channel and Huon Estuary, centered on providing an insight into the effectiveness of different farming arrangements and procedures as well as siting of algal farms.

Chapters 2-5 of this thesis were all prepared as standalone publications and so any redundancy in the form of repeated contextual information contained in the introduction section of each chapter was unavoidable.

CHAPTER 2

MODELLING MACROALGAE GROWTH AND NUTRIENT DYNAMICS FOR INTEGRATED MULTITROPHIC AQUACULTURE

Preface: One of the first objectives of this research was to identify the species of macroalgae that would be used in the subsequent quantification of IMTA. This was achieved by developing an IMTA process model and using it to compare the bioremediation capacity of three candidate species of macroalgae.

This chapter represents the first objective. The successful species is determined through subsequent application of the model developed herein. The bioremediation capacity of each species is examined through a range of environmental conditions which assists our understanding of IMTA.

This work has been published in a refereed journal and is presented below in an identical form. The citation for the original publication is:

Hadley S, Wild-Allen K, Johnson CJ, Macleod CK (2015) Modeling macroalgae growth and dynamics for integrated multi-trophic aquaculture. J Appl Phycol 27:901-916

Abstract

Integrated Multi-Trophic Aquaculture (IMTA) is being explored on both economic and environmental grounds in many traditional aquaculture regions. To test a variety of suitable macroalgae species and management scenarios, a numerical model is developed to quantify the remediation of dissolved nutrients and production of macroalgae near a nutrient source. Differences in the morphological, physiological and economic characteristics of different macroalgae species can provide flexibility when considering the cost and benefit of farming macroalgae. Results show that of the three species studied *Macrocystis pyrifera* removed 75% of DIN input from a point source, while *Porphyra umbilicalis* and *Ulva lactuca* removed *5%.* Both *M. pyrifera and P. umbilicalis* have reduced bioremediation capacity at increasing flow rates. *U. lactuca* showed increased bioremediation potential as flow rate increased from low to moderate flows. Increasing the optical depth increased the bioremediation potential of *M. pyrifera* for moderate values of the light attenuation coefficient, whereas bioremediation was unaffected by optical depth for both *U. lactuca* and *P. umbilicalis*. Harvesting increased bioremediation capacity of all species by up to 25 fold dependent on the establishment phase and harvesting frequency. We conclude that the choice of macroalgae species greatly affects the success of IMTA and both harvesting and farm arrangements can be used to greatly optimize bioremediation.

2.1 Introduction

An important potential environmental impact of salmonid farming is the accumulation of waste products in the waterway. In estuaries where water circulation may be restricted, there is a possibility that the accumulation of farm waste will form a nutrient rich system with a resultant shift in trophic status (Wild-Allen et al. 2010). Integrated multi-trophic aquaculture (IMTA), which involves farming of fed species like finfish together with 'extractive' species such as seaweeds and filter feeders to take up inorganic and organic nutrients respectively, has the potential to mitigate the environmental impacts of salmon aquaculture (Buschmann et al. 2008).

The extractive species can have economic value in their own right. IMTA takes a more balanced 'whole of ecosystem' approach to management, and typically takes into consideration site specificity, operational limits, revenues and food safety guidelines, as well as environmental quality and regulations (Troell et al. 2009) . There have already been some empirical studies into the effects of the nutrient output from fish farms on the growth of macroalgae (Buschmann et al. 2008; Hernandez et al. 2005; Sanderson et al. 2008). These studies found that macroalgae biomass increased in the presence of the fish farms but concluded that more detailed studies were needed to model nutrient dynamics, optimize farm design and identify suitable seaweed species, all which may be site specific. Empirical studies have been conducted to show comparisons between different species in the filtration of DIN from fish effluent (Hernandez et al. 2002; Hernandez et al. 2005). However these studies were conducted in tanks and plant morphology was not considered.

Results from small-scale systems do not necessarily extrapolate to large-scale operations because the removal of nutrients involves non-linear interactions between many variables. A modeling approach can help to understand these interactions, as full-scale trial operations may be prohibitively expensive. Models have been used to quantify the potential benefits of IMTA in an existing aquaculture system (Broch et al. 2013; Ren et al. 2012; Silva et al. 2012), however in these studies the assessment of macroalgae was limited to one species. Buschmann et al. (2008) showed that two commercial macroalgal species in Chile had similar bioremediative potential but at differing cultivation depths. This has significant implications for any potential farming operation. A key goal in implementing IMTA is to optimize the ratio of fed to extractive species (based on local hydrodynamic, physical and chemical water quality characteristics) to maximize the overall cost-benefit ratio. Another key goal is to identify an optimal harvesting strategy. Frequent harvesting enables constant removal of nutrients from the water (Chopin et al. 1999), but harvest strategies have to guarantee an increase in bioremediation and need to be balanced by economic considerations.

Species previously identified as most suitable for IMTA are those that are at their most productive in summer; have high rates of nutrient uptake (and thus high growth rates); have economic value in their own right; and are easily cultivated (Troell et al. 2009). Identifying suitable seaweed species and determining farm design to optimize the impact and economic return of IMTA will be aided greatly by development of suitable models that can be applied readily to locations anywhere in the world.

In this paper we apply a macroalgal growth model to compare the bioremediation capacity of three species of macroalgae in a flexible IMTA environment. Using a set of scenarios we examine the effect of variation in ammonium loads, refresh rate, optical depth and harvesting schemes, on seasonal yield of macroalgae.

2.2 Model description

The macroalgal growth model we used here is based on those originally described by Solidoro et al (1997) and Aldridge and Trimmer (2009). We have introduced a term for the increase in height of *Macrocystis pyrifera* based on biomass. We can use this term to assess the potential difference between kelp and smaller macroalgae grown for the purposes of IMTA. We are simulating a mesocosm, which represents a macroalgal farm with a salmon farm point source inputting a nitrogen load into the farm volume. Here we present a brief description of the state equations; more detailed processes and parameter information is included in appendix 2-A.

Dissolved inorganic nitrogen (DIN) is modeled in two forms: nitrate (NO_3; $\mathrm{mg\,N\,m^{-3}}$) and ammonium (NH_4; $\mathrm{mg\,N\,m^{-3}}$) (Figure 2-1). This allows distinguishing the output from the salmon farms, which is largely in the form of ammonium (~97% of ammonia derived

from the salmon is assumed to be protonated to ammonium instantly), from background concentrations of ammonium and nitrate. The currency of N is chosen for this study because this nutrient limits autotroph growth in the region (Thompson et al. 2005). Dissolved inorganic phosphorous (DIP) is a potentially limiting nutrient in estuarine systems however it is also output as waste from the salmon farms. The ratio of DIN to DIP output from salmon farms ranges from 5:1 to 12:1 (mol:mol) (Wang et al. 2012; Wild-Allen et al. 2010) which is well below the Redfield ratio of 16:1 and Atkinson ratio 30:1 for phytoplankton and benthic marine plant tissue composition. We therefore assume DIN remains in shortest supply and is the limiting nutrient in proximity to the fish farms.

The total concentration of DIN in the water passing through the macroalgae farm is calculated from the combination of the concentration of the inflow at the background reference concentration, $\mathrm{NX_{xref}}$, and the outflow at the macroalgae farm's internal concentration, $\mathrm{NX_x}$. There are internal DIN losses due to farmed macroalgae as well as transformations due to the processes of nitrification and remineralisation and an input of ammonia from the salmon farm, which gives:

$$\mathrm{V_{farm}}\ \frac{\mathrm{dNH_4}}{\mathrm{dt}} = \mathrm{F_{in}NH_{4ref}} - \mathrm{F_{out}NH_4} - \mathrm{f(NH_4, Q)BV_{MA}}\ + \mathrm{Fish_{in}}\ \ + \mathrm{V_{farm}r_L D} - \mathrm{V_{farm}r_N NH_4} \quad (2\text{-}1)$$

$$\mathrm{V_{farm}}\ \frac{\mathrm{dNO_3}}{\mathrm{dt}} = \mathrm{F_{in}NO_{3ref}} - \mathrm{F_{out}NO_3} - \mathrm{f(NO_3, Q)BV_{MA}}\ + \mathrm{V_{farm}r_N NH_4} \quad (2\text{-}2)$$

$\mathrm{V_{farm}} = \mathrm{z\,A_{farm}}$ is the volume of our macroalgae farm. Here z is cultivation depth and A_{farm} is the macroalgae farm area. Similarly $\mathrm{V_{MA}} = \mathrm{h_{MA}\,A_{farm}}$ is the volume occupied by the macroalgae (inside $\mathrm{V_{farm}}$) with $\mathrm{h_{MA}}$ the height of the macroalgae in m. In (2-1) and (2-2), $\mathrm{F_{in}} = \mathrm{F_{out}}$ represents the flow rate through $\mathrm{V_{farm}}$. B (Eq. 2-A9) represents biomass, $\mathrm{f(NX_x, Q)}$. (Eq. 2-A1) controls the uptake rate of $\mathrm{NX_x}$ by macroalgae dependent on the internal quotient Q (Eq. 2-A10). $\mathrm{Fish_{in}}$ is the point source input of $\mathrm{NH_4}$ from the salmon farm into $\mathrm{V_{farm}}$. The term $\mathrm{r_L D}$ represents the remineralisation of detritus into $\mathrm{NH_4}$. Finally, $\mathrm{r_N NH_4}$ is the nitrification of ammonia to nitrate.

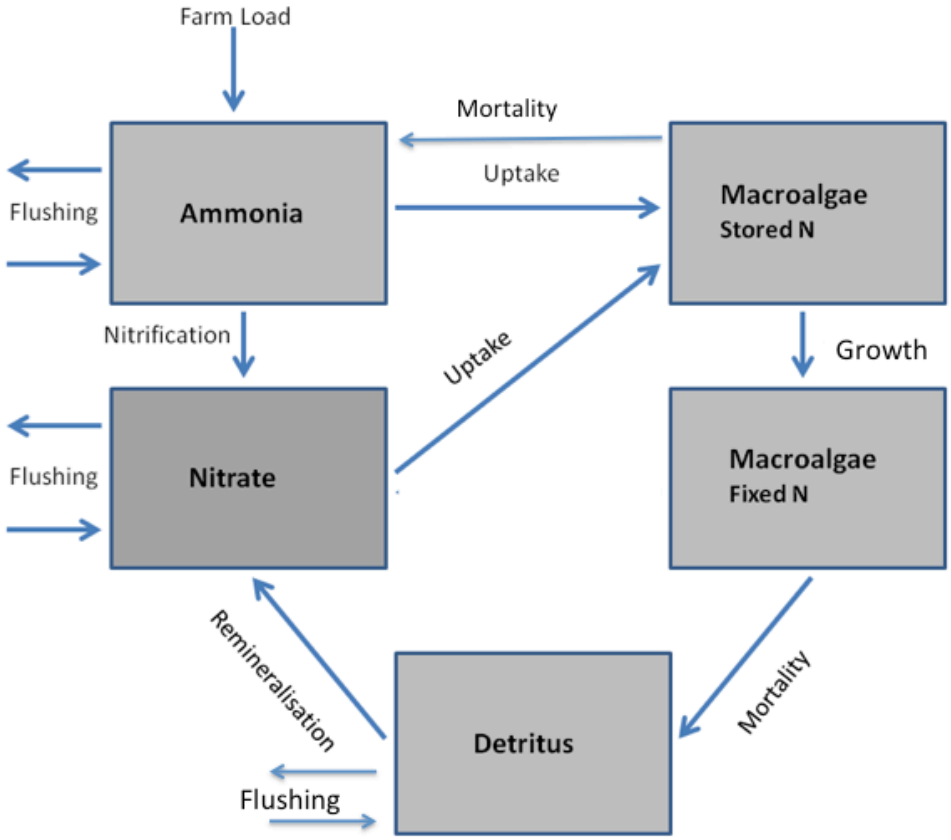

Figure 2-1: Biogeochemical model of nutrient uptake by macroalgae. A load is placed on the system by the salmon farms in the form of dissolved ammonia. This is either absorbed by the algae or nitrified (to nitrate) in the water column. The algae have a two-step uptake process where nitrogen is first stored in intracellular pools and then assimilated into the algae's cellular structure at a rate dependent on environmental factors. Finally the algae dies and fixed N is returned to detrital pools and stored N is returned to ammonia.

In (2-1) and (2-2) we divide through by V_{farm} to get

$$\frac{dNH_4}{dt} = \lambda_R(NH_{4ref} - NH_4) - f(NH_4, Q)B[\max(\frac{h_{MA}}{z}, 1)] + N_{farm} + r_L D - r_N NH_4 \quad (2\text{-}3)$$

$$\frac{dNO_3}{dt} = \lambda_R(NO_{3ref} - NO_3) - f(NO_3, Q)B[\max(\frac{h_{MA}}{z}, 1)] + r_N NH_4 \quad (2\text{-}4)$$

Here λ_R is the refresh rate which is the ratio F_{in}/V_{farm} and is a measure of how quickly the ambient nitrogen concentration inside V_{farm} returns to reference level without macroalgae present. We use this formulation (Aldridge and Trimmer 2009) to provide a method for examining effect of the flow rate on algae growth in the absence of an advection diffusion model. The default value for λ_R = 0.25 d^{-1} is as used by Aldridge and Trimmer (2009), but we vary this parameter to examine the effect of flow rate on the algae growth. The term $\max\left(\frac{h_{MA}}{z}, 1\right)$ is introduced in this model and determines the proportion

of DIN the macroalgae can access in the farm volume (the maximum value of this term is 1 when macroalgae reaches the water surface). Finally, N_{farm} is the daily input of ammonia from the salmon farm averaged over our macroalgae farm volume.

In the model the seaweeds *Ulva lactuca* (Chlorophyta) and *Porphyra umbilicalis* (Rhodophyta) are given a constant height,
h_{MA}= 0.2 m, taken from literature values (Table 2-A2.) The giant kelp *Macrocystis pyrifera* (Ochrophyta) is allowed to change its height according to an allometric term,

$$h_{MA} = (0.00174 N_f / num\_fronds)^{1.047} \quad \text{(Eq. 2-A11 in appendix)}$$

This term is derived from the work by Utter and Denny (1996) relating frond mass to height for *M. pyrifera*. In our model we determine mass per m^2 of macroalgae but not the number of fronds within this area. We introduced the dimensionless parameter num_fronds to scale the macroalgae height within an area. It represents the average number of *M. pyrifera* fronds in per area, where we are assuming that a plant consists of several fronds all the same length h_{MA}. The value of $num\_fronds = 7$ (dimensionless) was determined through model calibration. This involved running the model for different values of num_fronds, with a value of 7 resulting in *M. pyrifera* height increasing at a realistic rate. *M. pyrifera* eventually achieves a maximum height, equivalent to cultivation depth, with the parameter num_fronds controlling how quickly it achieves this maximum. The increase in height of the kelp effectively increases both its exposure to the DIN passing through the farm volume and its access to light.

Macroalgal growth is modeled as a two-step process. First DIN is taken up into intracellular pools as an internal reserve of stored nitrogen (N_s; $mg\ N\ m^{-3}$), and then N_s is converted into fixed nitrogen (N_f; $mg\ N\ m^{-3}$) resulting in increased macroalgae biomass B. The uptake of N_s is observed to be independent of light (Aldridge and Trimmer 2009) and is modeled as dependent on the external concentration of DIN (ammonia and nitrate) and the internal nitrogen quota Q. The conversion of N_s to N_f (growth) is dependent on internal reserves, light and temperature.

$$\frac{dN_s}{dt} = f(NX_x, Q) Bmax(\frac{\mathbf{h_{MA}}}{\mathbf{z}}, 1) - \mu g(E, Q, T) N_s - d_M N_s \qquad (2\text{-}5)$$

$$\frac{dN_f}{dt} = \mu g(E, Q, T) N_s - d_M N_f \qquad (2\text{-}6)$$

In equations 2-5 and 2-6, $\mu g(E, Q, T)$ (eq. 2-A2) represents the growth function for macroalgae dependent on light (E), internal nutrient reserves (Q) and temperature (T), whilst $d_M N_s$ and $d_M N_f$ are mortality terms. The breakdown of macroalgal tissue forms detritus (D; $mg\ N\ m^{-3}$), with subsequent remineralisation of D back to NH_4 as well as

release of N_s (from lost tissue) as NH_4. We also model the loss of detritus from the farm volume, with D_{ref} the background concentration of the natural system.

$$\frac{dD}{dt} = \lambda_R(D_{ref} - D) + d_M N_f - r_L D \qquad (2\text{-}7)$$

Equations 2-3 to 2-7 form the state equations for our system.

2.2.1 The Environment

The model was forced with a seasonal cycle of irradiance, temperature and nutrients, using the functional form,

$$X = X_{av} + SD * \sin\left(\frac{2\pi t}{365} + t_s\right). \qquad (2\text{-}8)$$

Here X is the instantaneous value of one of the environmental variables; X_{av} is the annual mean; SD is the standard deviation from the annual mean; t is time (days) and t_s (days) controls the phase shift of the sine function (nutrients have peak concentrations in winter, whilst PAR and temperature have peak values in summer). The values for temperate Australian waters were obtained from the CSIRO Atlas of Regional Seas (CARS) database (CSIRO 2009) for (approximate) latitude 43.0902 (S) and longitude 147.0231 (E) (Figure 2-2).

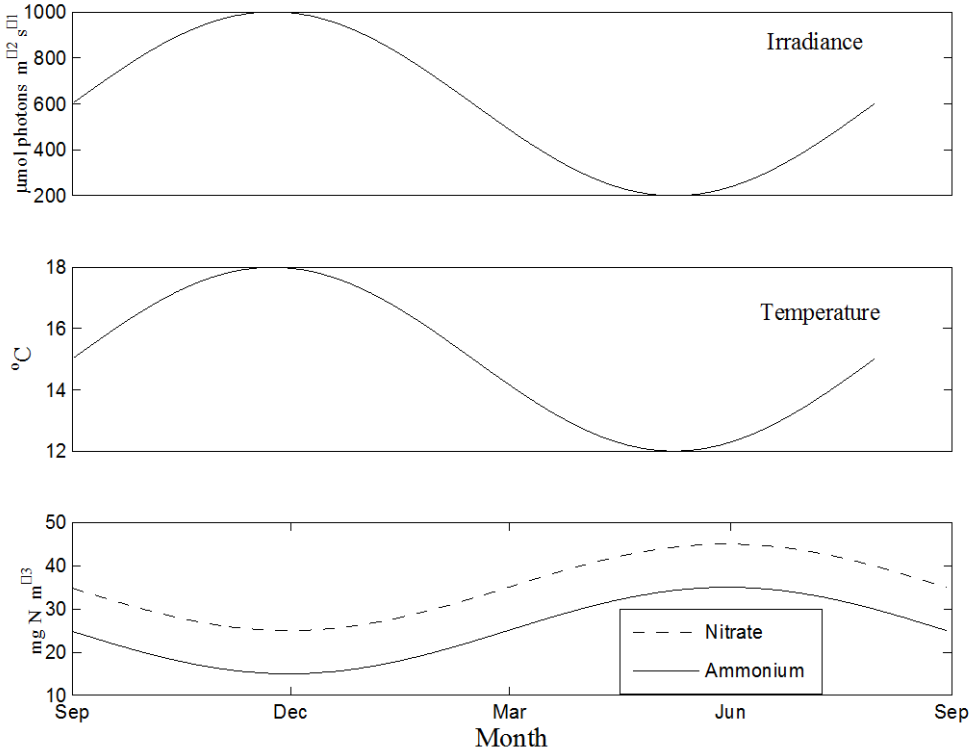

Figure 2-2: The irradiance is PAR and is approximated by a smooth function, to represent the range and seasonal strength typical of the region, with a peak in summer months. This is the same seasonal signal for sea temperature. Ambient nitrate and ammonia (NX_x) are highest in winter.

2.2.2 Macroalgae Species

The three species of macroalgae selected for comparison (*Ulva lactuca*, *Porphyra umbilicalis*; and *Macrocystis pyrifera*) all occur naturally in southeast Tasmanian waters (Sanderson and Di Benedetto 1988), and are suited to the local conditions, which is an important factor in choosing a suitable species (Carmona et al. 2006). All three have both high growth rates and low nitrogen storage capacity. Each of these species has been tested experimentally for potential in IMTA (Buschmann et al. 2008; Carmona et al. 2006; Yokoyama and Ishihi 2010) with encouraging results.

U. lactuca, *P. umbilicalis* and *M. pyrifera* differ in their economic value, bioremediation potential, and conservation value to the natural ecosystem. The potential growth of each species is distinguished in our model by the individual species parameters (Table 2-A2, Appendix 2-A). We also differentiate between the smaller seaweeds *U. lactuca* and *P. umbilicalis* (height = 0.2 m), and the giant kelp *M. pyrifera* (variable height). We use this variation in height to investigate how kelp optimizes its light environment and increases its nutrient capturing capacity in contrast to the smaller species that do not have the ability to grow over a large range of heights.

2.3 Model Simulations

All model simulations described in this section are run over a growing season of 365 days (unless otherwise stated) beginning in spring (September).

2.3.1 General Behavior

The following simulations are designed to establish the general behavior of our model. Firstly we conduct a reference run using the parameter values specified in table 2-A2 for each algal species and the environmental forcing outlined in section 2.2.1 The reference level of input of ammonium from the salmon farms is set at $\mathrm{N_{farm}} = 100\ \mathrm{mg\ N\ m^{-3}d^{-1}}$. The initial concentrations of $\mathrm{N_f}$ and $\mathrm{N_s}$ were set to $100\ \mathrm{mg\ N\ m^{-3}}$ in all model runs. We use this reference run to establish the bioremediation capacity of each species under 'typical' site conditions. We then look at the effect that changing the ammonium output from the salmon aquaculture has on the model results. We use two values of $\mathrm{N_{farm}} = 50$, $100\ \mathrm{mg\ N\ m^{-3}d^{-1}}$ and run the model forward until steady state is reached, and then compare the results for our two values. Finally we run the model with $\mathrm{N_{farm}} = 5000\ \mathrm{mg\ N\ m^{-3}d^{-1}}$ so that growth achieves steady state due to light limitation (nutrient replete system) and analyze the results.

2.3.2 Model validation

The purpose of this study is to apply a macroalgae model to compare the growth/bioremediation capacity of 3 different species of macroalgae in an IMTA environment. In order to validate our results we need to offer evidence that the model is able to offer reasonable simulations of macroalgae growth for all of three species examined. This gives us confidence in the results from the simulations carried out in our comparison study. We establish the fitness of purpose of our model by comparing model growth rates against those published in empirical studies on IMTA for each algal species. To do this we use the environmental forcing, DIN loads and growth period outlined in each empirical study in our model setup and compare the growth rates predicted by our model results with the literature values according to the formula,

$$\mathrm{SGR} = 100 * \ln(\mathrm{w_t} - \mathrm{w_o})/\mathrm{t} \qquad (2\text{-}9)$$

Where w_0 is the initial weight of the macroalgae and $w_t$is weight at the end of the growing period t.

2.3.3 Sensitivity Analysis

To determine the sensitivity of the model to changes in a parameter value, we perturb each parameter in turn by 10% and assess the sensitivity according to

$$\text{Sensitivity} = \frac{\left(\text{V(1.1p)-V(0.9p)}\right)}{0.2\text{V(p)}} \quad \text{(2-10)}$$

where $\mathrm{V(p)}$ is the output from the model with a parameter value equal to p, and $\mathrm{V(1.1p)}$ and $\mathrm{V(0.9p)}$ represent the model output with the parameter equal to 110% and 90% of the value of p respectively (Everett et al. 2007) . This normalized relative sensitivity (2-10) is equivalent to the relationship.

$$\frac{\Delta \ln(\mathrm{V(p)})}{\Delta \ln(\mathrm{p})} \quad \text{(2-11)}$$

so that Sensitivity = 2 implies $\mathrm{V(p)} \propto \mathrm{p}^2$ and therefore a doubling of the parameter value p results in $\mathrm{V(2p)} \propto 4\mathrm{p}^2$, i.e. a fourfold increase in output. In the sensitivity analysis results N_f is used for the model output V in (2-10).

2.3.4 Flow Rate

In the model refresh rate is used a proxy for flow and thus by varying λ_{R} we can investigate the effect of changing the flow rate on the model state variables for each species. In this simulation we run the model using the reference values established in section 2.3.1 with the exception that we vary the value of the refresh rate parameter. We use two values of the refresh rate parameter, the first $\lambda_{\mathrm{R}} = 0.05\ \mathrm{d}^{-1}$ represents a five-fold decrease in reference value given in table 2-A2 (λ_{R}= $0.25\ \mathrm{d}^{-1}$) and this represents low flow conditions (in this simulation). The second value, $\lambda_{\mathrm{R}} = 1.0\ \mathrm{d}^{-1}$ is a four-fold increase in the reference value and is representative of higher flow conditions. We then compare the model results to assess the effect of flow rate on system dynamics.

2.3.5 Optical Depth

Optical depth is the product of the actual cultivation depth z and the light attenuation coefficient of the water $\mathrm{K_d}$. For this simulation we keep z constant at 3 m and vary K_d. We set the reference value for $\mathrm{K_d} = 0.1\ \mathrm{m}^{-1}$ (Table 2-A2) which is equivalent to the background light attenuation coefficient of seawater (K_w). In this simulation we include attenuation due to coloured dissolved organic matter (CDOM) (we are not considering phytoplankton in this study). Light attenuation due to CDOM in the Huon Estuary (site of the environmental forcing in section 2.2.1) can range between 0.1-6.0 m^{-1} for surface water and 0.1-2.0 m^{-1} at a depth of 3 m (Clementson et al. 2004) . We examine the response of each species to a change in the light field by running the model for varying $\mathrm{K_d}(0.2, 0.6 \text{ and } 1.0\ \mathrm{m}^{-1})$ and compare the model results.

2.3.6 Harvesting

We assess the effect of harvesting algal biomass on the model results for each species. Thinning of crops is a common farming practice that optimizes growth by reducing the limiting effects of self-shading. Harvesting can also be imposed by the economic demand of market supply. In practice *P. umbilicalis* has been traditionally left for an initial phase of five months and then harvested at two weekly intervals, while *U. lactuca* has a lifespan of approximately three months (ElkhornSlough.org 2012) and so must be harvested more regularly. Giant kelp fronds typically have a lifespan of at least six months (North et al. 1986) , whereas *P. umbilicalis* can live at least a whole season (MarLIN 2012).

We define a harvesting scheme as (establishment phase, harvest frequency). The establishment phase is the period that macroalgae is grown before harvesting commences. The harvesting frequency is the time between harvests. 'Harvest amount' is the percentage of total macroalgae in the farm that is taken per harvest. We have constructed 9 schemes (Table 2-1) varying in establishment phase and harvesting frequency. Each scheme incorporates the lifespan of the species being harvested and ensures that there is no harvest interval greater than the maximum age of a frond so that we can discount natural losses due to senescence.

Table 2-1: A harvesting scheme is defined by the establishment period and harvesting frequency. The 3 establishment periods and 3 harvesting frequencies combine to form the 9 schemes we examined.

Scheme	Establishment Period (days)	Harvest frequency (days)
1	30	14
2	30	28
3	30	90
4	60	14
5	60	28
6	60	90
7	90	14
8	90	28
9	90	90

For each scheme the model is run forward until t=establishment phase (est) days. We then remove a fraction H=0.2 (25%) of both $\mathrm{N_f}(\mathrm{t} = \mathrm{est})$ and $\mathrm{N_s}(\mathrm{t} = \mathrm{est})$ and restart the model with new initial conditions,

$$[\mathrm{NH_4}(\mathrm{t} = \mathrm{est}); \mathrm{NO_3}(\mathrm{est});\ (1 - \mathrm{H})\mathrm{N_s}(\mathrm{est}); (1 - \mathrm{H})\mathrm{N_f}(\mathrm{est});\ \mathrm{D}(\mathrm{est})].$$

We repeat this process running the model forward for each harvesting (har.) period and removing the same proportion of $\mathrm{N_f}$ and $\mathrm{N_s}$ until the end of the season. The accumulated total of removed $\mathrm{N_f} + \mathrm{N_s}$ is added to the end of season amount of $\mathrm{N_f} + \mathrm{N_s}$ to give a total N for each scheme. We repeat the simulation for H=0.5 i.e. a 50% removal rate.

The simulations for *M. pyrifera* are conducted so that the plants are thinned with no reduction in height (and height is constant for the other species). Model runs are conducted for each species at the reference values.

2.4. Simulation Results

All state variables are presented in terms of mass per area rather than mass per volume for easier interpretation of the results. We define the following terms used in this section: Fixed N = $\mathrm{N_f} * \mathrm{h_{MA}}\ (\mathrm{mg\ N\ m^{-2}})$; Stored N = $\mathrm{N_s} * \mathrm{h_{MA}}\ (\mathrm{mg\ N\ m^{-2}})$; and Total N removed = Fixed N + Stored N which is the total amount of nitrogen removed by the macroalgae per unit area of the macroalgal farm.

2.4.1 General Behavior

We completed a reference run (outlined in section 2.3.1) for each species. From the model results we calculated the daily accumulated N per unit area of macroalgae farm input from the salmon aquaculture activity as Accumulated N = $\mathrm{N_{farm}tz}\ (\mathrm{mg\ N\ m^{-2}})$. We then compared Total N removed, Accumulated N and the difference (Accumulated N – Total N removed) for each species (Figure 2-3). These results show the bioremediative capacity of each species at a reference site by directly comparing the amount of N put into the system by aquaculture with the amount removed by the macroalgae. This shows that *M. pyrifera* is able to significantly impact the DIN from mid summer (Feb.) After April the bioremediated input from the salmon farm no longer accumulates but instead reduces, eventually becoming approximately constant (Figure 2-3; dotted line) because the growth of the macroalgae is matching the input from the salmon farm (Figure 2-3; solid line). End of season values for the Accumulated N and Accumulated N – Total N (Figure 2-3; dashed versus dotted lines) indicate that *M. pyrifera* has removed approximately 75% of the salmon farm output of DIN. Using the same comparison, *U. lactuca* and *P. umbilicalis* remove only approximately 5% each.

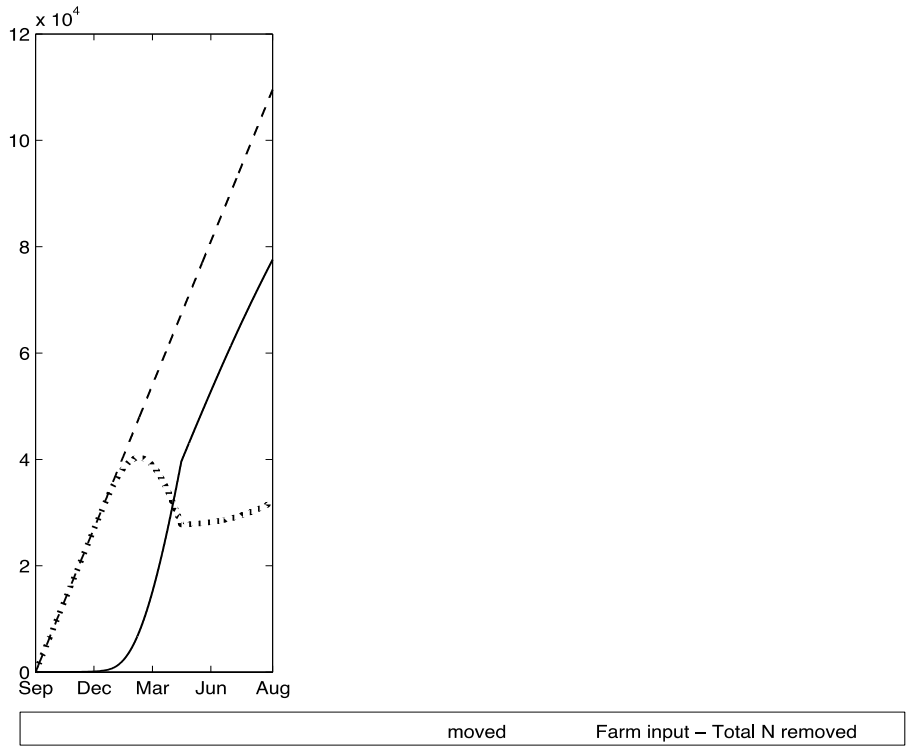

Figure 2-3: The bioremediation of N_{farm} for each species per m^2 of the macroalgae farm. The dashed line shows the farm input over a season per m^2. The solid line shows the total N removed by macroalgae per m^2 and the dotted line is the net N input into the system, i.e. farm input – total N removed by macroalgae. We multiplied $\mathrm{N_{farm}}$ by the water depth (z) to calculate the salmon load per m^2. Similarly we multiplied $(\mathrm{N_f} + \mathrm{N_s})$ by the instantaneous height of the macroalgae ($\mathrm{h_{MA}}$) to calculate the total N.

If farm loads are increased all three species eventually reach steady state (for all loads) after 10 years (Figure 2-4). In the nutrient limited cases when $\mathrm{N_{farm}} = 50$ (solid line) and $100\ \mathrm{mg\ N\ m^{-3} d^{-1}}$ (dashed line) respectively, a doubling in farm load results in a doubling of end of season yield of Fixed N. The trajectories of Fixed N are similar for *U. lactuca* and *P. umbilicalis*, including similar final steady state values at all rates of farm input. The final Fixed N for the *M. pyrifera* is an order of magnitude (x10) larger than those obtained by the smaller species at the lower loads, and double that of the other two species at the highest value of farm load. In the nutrient replete system (dotted line), model results gave the maximum end of season biomass for each species as: *M. pyrifera* ~ 86–94 $\mathrm{kg\ ww\ m^{-2}}$; *P. umbilicalis* ~ 23-26 $\mathrm{kg\ ww\ m^{-2}}$ and *U. lactuca* ~ 24-27 $\mathrm{kg\ ww\ m^{-2}}$.

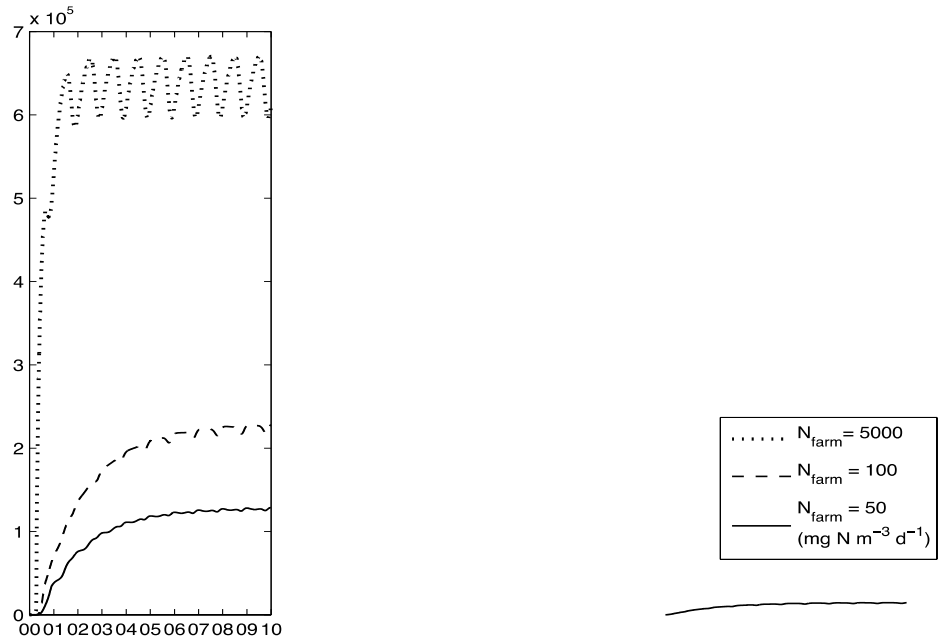

Figure 2-4: The steady state of fixed N as we increase the value of $\mathrm{N_{farm}}$. We multiply $\mathrm{N_f}$ by the instantaneous macroalgae height ($\mathrm{h_{MA}}$) to calculate fixed N for each species per $\mathrm{m^2}$. Only the value of $\mathrm{N_{farm}}$ is changed between model runs, and all other environmental forcing is kept at the reference level. Growth is eventually limited by the amount of N in the system for the two lower values of $\mathrm{N_{farm}}$. At $\mathrm{N_{farm}} = 5000\ \mathrm{mg\ N\ m^{-3}\ d^{-1}}$ we are simulating a nutrient replete system where growth is eventually limited by light for all three species.

2.4.2 Model validation

The Specific Growth Rates (SGR) predicted by the model (Table 2-2) are similar to the results reported for each species from empirical experiments. The experiments with *P. umbilicalis* and *M. pyrifera* were conducted around fish farms while the empirical work measuring growth of *U. lactuca* was conducted in tanks using effluent from fish (Neori et al. 1991) and abalone (Robertson-Andersson et al 2008) culture respectively.

Table 2-2: Comparison of the growth rates as determined by the model result with that for the same species evaluated in a field based IMTA experiment. All the studies in table 2 define Specific Growth Rate as $\mathrm{SGR} = 100 * \ln(\mathrm{w_t} - \mathrm{w_o})/\mathrm{t}$, where $\mathrm{w_t}$, $\mathrm{w_0}$ are the weight of algae at time t and 0 respectively and t is the growing period.

Species	DIN $\boldsymbol{\mu M}$	SGR % ($\mathbf{g\ ww\ d^{-1}}$)	Study
M. pyrifera	0.08-30	6 (t = 9 months)	(Buschmann et al., 2008)
M. pyrifera	10-13	4	This study
U. lactuca	10 - 78	7.4-17.9 (t = 2 weeks)	(Neori et al. 1991)
U. lactuca	5.0	1.6-6.3 (t = 2 weeks)	(Robertson-Andersson et al., 2008)
U. lactuca	10 - 13	7	This Study
P. umbilicalis	150	13.1 (t = 4 weeks)	(Carmona et al., 2006)
P. umbilicalis	150	16	This study

2.4.3 Sensitivity analysis

The model is relatively insensitive to the range of parameter values defining *U. lactuca* and *P. umbilicalis* (Table 2-3). For *M. pyrifera* the model shows mild sensitivity to the parameters Q_{min}, I_s and K_c. Two of these are related to the internal storage capacity of *M. pyrifera* whilst the saturation constant dictates sensitivity to photoinhibition.

Table 2-3: Sensitivity analysis results are based on a comparison of the end of season total of N_f using Eq. 9. We show the 5 most sensitive parameters for each species where an absolute value of 0.3 is determined as the threshold for the model to be sensitive to the parameter. A negative value means total N_f decreases as the parameter increases.

M. pyrifera		*U. lactuca*		*P. umbilicalis*	
Parameter	Sensitivity	Parameter	Sensitivity	Parameter	Sensitivity
Q_{min}	-0.82	d_M	-0.24	d_M	-0.23
I_s	0.53	r_L	0.11	Q_{min}	-0.18
K_c	0.44	Q_{min}	-0.10	r_L	0.10
K_d	0.29	T_0	-0.05	$\mathbf{V_{NH_4}}$	0.09
d_M	-0.25	μ	0.05	μ	0.07

2.4.4 Flow Rate

At the lower flow rate *M. pyrifera* and *P. umbilicalis* achieve consistently higher remediation over the whole season than that achieved at the higher flow (Figure 2-5). This difference is greater for *P. umbilicalis* particularly at the end of the season where total N for *M. pyrifera* appears to converge for both values of λ_R. For *U. lactuca,* initially total N increases at a faster rate in low flow conditions (compared with higher flow) but this rate slows and crosses the trajectory for total N under the higher flow conditions about mid season, then continues at a lower rate until the end of the season. Bioremediation capacity is slightly increased for *U. lactuca* under higher flow conditions.

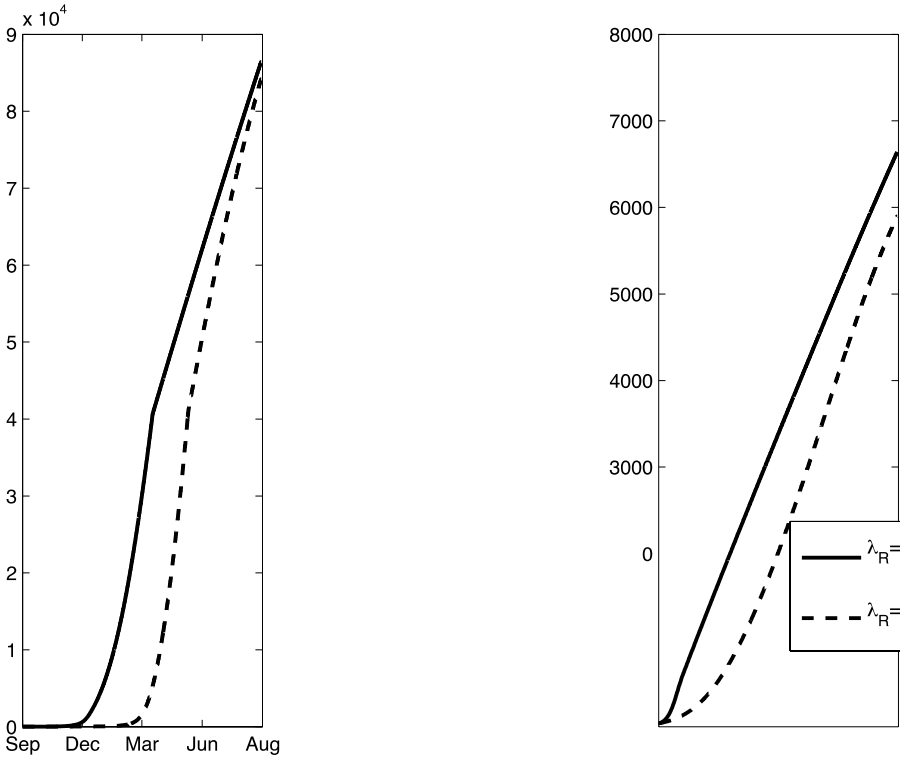

Figure 2-5: Total N (=$(N_s + N_f)h_{MA}$) removal by per m^2 by each species for two values of the refresh rate. By setting $\lambda_R = 0.05\ d^{-1}$ (solid line) we are simulating growth in low flow conditions. Setting $\lambda_R = 1.0\ d^{-1}$ (a 20 fold increase in net flow) simulates higher flow conditions. All other environmental forcing is kept at the reference level.

2.4.5 Optical Depth

Under low light, photosynthetic growth (fixed N) is less for *U. lactuca* and *P. umbilicalis* (Figure 2-6) and growth strictly increases as light increases. For *M. pyrifera* photosynthetic growth is lowest when the light is highest. This species also has the highest growth at the mid-range of the optical depths examined. As the photosynthetic growth decreases, stored N increases for all three species. The net effect of this is an unchanged bioremediation capacity (total N) for both *U. lactuca* and *P. umbilicalis* across all optical depths examined. The bioremediation capacity of *M. pyrifera* is lowest in highest light and greatest at the mid-range.

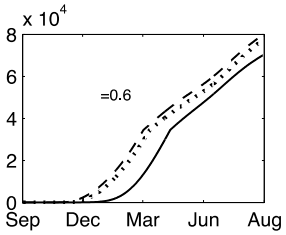

Figure 2-6: Fixed N, Stored N and Total N for each species at increasing values of the light attenuation coefficient K_d. The increase in K_D simulates increasing turbidity in the water column. Environmental forcing was kept at the reference level with only k_D varying.

2.4.6 Harvesting

The results for all three species (Figure 2-7) show that, compared with non-harvested crops, schemes with an establishment phase of 30 days result in a decrease in bioremediation (total N); 60 days results in an approximate doubling of bioremediation; and 90 days results in the greatest increase in bioremediation, but which varied greatly depending on harvest frequency. Across all schemes total N increased with establishment phase and decreased with harvesting frequency. As the percentage removed (H) increased, total N removed increased for schemes with establishment phases of 90 days, but in the other schemes the effect was negligible. For all macroalgae, schemes with a 90-day establishment period resulted in a 5-25 fold increase in bioremediation dependent on both harvesting frequency and H.

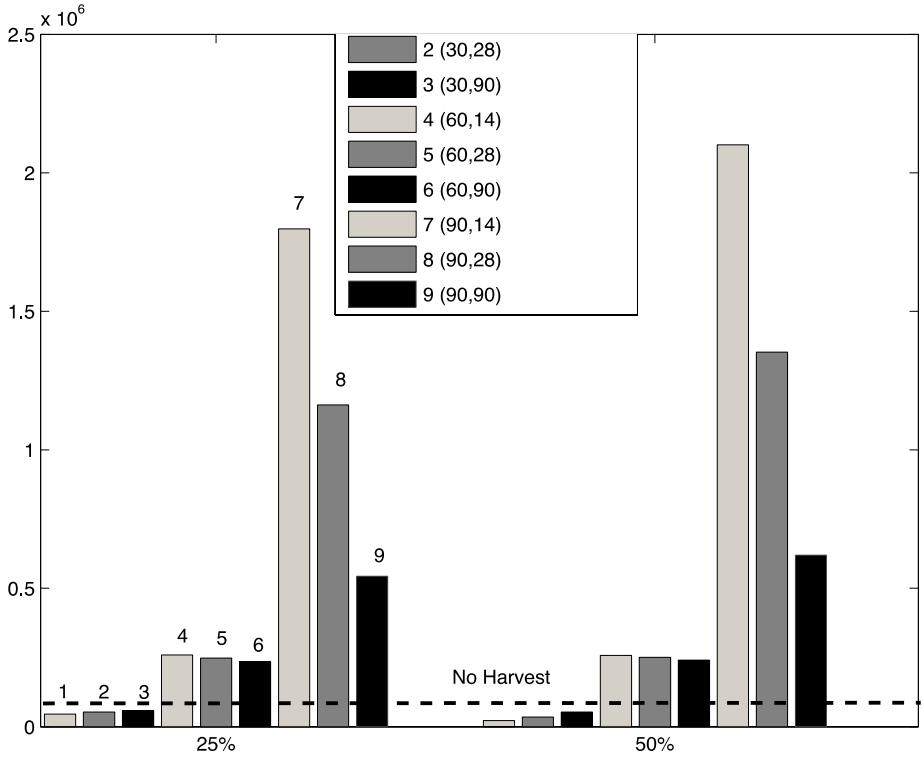
x 10^6
2.5
2
1.5
1
0.5
0
2 (30,28)
3 (30,90)
4 (60,14)
5 (60,28)
6 (60,90)
7 (90,14)
8 (90,28)
9 (90,90)
1
2
3
4
5
6
7
8
9
No Harvest
25%
50%

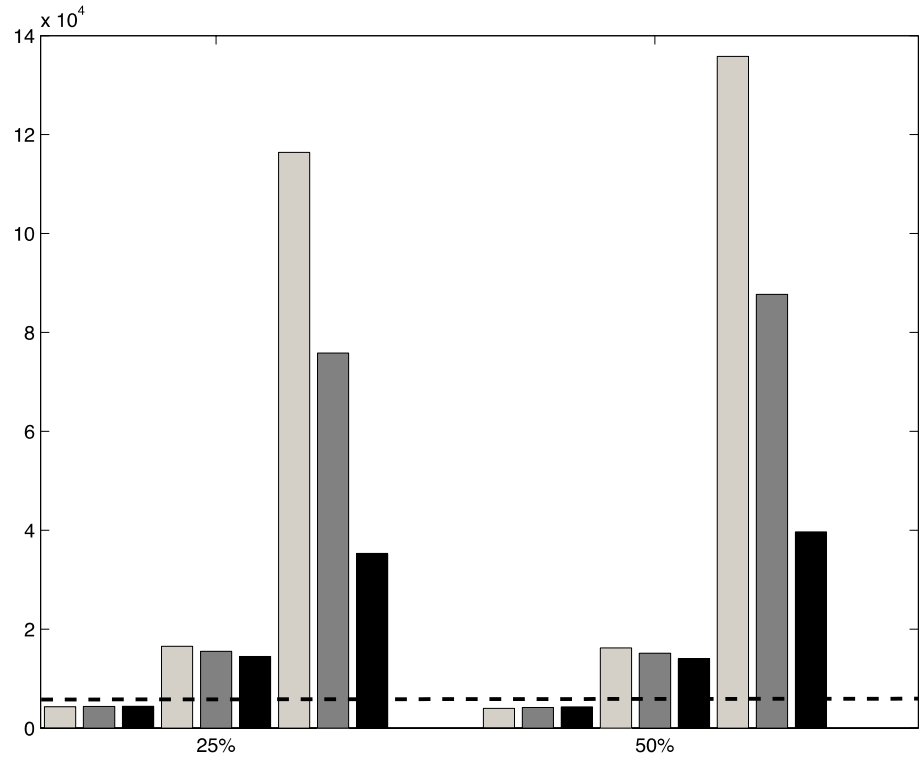
x 10^4
14
12
10
8
6
4
2
0
25%
50%

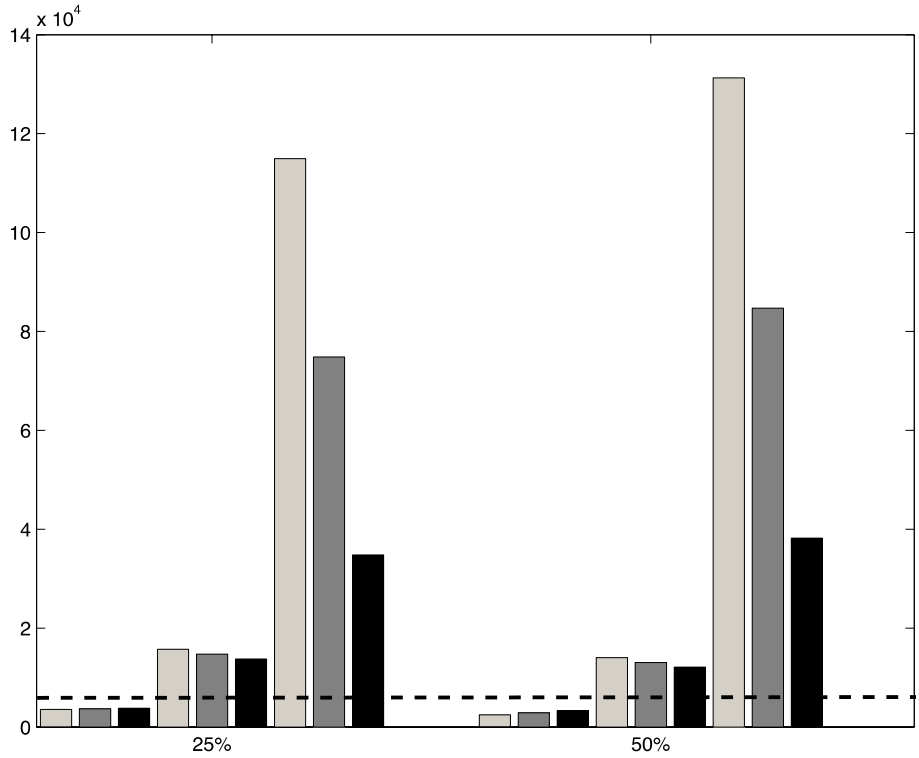

Figure 2-7: Total N removed by each species. The total N removed is calculated for each harvesting scheme 1-9 with at first 25% removed per harvest and then 50%.

2.5 Discussion

2.5.1 General model behavior

An aim of the study was to quantify the bioremediation potential of three macroalgae species within the context of a modeling approach. The model indicates conclusively that of our three species *M. pyrifera* is the most effective at removing the ammonia in a near field i.e.75% of farm load, whereas the two smaller species remove only 5% each. However, beginning the simulation in September, it took until March for *M. pyrifera* to better the removal rates of the other algae. Although we did not simulate phytoplankton in this study, in the natural environment phytoplankton may remove the DIN before *M. pyrifera* is able to, thus reducing its growth and therefore its height and bioremediation capacity. Growing *M. pyrifera* earlier in the season may be an option as they may be at the height required to remove adequate quantities of DIN before phytoplankton become active (spring/summer). However the light climate may not be adequate to achieve the growth rate required in which case growing kelps over consecutive seasons would seem a sensible solution. An obvious conclusion is that, in the near field case, the height of macroalgae is a critical factor in its bioremediation potential. It may be possible to grow several of the smaller species on vertical lines to increase their vertical distribution.

Macroalgae growth reaches steady state due to nutrient limitation when $Q \sim Q_{min}$ at which point $N_s \sim 0$, i.e. stored nitrogen is close to 0. Theoretically macroalgae could be grown in the long term around a constant N source and after a period (10 years in this case) it would match its growth exactly to the input source to achieve a system in equilibrium (although this does not take into account environmental losses, changes in seasonal cycle and natural senescence). In the case of light limitation the algae could not grow past a maximum biomass and its bioremediation capacity would have reached its upper limit. In this experiment the simulated final biomass for all three species due to light limitation is; *M. pyrifera* ~ 86–94 $kg\ dw\ m^{-2}$; *P. umbilicalis* ~ 24-27 $kg\ dw\ m^{-2}$ and *U. lactuca* ~ 23-26 $kg\ dw\ m^{-2}$. *U. lactuca* grown in a land-based IMTA facility demonstrated a production potential of 4.5 $kg\ dw\ m^{-2}$ (Bruhn et al. 2011) . It is therefore plausible that *U. lactuca* could reach the concentration found in this study before self-shading stops growth entirely. Although we have not found similar empirical results for our other two species, we interpret the results for *U. lactuca* as partial validation for the light component of the model.

2.5.2 Model validation

Similar formulations of the model used in this study have previously been validated against observation for different species of macroalgae (Aldridge and Trimmer 2009; Solidoro 1997). The results of our validation were conclusive in predicting growth rates achieved in field IMTA experiments for the species studied here. The model (eqns. 2-3 to 2-7) has been partially validated using a fitness for purpose criteria (Rykiel 1995).

2.5.3 Sensitivity Analysis

The sensitivity analysis showed the model is not sensitive to parameter values in the range describing *U. lactuca* and *P. umbilicalis*. Our three species in effect represent a large perturbation of the parameter space and it is encouraging to note that the model is not unduly sensitive across this perturbation which is evidenced by the fact that end of season N_f were similar across all species for each value of farm loading investigated. The model for *M. pyrifera* showed the greatest sensitivity to parameter perturbations, where Q_{min}, I_s and K_c all showed sensitivities above the 0.3 threshold (section 2.3.3). Firstly the growth model had a slightly different formulation for *M. pyrifera,* where the h_{MA} varied. *M. pyrifera* has the lowest nitrogen storage capacity of the 3 species, and decreasing this capacity further decreases growth. Increasing K_c increases growth rate by allowing the macroalgae to fix a greater proportion of internal nitrogen before its growth is satiated. *M. pyrifera* is sensitive to photoinhibition in the field (Buschmann et al., 2008) and increasing I_s reduces this effect, i.e. increases growth rate. Overall the model is not unduly sensitive however it is important to make parameters as realistic as possible to constrain model output to reasonable values.

2.5.4 Flow rate

The uptake of DIN into the macroalgae is modeled as dependent on biomass concentration (Eqns. 2-3 & 2-4). As λ_R increases so too does the rate at which N_{farm} is flushed out of the macroalgae farm. Conversely the farm volume is being replenished by

external DIN at an increasing rate. The net effect on bioremediation resulting from the increase in refresh rate is an end of season increase in total N for *U. lactuca* and decrease for the other two species. Of the species investigated, *U. lactuca* has the highest growth rate and is able to reach the biomass required to remove DIN at a rate that enables it to surpass the growth rate at the lower flow regime. Al-Hafedh et al. (2014) found that increasing the rate of effluent flow increased biomass yield for *U. lactuca* and that flow rate was more important in this regard than stocking density.

Although *M. pyrifera* and *P. umbilicalis* showed reduced bioremediation capacity, as flow rate increased after March total N increased faster under higher flow for both. This may be due to the seasonal increase in background DIN. Although maximum growth rate is important in achieving the biomass required to remove the DIN under higher flow, it is not the only element important in optimizing DIN removal in the model. *P. umbilicalis* has a higher maximum growth rate (μ) than *M. pyrifera,* however the latter species was less sensitive to the change in flow when comparing end of season total N. The reason for this may be in the uptake term in (2-3). Here uptake depends partly on the ratio of algal height to water depth $\mathrm{h_{MA}/z}$. For *M. pyrifera* this term is always increasing, however in general there will eventually be a limit to how fast the flow can be before DIN is washed away before the algae can take it up. Hepburn et al. (2007) found that *M. pyrifera* had greater growth rates at wave exposed sites than at sheltered sites. Faster flow can reduce the boundary layer around the macroalgae blades increasing the uptake (Wheeler 1980), although our model does not explicitly model DIN uptake dependent on boundary layer dynamics. Future models may need to incorporate a mechanistic term relating flow and uptake to further understand this dynamic.

2.5.5 Optical depth

For both *U. lactuca* and *P. umbilicalis* an increase in light attenuation resulted in reduced growth rate from April (autumn) through to August (late winter). This result is more pronounced for *P. umbilicalis. M. pyrifera* showed highest growth at $\mathrm{K_d} = 0.6\ \mathrm{m^{-1}}$ and lowest at $\mathrm{K_d} = 0.2\ \mathrm{m^{-1}}$, which we interpret to indicate photoinhibition limiting growth when light attenuation is low. *M. pyrifera* has the lowest saturation point $(\mathrm{I_s})$ of our three species. If the value of $\mathrm{I_s}$ for *M. pyrifera* is increased to that of *U. lactuca* then it displays the same relationship between optical depth and growth as do the two smaller species (results not shown; $\mathrm{I_s}$ is the parameter that determines the magnitude of photoinhibition on macroalgal growth). The results at the high to mid range of optical depth for *M. pyrifera* imply that although optical depth may reduce photoinhibition there is a point when light levels become too low and growth is reduced. As *M. pyrifera* was allowed to increase its height, in summer where it would be close to the surface the potential for photoinhibition should increase. However the resultant increase in biomass should act to counter this effect through self-shading. *M. pyrifera* has been shown to be particularly susceptible to photoinhibition, particularly at midday, when cultivated near fish farms in Chile in spring and summer (Buschmann et al. 2008). Broch et al (2011) found cultivation depth did not greatly influence seasonal biomass for the species *S. latissima* in a similar modeling

approach, however they used a K_d = 0.07 m^{-1} which was considerably lower than the range of attenuation coefficients used here.

As fixed nitrogen increased/decreased for each species, so stored nitrogen decreased/increased for each of our optical depth experiments. The combined effect of this meant that for *U. lactuca* and *P. umbilicalis* the total remediated nitrogen was the same at all three optical depths. This implies that the algae with lower biomass may have higher stored N content. Broch et al. (2011) use a more complex formulation for internal nutrient composition in their macroalgae model, using the internal reserves of carbon and nitrogen to dynamically determine the stoichiometric ratio of carbon to nitrogen which yielded more realistic (and perhaps more interpretable) results. Nonetheless our simpler formulation based on Solidoro et al. (1997) is sufficient to show that the relationship between N storage and fixation will both influence the cultivation strategy for IMTA as well as having clear economic implications.

2.5.6 Harvesting

The establishment phase appears crucial to a successful harvesting scheme. All three algae possess a high maximal growth rate (μ) and so are able to fix N very efficiently. The key to successful bioremediation in the early stages of growth is for each species to achieve a biomass capable of removing DIN in sufficient quantities to fuel their high demands. Eventually the biomass achieves a density where light and nutrient limitation act to reduce their growth rate considerably. At this point harvesting frequency becomes important as this reduces the limiting effect and thus stimulates higher growth rates. This is why total N reduced with harvesting frequency for schemes with a 30 day establishment phase but increased with harvesting frequency for those with 60 and 90 day establishment phases. This could also explain the variability in the results for H=0.25 and H=0.5. In their simple model for seaweed growth, Lee and Ang (1991) found the optimal harvest strategy had the same period as the macroalgal growth and mortality terms. We note however that unlike our system, their model treats harvesting as continuous and not a discrete process, and that it does not include DIN uptake as stored N, while it does show the importance of incorporating growth rate variability with harvesting strategies.

Harvesting strategies from other studies have focused on the sustainability and/or reduction of natural populations of macroalgae and so a direct comparison with our findings is not appropriate. Kelp harvesting is also done in practice by reducing the height of the kelp and not by thinning of the plants, as was the case in our simulation. We decided on this strategy because we consider plant height to be a vital component of bioremediation. We acknowledge that in deciding on a harvesting strategy there are many other elements to consider, including market demand, cost of harvesting, price etc. (Troell et al. 2009). In addition we have not considered diurnal effects on growth/uptake rates, and this may influence the time of day for harvest. In an IMTA arrangement, the diurnal profile of ammonium discharge from the salmon may affect the ambient nutrient concentrations, which in turn may also have a significant impact on harvest strategy.

2.5.7 Improvements to the model

Macroalgal communities in Nature can fluctuate between high and low standing biomass due to factors such as grazing pressure, hydrodynamic losses, other seasonal forcing or natural senescence. Our macroalgae model does not simulate a steady state biomass subject to long term population dynamics but an increasing biomass grown under optimal conditions. Of the modifying factors just mentioned, mechanical and grazing losses could theoretically be controlled, or at least better understood, in a farming context.
Natural senescence has an unavoidable effect on macroalgae losses. A recent model for age related senescence of *M. pyrifera* fronds (Rodriguez et al. 2013) showed that progressive senescence accounted for 73% of the variation in biomass between kelp communities. Incorporating a mortality term based on natural senescence may form part of a more realistic model and also aid in the search of an optimal harvesting scheme.

We have used the formulation of Solidoro et al (1997) for growth dependent on the internal nitrogen quota Q. We believe this formulation was appropriate for application in this study. However this model does not incorporate carbon uptake dynamics, which are important in representing the internal macroalgae dynamics that determine N fixation. Formulations similar to those presented by Broch et al (2013) would be necessary to more accurately represent growth dynamics and seasonal biomass estimates. In a future study we intend to include our model in a fully coupled 3D hydrodynamic, biogeochemical and sediment model of the region to examine the growth dynamics of our species in a more realistic environment that includes competition with phytoplankton and sporadic access to nutrients.

2.5.8 Conclusion

This study shows that IMTA offers a flexible solution to bioremediation of the nutrients input into an ecosystem from finfish aquaculture. We have shown that in a near field scenario, of the three species we considered only the giant kelp, *M. pyrifera*, offers reasonable bioremediation of salmon farm ammonium in the absence of harvesting. Increasing water flow reduced total N removal by *M. pyrifera* (marginally) and *P. umbilicalis* over a season, whilst total N removal for *U. lactuca* increased with water flow. Increasing optical depth increased the total N removed by *M. pyrifera* at low to moderate optical depths but had no effect on total N removed by *U. lactuca* and *P. umbilicalis.* Harvesting had a positive effect on total N removal by all three species when harvesting commenced after 60 days. Greatest removal occurred when harvesting began after 90 days with an interval of two weeks thereafter, and there was a minor improvement if 50% of the biomass was removed per harvest instead of 25%. Optimal harvesting resulted in a 20-25 fold increase in bioremediation capacity across our three species.

Appendix 2-A

Table 2-A1: Biological intermediate processes.

Symbol		Description	Formula	Unit
$f(N, Q)$	2- A1	Uptake of external N source into internal reserve.	$\frac{V_M N}{K_{1/2}+N}\ \frac{Q_{max}-Q}{Q_{max}-Q_{min}}$	$mg\ N\ g^{-1}\ dw\ d^{-1}$
$\mu g(E, Q, T)$	2-A2	Growth function for macroalgae.	$\mu g(E)g(Q)g(T)$	d^{-1}
$g(E)$	2-A3	Growth limitation due to light.	$\frac{e}{K*h}\left(e^{-\frac{E_z e^{-Kh}}{I_s}}-e^{\frac{E_z}{I_s}}\right)$	Dimensionless
$g(T)$	2-A4	Growth limitation due to temperature.	$\frac{1}{1+\exp(-(T-T_0)/T_r)}$	Dimensionless
$g(Q)$	2-A5	Growth limitation due to internal nutrient reserves.	$\frac{Q-Q_{min}}{Q-k_c}$	Dimensionless
E_z	2-A6	Irradiance at top of macroalgal canopy.	$E_0 e^{-Kz}$	$\mu mol\ photons\ m^{-2}\ s^{-1}$
K	2-A7	Extinction rate of light due to water and algae.	$K_d + K_{MA}$	m^{-1}
K_{MA}	2-A8	Extinction rate of light due to algae.	$N_f a_{cs}(\max\left(\frac{h}{z},1\right))(\min(h,z)^{-1})$	m^{-1}
B	2-A9	Biomass of dry macroalgae.	$N_f {Q_{min}}^{-1}$	$g\ dw\ m^{-3}$
Q	2-A10	Internal nutrient quota of macroalgae	$Q_{min}\left(1+N_s {N_f}^{-1}\right)$	$mg\ N\ g^{-1}\ dw$
h_{MA}	2-A11	Height of *Macrocystis*	$(0.00174 N_f/\text{num\_fronds})^{1.047}$	m

Table 2-A2: Parameters for the macroalgal growth model

Symbol	Description	Units	Macrocystis	Ulva	Porphyra
μ	Max. Growth Rate	d^{-1}	0.2 [1]	0.45 [6]	0.33 [10]
V_{NH_4}	Max. Uptake Rate (Amm.)	$mg\ N\ g^{-1}\ dw\ d^{-1}$	8.0 [2]	124.0 [6]	60.0 [11]
V_{NO_3}	Max. Uptake Rate (Nit.)	$mg\ N\ g^{-1}\ dw\ d^{-1}$	10.3 [3]	39.0 [6]	25.0 [12]
K_{NH_4}	Half Sat. Const. (Amm.)	$mg\ N\ m^{-3}$	74.2 [2]	700.0 [6]	700.0 [12]
K_{NO_3}	Half Sat. Const. (Nit.)	$mg\ N\ m^{-3}$	182.0 [3]	70.0 [6]	300.0 [12]
Q_{max}	Max. Internal Nitrogen	$mg\ N\ g^{-1}\ dw$	25.0 [1]	42.0 [6]	70.0 [13]
Q_{min}	Min. internal Nitrogen	$mg\ N\ g^{-1}\ dw$	7.0 [4]	13.0 [6]	14.0 [10]
K_c	Half Growth Const.	$mg\ N\ g^{-1}\ dw$	6.0 [5]	7.0 [6]	7.0 [10]
T_0	Optimal Temp.	°C	12.0 [6]	12.0 [6]	12.0 [6]
T_r	Range of Optimal Temp.	°C	1.0 [6]	1.0 [6]	1.0 [6]
I_S	Saturation Irradiance	$\mu mol\ photons\ m^{-2}\ s^{-1}$	134.0 [7]	200.0 [6]	277.0 [13]
a_{cs}	Nitrogen Specific Shading	$m^2\ mg^{-1}\ N$	0.0001 [8]	0.00033 [9]	0.00036 [14]
d_m	Mortality Rate	d^{-1}	0.003 [9]	0.003 [9]	0.003 [9]
h_{MA}	Height of U. lactuca, P. umbilicalis	m	-	0.2 [9]	0.2 [9]
num_fronds	Number of Fronds	Dimensionless	7.0 [15]	-	-
r_L	Remineralisation Rate	d^{-1}	0.2 [16]	0.2 [16]	0.2 [16]
r_N	Nitrification rate	d^{-1}	0.1 [16]	0.1 [16]	0.1 [16]
λ_R	Refresh rate	d^{-1}	0.25 [15]	0.25 [15]	0.25 [15]
K_d	Light attenuation coefficient	m^{-1}	0.1 [16]	0.1 [16]	0.1 [16]

Source: [1]Zimmerman and Kremer (1984) [2]Haines and Wheeler (1978) [3] Gerard (1982) [4]Lobban and Harrison (1994) [5]Carmona et al. (2001) [6]Solidoro et al (1997) [7]Buschmann et al. (2008) [8]Enriquez et al. (1994) [9]Trancoso et al. (2005) [10]Hafting (1999) [11]Johansson (2002) [12]Pedersen et al. (2004) [13]Carmona et al. (2006) and Pedersen et al. (2004) [14]Markager and Sand-Jensen (1996) [15] Calibration [16]Wild-Allen et al. (2010)

CHAPTER 3

A BAYESIAN APPROACH TO ACCOUNT FOR MULTIPLE SOURCES OF UNCERTAINTY IN A MACROALGAE BASED INTEGRATED MULTITROPHIC AQUACULTURE MODEL

Preface: Adequately quantifying uncertainty in a model output is fundamental to the inference that can be made from the results. In this chapter a powerful Bayesian inference tool is applied to the original IMTA model. The model was recast in stochastic form by allowing some sub-processes to vary in time; expressing uncertainty in these model processes. Probability distributions replaced constant values for each parameter; expressing uncertainty in the parameters. Uncertainty in the model output was quantified by running the stochastic model with parameter priors.

Observations from an IMTA experiment were introduced to reduce the uncertainty in the model output. This resulted in a shift of some parameters away from their prior values. The method used here not only allows both quantification and reduction of model uncertainty but also provides a method of using data to inform our understanding of the model.

At the time of thesis submission, this work was submitted to a refereed journal and was subsequently accepted with minor revisions on 25th August 2015. It is presented below in the submitted form. The intended citation for the original publication is:

Hadley S, Jones E, Wild-Allen K, Johnson CJ, Macleod CK (2015) A Bayesian inference approach to account for multiple sources of uncertainty in a macroalgae based integrated multi-trophic aquaculture model. Submitted to Env Mod Soft, accepted with minor revision 25/8/2015.

Abstract

A Bayesian inference method was employed to quantify uncertainty in an Integrated Multi-Trophic Aquaculture (IMTA) model. In addition, a more realistic set of model parameters was sought through the conditioning of posterior distributions on empirical data. This enabled reformulating a deterministic biogeochemical IMTA model within a Bayesian Hierarchical Modeling (BHM) framework. Unresolved time varying processes were modelled using first order auto-regressive processes which yield a stochastic process model to represent model uncertainty. Uncertainty in the model parameters was formally accounted for using "prior" distributions. Empirical observations of the height and weight of *M. pyrifera* (kelp) grown around salmon pens in southern Chile were assimilated into the BHM using a Sequential Monte Carlo method implemented within the LibBi package (www.libbi.org). Three data sets corresponding to high, medium and low seeding densities of kelp sporelings on a long-line placed near the salmon pens were used. The observational data were assimilated into the model, which reduced the uncertainty considerably when compared with the non-assimilating runs. The results showed that each of the data sets constrained the model solutions for both the observed variables of height and weight as well the unobserved state variables of ammonium, nitrate, and fixed and stored nitrogen. Learning based on a comparison between the prior and posterior marginal distributions was observed for a subset of model parameters, which varied with seeding density. To estimate the degree of learning from the observations, the Kullback-Liebler (KL) divergence metric was estimated. By assimilating the observations, the reduction in uncertainty of the state and parameters was approximately 90%. Bivariate parameter interactions were used to display learning not observed in the marginal plots. Density dependent information carried in the observations informed the model, consistent with our understanding of the underlying processes for macroalgal growth. Results from this study suggest that a low (3 sporelings per metre) to medium (6 sporelings per metre) seeding density results in the most efficient removal of excess nutrients in this simple system.

3.1 Introduction

The environmental, economic and social implications of ecosystem disturbances generated by the aquaculture industry have been widely reported (Buschmann et al. 2009). Integrated Multi-Trophic Aquaculture (IMTA) (Troell et al. 2009) involves joint farming of a 'primary' species together with other species that take up 'waste' (e.g. nutrients, particulates) produced in the farming process. This integrated approach provides both a method of removing problematic waste, as well as offering potential economic benefits through the cultivation of a new crop. Because empirical investigations to quantify the effectiveness of IMTA are expensive, and the results do not necessarily extrapolate to full-scale operations given inherent non-linearity in the scaling of these systems (Hadley et al. 2015), modelling studies emerge as a particularly useful approach to investigate the potential of IMTA. In order to validate model output some of the modelling investigations of IMTA have incorporated results from concurrently run empirical growth experiments (Broch

et al. 2013) or compared results with those from existing IMTA operations (Ren et al. 2012). However data assimilation methods, which improve model parameterisation and constrain model output to observed values and thereby reduce model uncertainty, have not yet been included in the modelling process.

Data assimilation provides a robust statistical method to combine information from numerical models and observations in the presence of model error and sparse observations (Wikle et al. 2013). Deterministic biogeochemical (BGC) models are typically assessed against empirical data, and many are highly parameterised with a degree of uncertainty surrounding parameter values due to varying results from field-based studies (Planque et al. 2014). Furthermore, while the parameters in a deterministic model are constants they in fact often represent processes that in reality vary in time. It follows that useful quantification of model uncertainty provides an envelope of confidence around the model solution, and statistical methods have been developed recently that use observations to objectively reduce model uncertainty (e.g. Parslow et al. 2013 and Dowd et al. 2014). This is critical to models such as those used for IMTA, where the results can influence decisions such as whether to undertake expensive full-scale farming operations. Simply perturbing parameters through a range of possible values may lead to wildly divergent solutions in a non-linear deterministic model. However, by capitalising on data assimilation methodology, observations from empirical experiments can be used to objectively quantify and constrain both model parameters and solutions (Jones et al, 2012; Parslow et al, 2013). Recent advances in statistical methodology and computing allow for the problem to be cast in the Bayesian Hierarchical Modelling (BHM) framework (Cressie and Wikle 2011), which allows samples of parameters and state variables to be drawn from the posterior distribution that is conditioned on the empirical data.

The use of BHMs (Dowd et al. 2014; Parslow et al. 2013; Jones et al. 2010) is a method currently attracting interest due to its treatment of model uncertainty. A BHM is constructed from a state space model (SSM) through a process of reformulating the SSM so that the three main areas of model uncertainty, i.e. observations, process and parameters, can be treated individually. In this approach the deterministic BGC model is stochasticised by identifying the time-varying processes in the model and representing them by a random process rather than a constant parameter. In their study, Parslow et al. (2013) replaced a constant parameter representing phytoplankton community structure in a deterministic NPZD model with an autoregressive process. This both captured the observed natural variability seen in phytoplankton communities despite that in general the underlying process for this variation is not well understood.

To account for uncertainty in the remaining parameters, constant values are replaced by probability distributions. Finally a data model is constructed from field-based observations. The newly formed process, parameter and data models combine to make the BHM. Once in this format, Bayesian inference techniques are employed to exploit the conditional dependencies between the sub-models to enable a reduction in parameter and process uncertainty. To solve these complex systems, powerful computational techniques are required.

This reformulation into statistical-biophysical models combined with the advancements in distributed node (cluster) architecture supercomputers, has lead to powerful new computational techniques that solve complex model systems in a meaningful way. The particle filter Markov Chain Monte-Carlo (pMCMC) (Andrieu et al. 2010) method uses samples from the posterior to calculate a joint distribution of parameter and state. Using a pMCMC approach Parslow et al. (2013) showed learning in parameter space and also that the state variables can be considerably constrained when conditioned on observation. In general this approach can be applied to a range of problems in biogeochemical modelling.

In this study an IMTA approach was employed to examine the capacity of giant kelp (*Macrocystis pyrifera*) to take up excess nitrate released from finfish aquaculture farms. The overall aims of the work are to:

- Reformulate a macroalgae based IMTA (Hadley et al. 2015) model into a BHM and use the method of Parslow et al. (2013) to introduce stochasticity into some of the sub-processes and represent the other parameters using probability distribution functions.
- Use a pMCMC (LibBI) (www.libbi.org) approach to solve this system using observational results taken from a field based IMTA experiment.
- Analyse the posterior distribution to identify the potential of this approach to constrain the model output based on a set of observed data, and to determine the extent to which parameter learning occurs.

3.2 Methods

3.2.1 Governing equations for IMTA model

To simulate the growth of *M. pyrifera* in a near-field arrangement of IMTA we use the model developed by Hadley et al. (2015). It is assumed that nitrogen (N) is the limiting nutrient, and therefore all equations have a common currency of N and are locally mass conserving. The governing equations for the state variables are presented below, while details of the rate process equations are given in appendix 3-A:

$$\frac{dNH_4}{dt} = \lambda_R(NH_{4ref} - NH_4) - f(NH_4, Q)B + r_L D - r_N NH_4$$

$$\frac{dNO_3}{dt} = \lambda_R(NO_{3ref} - NO_3) - f(NO_3, Q)B + r_N NH_4$$

$$\frac{dN_s}{dt} = f(NX_x, Q)B - \mu g(E, Q, T)N_s - d_M N_s$$

$$\frac{dN_f}{dt} = \mu g(E, Q, T)N_s - d_M N_f$$

$$\frac{dD}{dt} = \lambda_R(D_{ref} - D) + d_M N_f - r_L D. \qquad (3\text{-}1)$$

The model (3-1) has 5 state variables all of which are in units of $\mathrm{mg\ N\ m^{-3}}$seawater. Ambient nitrogen taken up by the macroalgae is in two forms of dissolved inorganic nitrogen (DIN) namely ammonium ($\mathrm{NH_4}$) and nitrate ($\mathrm{NO_3}$). Parameters $\mathrm{NH_{4ref}}$, $\mathrm{NO_{3ref}}$ and $\mathrm{D_{ref}}$ represent the background concentrations of ammonium, nitrate and detritus respectively. The refresh rate λ_R determines how quickly the external ammonia, nitrate and detritus return to a background concentration in the absence of macroalgae. This term is used in the absence of an advection diffusion model (Aldridge & Trimmer, 2009). Once taken up, DIN is stored as intracellular nitrogen ($\mathrm{N_s}$), which is then fixed into the macroalgae cellular structure ($\mathrm{N_f}$). The uptake rate $\mathrm{f(NX_x, Q)}$ is dependent on both ambient concentrations of DIN and the internal quota, Q, of intracellular nitrogen (Solidoro et al. 1997). The instantaneous growth rate $\mu g(\mathrm{E, Q, T})$ is a product of maximum growth rate, μ, and the environmental variables PAR (E), temperature (T) and Q. $\mathrm{N_f}$ is returned to detritus (D) at a rate determined by the mortality term $\mathrm{d_M}$. Similarly decaying macroalgae returns $\mathrm{N_s}$ to $\mathrm{NH_4}$ at the same rate. D is remineralised at a constant rate $\mathrm{r_L}$. Finally $\mathrm{NH_4}$ is nitrified to $\mathrm{NO_3}$ at a constant rate $\mathrm{r_N}$.

The height of *M. pyrifera* $\mathrm{h_{MA}}$ varies according to the allometric relationship (Hadley et al. 2015),

$$\mathrm{h_{MA}} = (0.00174\mathrm{N_f}/\mathrm{n_{fronds}})^{1.047} \qquad (3\text{-}2)$$

Height change allows kelp to reach the light from depth. Since $\mathrm{h_{MA}}$is frond height (m), the parameter $\mathrm{n_{fronds}}$ is an average of the number of fronds within the unit volume.
Observations taken from the IMTA experiment used in the data model were of height and weight. The weight $\mathrm{w_{MA}}$ $(\mathrm{g^{-1}\ dw\ m^{-3}})$ is given by

$$\mathrm{w_{MA}} = \left(\frac{\mathrm{N_f}}{\mathrm{Q_{min}}}\right) * \mathrm{h_{MA}} \qquad (3\text{-}3)$$

Here $\mathrm{Q_{min}}$ is the minimum amount of structural nitrogen required for the macroalgae cells (Solidoro et al. 1997), while the remainder contributes to growth or respiration. Respiration is not modelled explicitly but is included in the growth term dependent on the internal quota Q. Two changes were made in the present model compared to the original. Firstly, the uptake limiting term $\min(1, \frac{\mathrm{h_{MA}}}{\mathrm{z}})$ (where z is the cultivation depth and $\mathrm{h_{MA}}$ the algae height) was removed; this term was derived to facilitate comparison between two size dependent functional groups of macroalgae. Secondly, the point source term representing the finfish farm output was removed; this excess nitrogen is assumed part of the background ammonium ($\mathrm{NH_{4REF}}$) term. Consequently, the present model (3-1) is a slight simplification of the original model, but still retains all the terms required to represent IMTA.

3.2.2 BHM framework

Formally, the BHM is represented as

$$[\mathrm{Y}, \mathrm{W}, \theta] = [\mathrm{Y}|\mathrm{W}, \theta_{\mathrm{Y}}, \theta_{\mathrm{W}}][\mathrm{W}|\theta_{\mathrm{Y}}, \theta_{\mathrm{W}}][\theta_{\mathrm{Y}}, \theta_{\mathrm{W}}] \quad (3\text{-}4)$$

Where $[\mathrm{A}|\mathrm{B}]$ is the conditional probability of A given B, Y is the data model, W is the stochastic process and $\theta_{\mathrm{Y}}, \theta_{\mathrm{W}}$ are the parameters (Parslow et al. 2013). In equation (3-4) the joint distribution of observation, process and parameters can be represented (using Bayes rule) as the product of conditional dependencies between these sub-components; thus offering a way in which to assess the individual component influence on the model output. In this approach we assume we already know θ_{Y} and only perform inference on θ_{W}. BHMs are probabilistic models, constructed from conditional probability distributions where the data are treated as conditional on the process and some parameters, and the process is treated as conditional on other parameters.
Using the three components for the BHM the model output is represented as

$$\mathbf{W} = [\mathbf{X}, \mathbf{B}]^{\mathrm{T}} \quad (3\text{-}5)$$

Here $\mathbf{X} = [\mathrm{NH_4}, \mathrm{NO_3}, \mathrm{N_s}, \mathrm{N_f}, \mathrm{D}, \mathrm{h_{MA}}, \mathrm{w_{MA}}]$ and $= [\mathrm{G_{max}}, \mathrm{N_{fronds}}, \mathrm{d_M}]$, and T denotes the transpose. This splits the state variables into the state space and the stochastic processes (see next section). The parameters are represented by

$$\boldsymbol{\theta} = [\boldsymbol{\theta}_{\mathbf{X}}, \boldsymbol{\theta}_{\mathbf{B}}]^{\mathrm{T}} \quad (3\text{-}6)$$

Here θ_X and θ_B are subsets of parameters that update either the state variables (X) or autoregressive processes (B) (see table 3-A2 in appendix). Furthermore these can be separated into the constants that affect the state and those that define the rate processes

$$\mathbf{C} = [\mathbf{C}_{\mathbf{X}}, \mathbf{C}_{\mathbf{B}}]^{\mathrm{T}} \quad (3\text{-}7)$$

Here $\mathrm{C_X}$ and $\mathrm{C_B}$ are the constants that update the state and stochastic parameters respectively (see table A3). For the stochastic processes the long-term expected value is where the function should be (e.g. μ_{Gmax} for the growth rate in table 3-A2) but this rate changes each model run with the new value dependent only on the previous value (Markovian process). The three component models of the BHM are now outlined.

3.2.2.1 The stochastic model

Following the method of Parslow et al. (2013) some of the parameters in (3-1) were made stochastic, assuming that these parameters represent sub-processes in the model that vary with time. In the model, maximal growth rate (μ), mortality rate $(\mathrm{d_M})$ and the number of fronds $(\mathrm{n_{fronds}})$ are considered the time varying processes. Although maximal growth rate is given a constant value in (3-1) it is known to vary with age for *M. pyrifera* (Haines & Wheeler, 1978). Similarly, mortality is represented as a constant fraction of the current

biomass (eqn. (3-1)) but in *M. pyrifera* mortality rate varies with both age and environmental pressures, and frond initiation rate also varies with time (Rodriguez et al., 2013). As these three processes are not well studied there is not the information to develop a mechanistic process model for each of them, and in any case this would require adding significant complexity to the process model. Instead literature values are used as the expected value (mean) of a first order stochastic process with a sigma function to represent randomness according to

$$\mathrm{B}(\mathrm{t}+\Delta\mathrm{t}) = \mathrm{B}(\mathrm{t}) \times \left(1 - \frac{\Delta\mathrm{t}}{\tau}\right) + \zeta_{\mathrm{B}}(\mathrm{t}) \times \Delta\mathrm{t}/\tau \qquad (3\text{-}8)$$

for $|1 - \Delta t| < 1$ (Parslow et al. 2013). Here $\mathrm{B}(\mathrm{t})$ is the process of interest (e.g. maximum growth rate), τ is the characteristic time for the autoregressive process (i.e. the timescale on which the growth occurs) and Δt is the discrete time step (1 day). Finally $\zeta_{\mathrm{B}}(\mathrm{t})$ is a series of independent and identically distributed Gaussian random variables.

3.2.2.2 Data model

The observations used in this study were taken from an IMTA experiment conducted around a salmon farm in the Calbuco region of Chile (A Buschmann et al. personal communication, 12th June 2013) (Fig. 1). *M. pyrifera* sporelings (small sporophytes) were attached to specially designed long-lines in three distinct densities: high = 7, medium = 6, and low = 3 sporelings per metre, with 9m of line for each density experiment. The long lines were anchored approximately 100 m from a salmon farm at a depth of 3 m, horizontal to the bottom. Measurements of frond length were taken for each individual kelp at the start of the experiment and twice more at 3 monthly intervals. The initial frond lengths were approximately 14cm (average) per sporeling. One measurement was taken at the end of the experiment for individual kelp weight. Work began July 14th 2007. The data model links the observations with the process model. Environmental forcing is taken from recordings of ammonium and nitrate concentration (3m), temperature (3m) and surface photosynthetically active radiation (PAR) for this region (Buschmann et al. 2008).

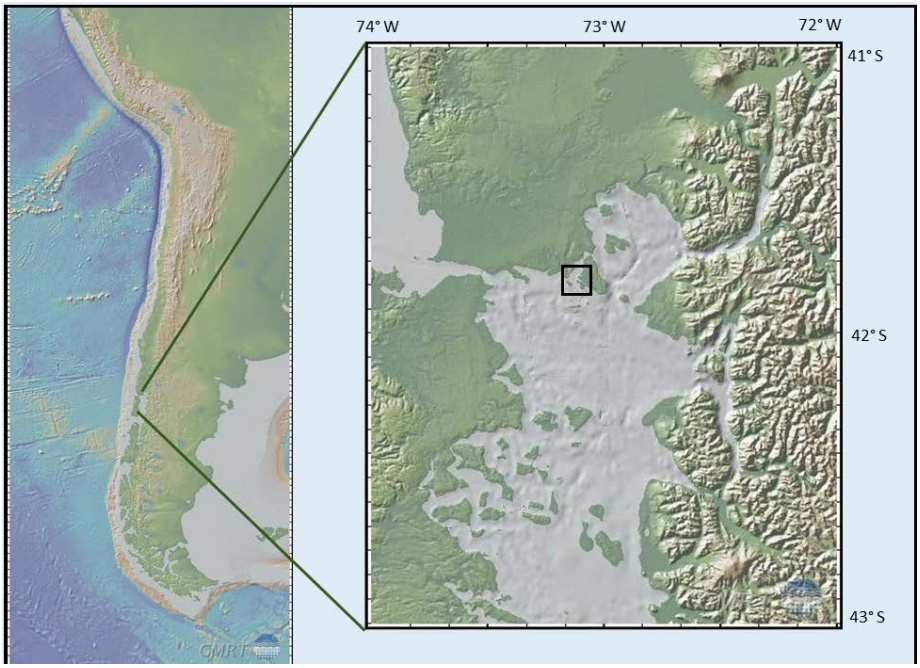

Figure 3-1: Map of the Calbuco region in southern Chile. The experimental data comes from the southern coast of the Isla Calbuco (A Buschmann et al. personal communication, 12th of June 2013), denoted with the black square, a site of intensive salmon aquaculture in Chile.

3.2.2.3 Prior model

In this approach constant parameters in the deterministic model (3-1) were replaced by probability density functions representing a range of possible values for each parameter. The priors were represented by a distribution over a mean for each parameter. The mean of each prior was found from a literature search for *M. pyrifera* growth and were the same as that used in Hadley et al. (2015). The parameters were assumed to be independent (of each other) and to have a log normal distribution, as is typical of many biological processes (Limpert et al. 2001). A prior standard deviation of 0.5 in log space was used for each parameter. The priors were assumed to be a relatively uninformative, which is important in this case as the 'sparse' data is able inform the posterior; a narrower parameter distribution could dominate the inference process. This represents a 50% uncertainty in log-space. We ran a sensitivity analysis of the posterior to the prior with this value at 1.0, 0.5, and 0.3. A prior uncertainty of 0.5 was chosen as it represents a relatively uninformative prior that is consistent with very few values or ranges reported in the literature. As more studies are published this prior uncertainty can be reduced. However, in the absence of published literature values, we have erred towards using relatively uninformative priors. The consequence of this is that for some parameters where the observation are uninformative, the marginal posterior distribution appears to be unchanged from the prior, however the observations have altered the posterior covariance such that parameters can no longer be considered independent. With the data model (observations), process model and prior model the system was then represented as a Bayesian Hierarchical Model (BHM) using the approach of Parslow et al. (2013).

3.2.3 Inference Method

The particle Markov Chain Monte Carlo (pMCMC) method was used to sample from the posterior distribution of our BHM. The particle filter provides estimates of $[\mathrm{Y}|\mathrm{X},\theta]$ and draws samples from the state. The Markov Chain Monte Carlo process is then used to sample θ, according to a Metropolis-Hastings accept/reject rule. The proposal densities samples a new value for θ, conditional on its current value,

$$\theta_{N+1} = \theta_N + q \qquad (3\text{-}9)$$

Here $q = N(\mu = 0, \sigma = \emptyset_B \times S)$ where S=0.05, a value which we chose based on calibration runs of the model.

In this study the model was run on LibBI (www.libbi.org, Murray 2013) which uses a Bayesian inference engine to solve state space models (SSM), reformulated as BHMs by employing pMCMC algorithm for parameter estimation. For each set of parameter values (sampled from the prior distributions) 1024 model runs (particles) were conducted. Each run differs due to the randomness in the autoregressive rate processes and a total of 11 independent MCMC chains of length 40,000 sample $[\theta]$. Samples from all 11 chains are pooled, ensuring the posterior distribution is adequately sampled.

3.2.4 Interpretation of the parameter posteriors

The posterior distribution of the parameters is a high-dimensional (17-D) space that may contain complex structures that do not project onto a 1 or 2-D surface, thus any information gain may not be immediately obvious from the marginal or pairwise distributions. Furthermore the model output may only be sensitive to a small subset of parameters. We present 4 methods for visualising and interpreting the posterior distribution:

1. An integrated metric to assess the overall information content using the Kullback – Liebler (KL) Divergence. The details of the KL divergence, including calibration of the method, are presented in Appendix 3-B.
2. The marginal normalised histograms for each parameter.
3. A subset of pairwise plots for a selection of parameters.
4. Parallel coordinate plots which connect individual sets of sampled parameters by lines that vary in brightness dependent on their likelihood of reproducing observations with the model output.

3.3 Results

A comparison of the model output for the observed state variables (macroalgal height and weight) conditioned on both the data (Y) and parameters (θ) (blue shaded area Figure 3-2) versus conditioning on θ (pink shaded area Figure 2) alone, showed an approximate 90% reduction in range, and this result is replicated across the three sets of density

dependent observations. However, in the high density situation the 95% credibility interval (shaded areas) for the posterior covers a considerable range of values i.e. 0 – 11 m and 0 – 60 kg for height and weight respectively (after 251 days). This demonstrates the uncertainty in the model output (for the observed variables) given the uncertainty in the parameter values.

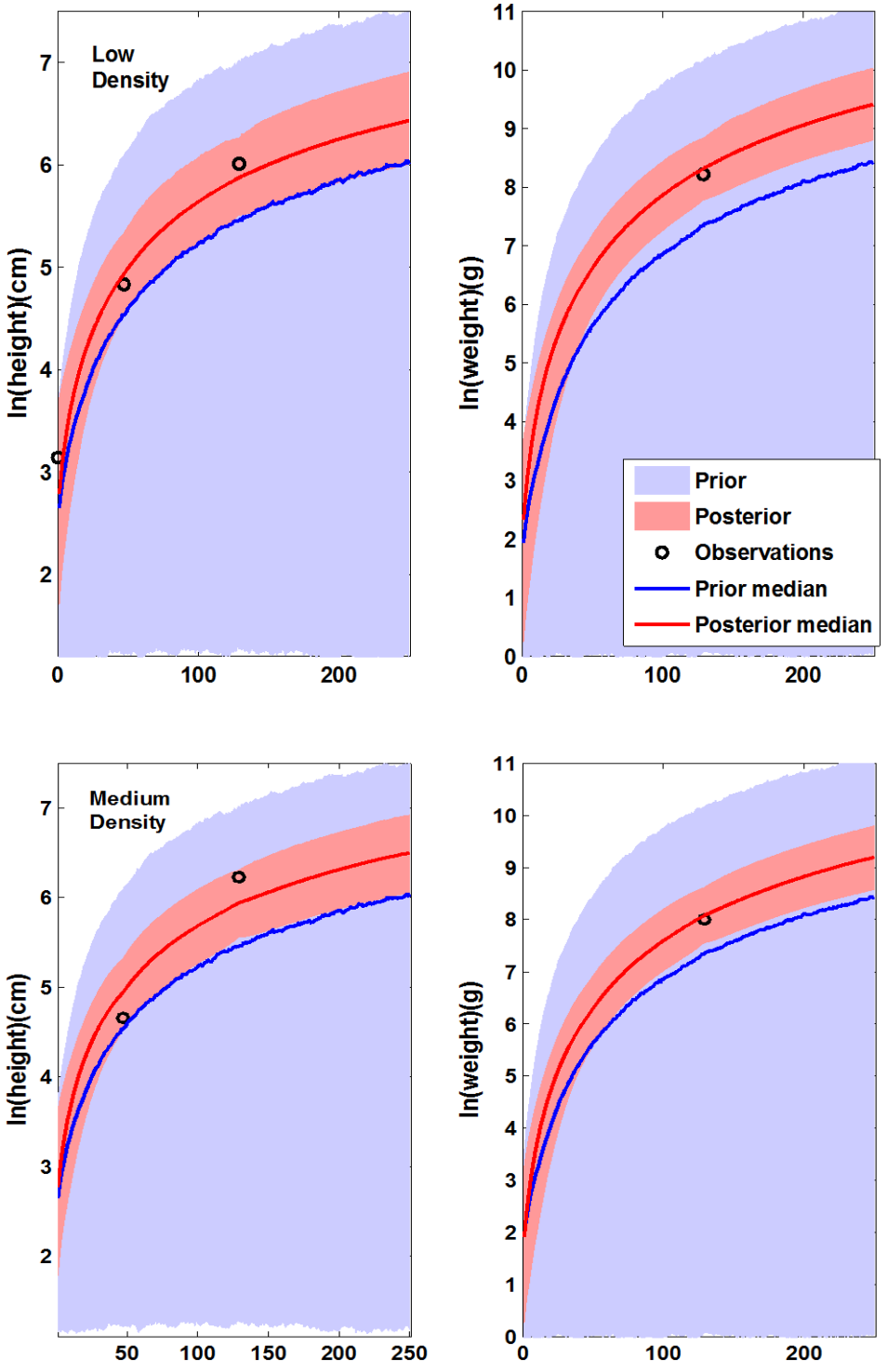

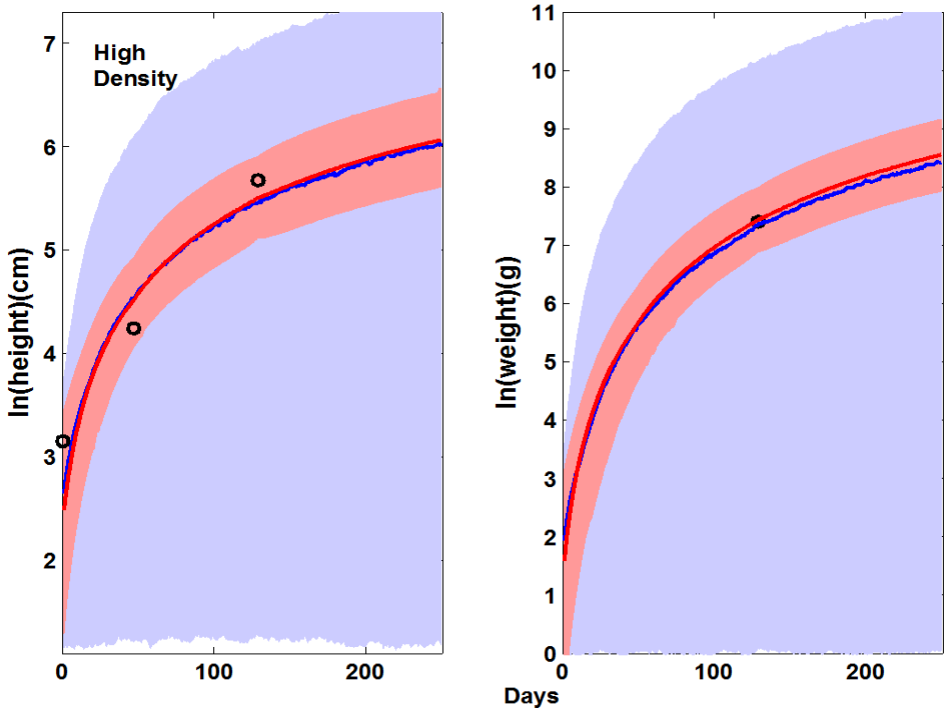

Figure 3-2: 95% confidence intervals for the posteriors of the observed variables; height and weight conditioned on the prior only (blue shaded area) and data plus the prior (pink shaded area.) Medians (in log space) for the posterior and prior data are shown as pink and blue line respectively, with the observations (circles) superimposed.

A direct comparison of the medians of the posteriors (Figure 3-3) showed that conditioning on the medium density data produced the tallest macroalgae at 6.5m, followed by low density at 6.0m and finally the high density observations at 4.0m, after 251 days. Using the same comparison test for weight established that conditioning on low density observations returned the highest end of season value at 12.0 kg, followed by 10 kg for the medium density observations and 5.0 kg for the high density observations. All three medians accurately predicted actual macroalgae height after 50 days but under predicted the height at 120 days. For macroalgae weight each of the three trajectories are closely aligned with observation.

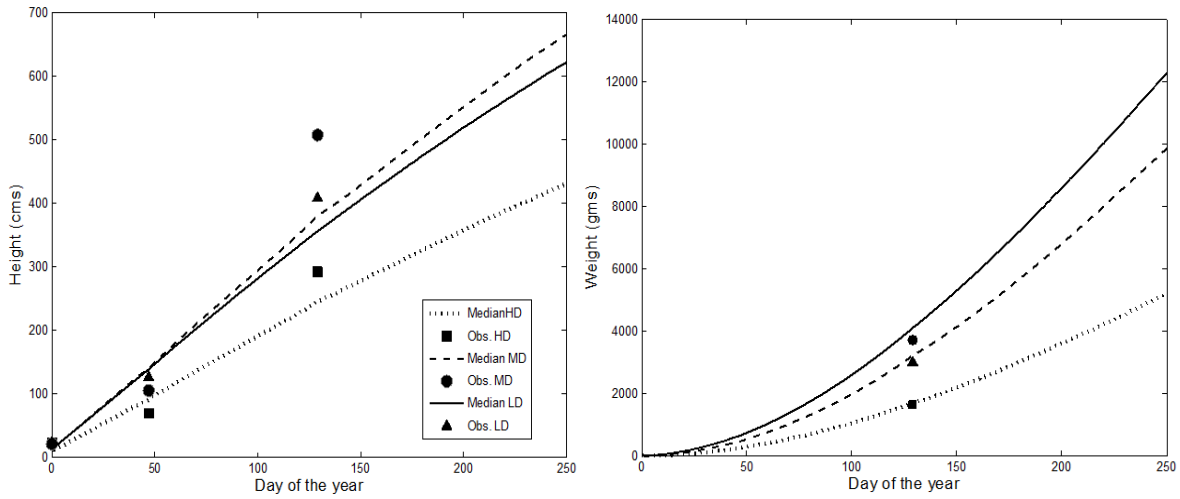

Figure 3-3: Shown are the Posterior medians for macroalgae height (cm) (left), and weight (g) (right) conditioned on the observations from each of the 3 density experiments,. Observations are overlaid. The model closely predicts height at 50 days but under predicts (height) at 130 days in all 3 cases. The model closely predicts the weight at 130 days in all 3 cases.

The definitive metric for bioremediation capacity of *M. pyrifera* is uptake rate (removal) of DIN. Estimating this rate indicated that the medium and low density sporelings removed approximately the same amount of DIN over the season (Figure 3-4) with the high density arrangements removing the least. This conclusion was based on the observable difference between the posterior and prior medians for all three plots. Once again the conditioning of the posterior on the data model constrained the model output by between 50 - 70% dependent on the data model used.

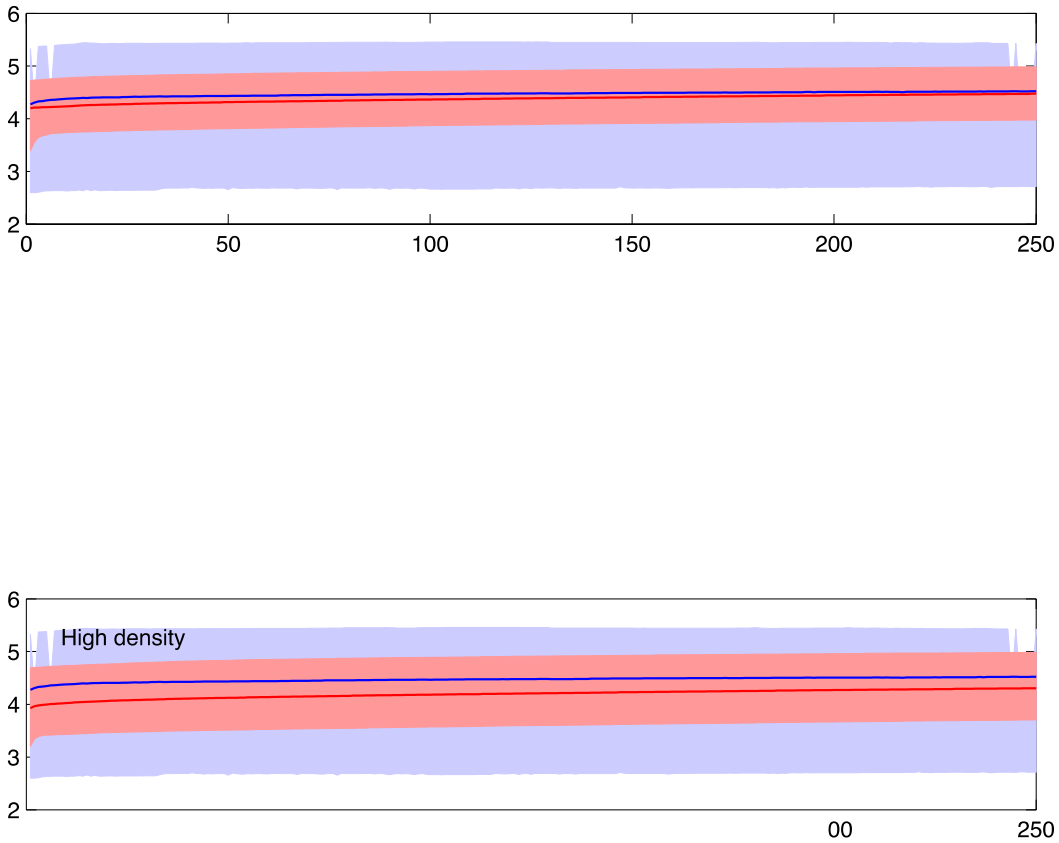

Figure 3-4: Model simulation of uptake of DIN by macroalgae at high, medium and low density seeding's. 95% confidence intervals for the posteriors of the uptake conditioned on the prior only (blue shaded area) and data plus the prior (pink shaded area.) (log space.) Medians (in log space) for the posterior and prior data are shown as pink and blue line respectively. A comparison between the medians in each plot shows high density seeding removing the least DIN over a season with medium and low density seeding's showing approximately the same uptake.

An inspection of the 95% credibility interval for the posteriors of the unobserved state variables (i.e. NH_4, NO_3, N_s, N_f and D) when $[X|\theta]$ (blue shaded regions in Figure 3-5) showed once again a considerable variation in the model output based on uncertainty in the parameters. Although the data models do not contain observations for any of these 5 variables, conditioning on observations for height and weight constrained the model output for 4 of them, namely NH_4, NO_3, N_f and N_s (pink shaded areas Figure 3-5). Moreover, this result was consistent for data from all 3 sets of observations. Only the posteriors for detritus D (when transformed back from log space) were not constrained by conditioning on the data models.

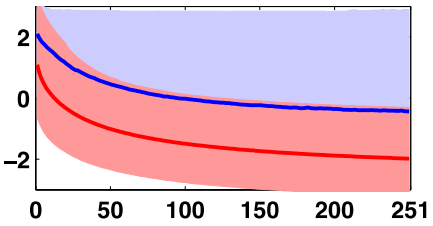

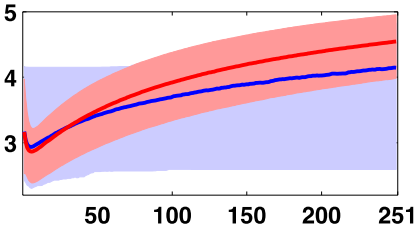

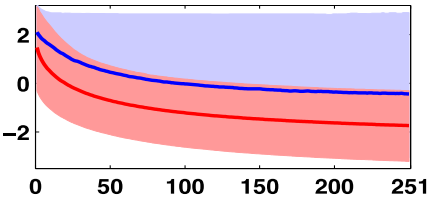

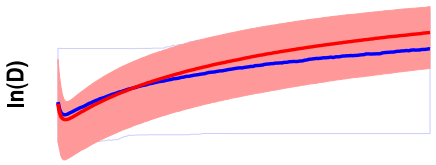

Medium Density

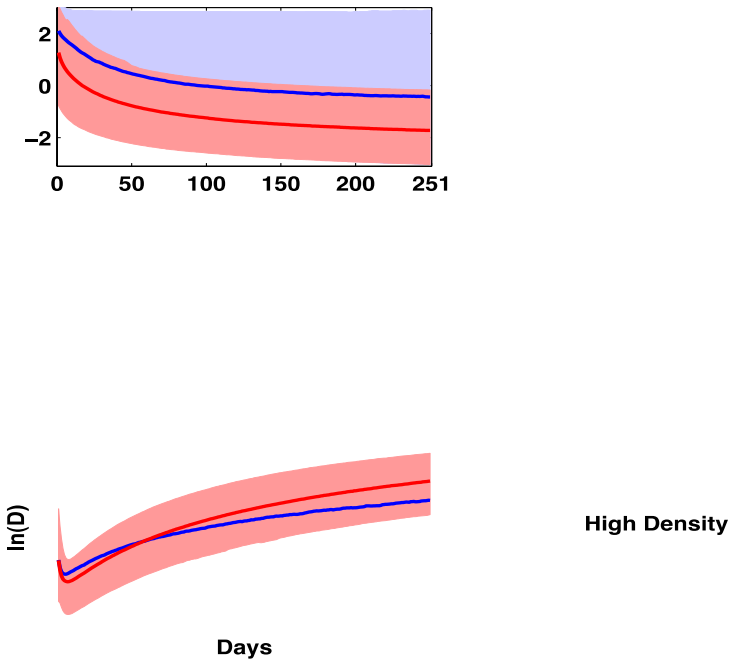

Figure 3-5: 95% confidence intervals for the posteriors of the unobserved variables; NH_4, NO_3, N_s, N_f, D conditioned on the prior only (blue shaded area) and data plus the prior (pink shaded area.) Medians (in log space) for the posterior and prior data are shown as pink and blue line respectively. For all 3 cases only in detritus D is not constrained by observations.

The KL divergence test was applied to the posterior of the parameters and showed that for a low density of initial sporelings the KL divergence had a value of 71.7903 (mean of 11 chains) with a variance of 0.1827 (variance in the means of each chain); for medium density the corresponding values were 77.5679 and 0.2582; and for high density 67.9248 and 0.2365. Based on calibration, which suggests a KL value of 58.2 was associated with a 10-fold reduction in uncertainty (App. 3-B), the KL divergence results indicate a 10-fold contraction in variance of the prior. However, this method does not give the direction of the contraction in parameter space. The fact that the variances were all low values indicated a convergence of the method. To observe the change in parameter space we examined the posterior distributions in detail.

The amount of parameter learning obtained was displayed through a comparison of the prior (blue lines Figure 3-6) and posterior (red histograms Figure 3-6) marginal distributions for each of the model parameters. Learning was observed as either a shift in the mean of the posterior away from that of the prior, or a contraction in the variance of the posterior compared to the prior. For each set of observations, several parameters showed learning; for parameters conditioned on the low density data model these were Q_{min} and λ_R; at medium density they were $Q_{min}, \lambda_R, \mu_{fronds}, \mu d_M$; and at high density, $Q_{min}, \lambda_R, K_{NH_4}, K_c, \mu_{fronds}$. It should also be noted that learning occurred in parameters controlling both the state and the stochastic processes.

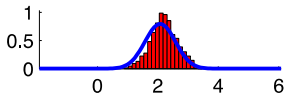
1
0.5
0
0
2
4
6

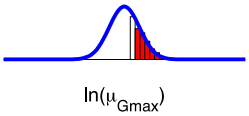
ln(μGmax)

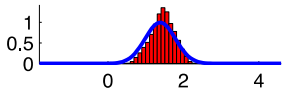
1
0.5
0
0
2
4

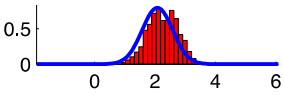
0.5
0
0
2
4
6

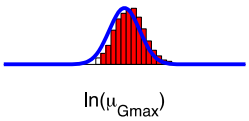
ln(μGmax)

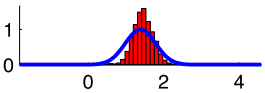
1
0
0
2
4

Figure 3-6: Comparison of the parameters controlling the state in the macroalgae model showing prior (blue line) and posterior (red histogram) outputs for low (top), medium (middle) and high-density (bottom) observations. Note: The final three parameters control the autoregressive process. The displacement of the posterior from the prior shows degrees of learning for that parameter.

A subset of parameter posteriors displayed as pairwise plots derived from kernel density estimates characterises the complex interactions involved in a 17D parameter space (Figure 3-7). This result was a qualitative investigation and so for brevity only parameter posteriors conditioned on data for the high-density sporelings were used. High density results were chosen because they displayed the most learning based on results for the marginal distributions only. For all six plots there was a contraction of the posterior from the prior for each parameter pair however, there were slight variations in each case. For the posterior the refresh rate λ_R correlated linearly with both μ_{fronds} and Q_{min}. The pairwise comparison of K_C and Q_{min} shows the contraction was skewed, pairing higher values of the former with lower values of the latter. Although the marginal distributions of the parameters r_L and r_N conditioned on the high-density observations (Figure 3-6) show only slight evidence of learning, the bivariate plot (Figure 3-7) for this pair showed a uniform contraction of the joint posterior distribution. A similar result is seen for the joint distribution of V_{NH_4} and K_{NH_4}, which together control the uptake rate of ammonia.

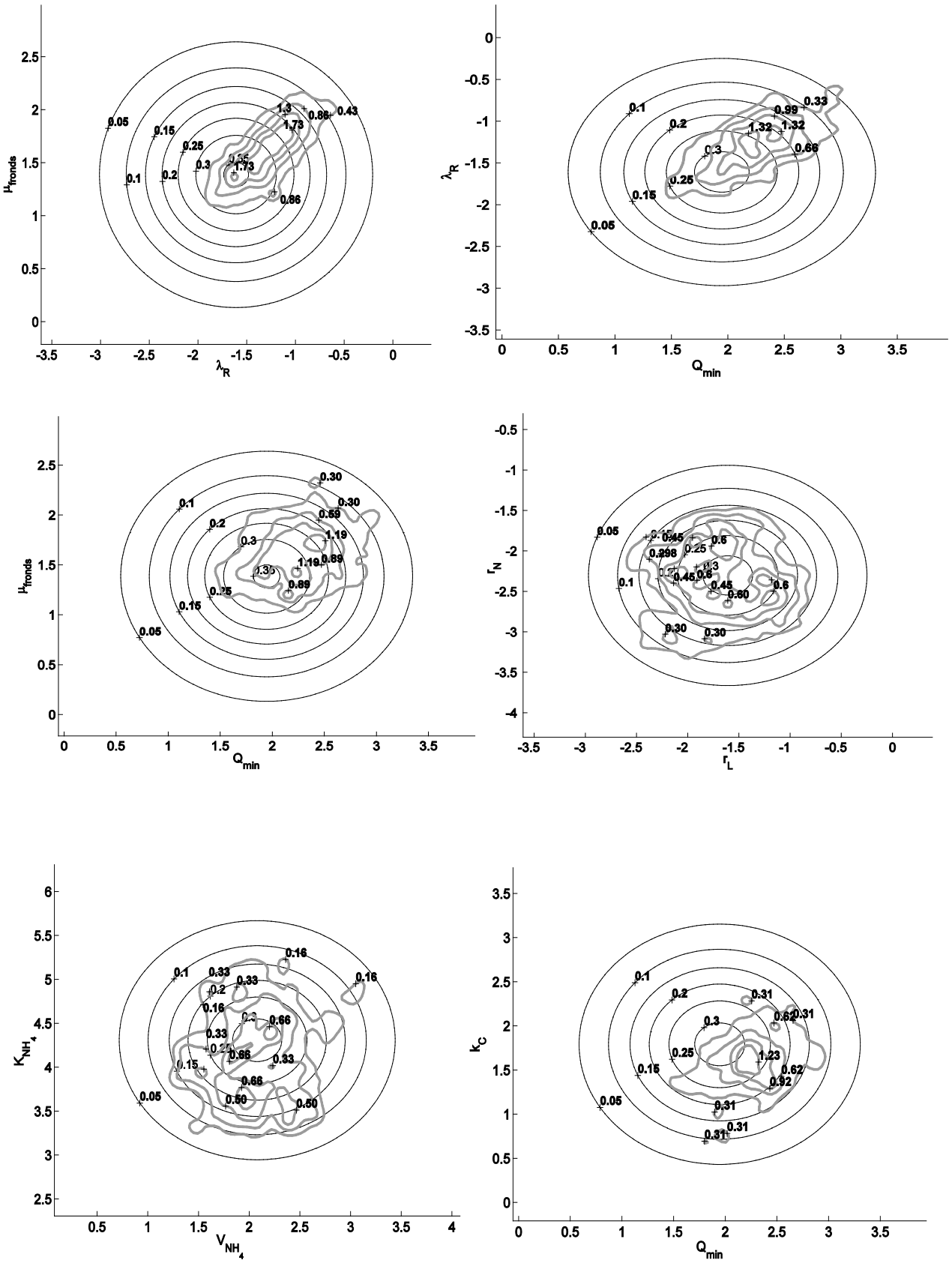

Figure 3-7: A sample of pairwise plots of parameters showing the different relationships observed. The black concentric circles denote the joint parameter space for the kernel density estimates (KDE's) of the priors. The

grey lines represent the KDE's for joint posteriors of the parameter pair conditioned on the observations from high-density sporelings experiment. The KDE represents the density of parameter values in pairwise parameter space.

Parameter dependence was examined even further through the construction of parallel coordinate plots (Inselberg 1998) (Figure 3-8.) Each line joins a set of parameters sampled from the posterior. In these plots the darker the line the greater the likelihood that the model will reproduce the observations using that set of parameters. A visual inspection of each plot shows that the range of parameter values (evaluated on the y-axis) narrows as the likelihood increases, i.e. lines were darker as they neared y=0. This result is interpreted as a contraction in the variance of the posterior distribution about the mean value. Furthermore, the clusters of dark lines are quite distinct between the 3 plots indicating density dependent effects in the model.

Within each plot the high likelihood modes (clusters of dark lines) diverged significantly for some parameters indicating that the model was capable of reproducing the observations using different mechanisms. An example of this is seen in the plot based on medium density sporelings data where two of these modes diverged around the adjacent parameter sets of $\mathrm{V_{NH_4}}$ and $\mathrm{K_c}$ with one mode pairing a 'high, low' value for $(\mathrm{V_{NH_4}}, \mathrm{K_c})$ whilst the other uses a 'low, high' pairing. Another interesting feature is seen in the posterior conditioned on low density observations (top plot Figure 3-8). Here the parameter $\mathrm{K_{NH_4}}$ has two different high likelihood modes passing through it with preference for either a low or high value of this parameter; however, the marginal of the posterior distribution for this parameter shows no learning. The key point is that the overall posterior for this parameter is left unchanged by the inference process yet preferred modes (sets of parameters) contain values (of $\mathrm{K_{NH_4}}$) from the tail of the prior distribution.

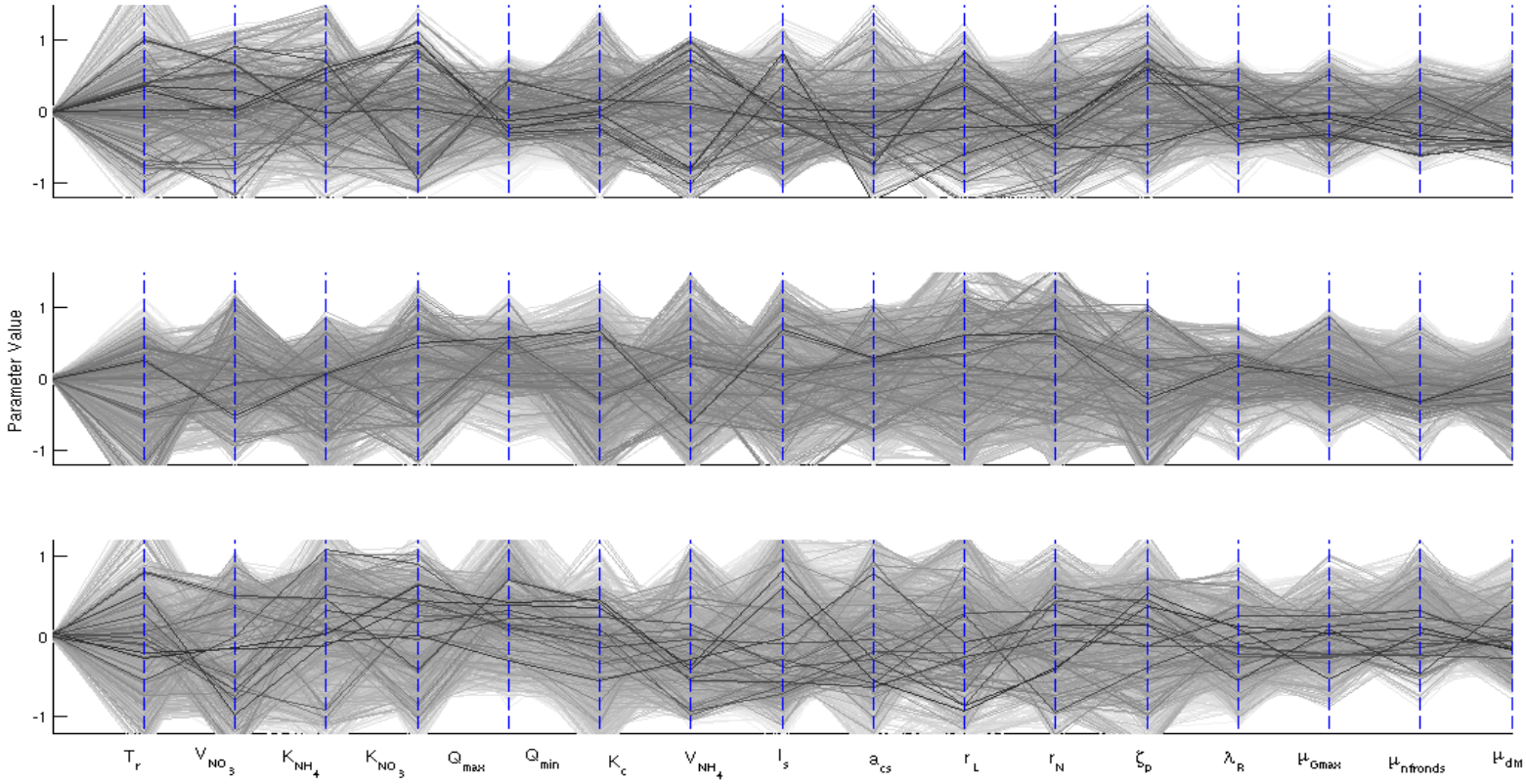

Figure 3-8: Parallel coordinate plot of the 17 parameters for the scenarios where *M. pyrifera* sporelings are seeded at low (top), medium (middle) and high (bottom) densities. Parameter values are scaled to make interpretation easier. The lines shown in each plot connect sub sets of parameter values used in the sampling process; the darker the line the higher the likelihood that the set of parameters would match the model output to observations.

3.4 Discussion

3.4.1 Visualising and interpreting the high dimensional posterior

The results highlight the complexity in the high dimensional posterior parameter space and the subsequent difficulty interpretation. It is helpful to begin by discussing the results for parameter learning.

3.4.1.1 Marginal posterior plots

In general the model was sensitive to Q_{min} and λ_R as these two parameters exhibited learning independent of the seeding density. In this context it is worth noting that in Hadley et al. (2015), the deterministic model was also sensitive to Q_{min}. This parameter is used within the model to convert N_f to biomass B (eqn. 3-A9), and it determines the uptake and growth rates (eqns. 3-A1 and 3-A5) and internal nitrogen quota Q (eqn. 3-A10). Given that Q_{min} has four functions within the model it is difficult to isolate the influence of this parameter. In contrast, λ_R had the sole function of determining how much time the kelp has to take up the external nutrients. Hadley et al. (2015) highlighted that a higher value of λ_R resulted in a comparatively reduced growth rate for *M. pyrifera* in the first half of the growing season, while in the second half of the season the higher value of λ_R resulted in a comparatively higher growth rate. Second order effects make it difficult to quantify how both Q_{min} and λ_R act individually to determine the model output. The interpretation of this result is that the posteriors are more representative of the true values of these parameters that are needed to represent the actual IMTA system studied.

The parameter μ_{fronds} was used to calculate the height and weight of *M. pyrifera* and therefore exerted strong influence over the model output for these observed variables. The posterior marginal distributions for μ_{fronds} were observably different in all 3 cases, which inferred density dependence in this process although, notably, this dependence was not explicitly modelled. The results indicate that the prior used for the parameter μ_{fronds} was more representative of a low density sporelings arrangement, where there was no change in the prior distribution. The shift in the mean of μ_{fronds} captured in the posterior distributions for the medium and high density arrangements showed that the prior was not suitable for IMTA at these densities. Its true value may vary considerably under a range of initial sporelings densities and intuitively it should increase with density. The parameterisation of this process therefore needs a different approach in future applications. In general it appears that there was parameter learning based on marginal distributions alone but due to both the density dependence effects observed in the posteriors and the high dimensional parameter space studied, there is a need to look at the other visualisation methods to properly characterise this learning.

3.4.1.2 Pairwise KDEs

A linear correlation was observed between λ_R and both μ_{fronds} and Q_{min} in the pairwise KDE plots. In general parameter correlation leads to an inability to identify between parameters, and thus a need for more empirical data to resolve (Li and Vu 2013.) Sampling from the posterior becomes more difficult unless the correlation is included in the proposal distribution. As mentioned previously, the refresh rate controls how much DIN

flows through the system. If λ_R increases, then DIN should flow through more quickly which can have differing effects on *M. pyrifera* growth depending on the state of the system. If the biomass of *M. pyrifera* is large enough it is able to take up the increased supply of the DIN. Even for quite large values of λ_R the biomass should eventually be large enough to efficiently remove DIN and in doing so considerably increase its growth and by extension its height and weight. In this case the system can also act to reduce the height and weight by increasing μ_{frond}, which will then match model output to observation.

Similarly, an increase in Q_{min} resulted in a decrease in *M. pyrifera* biomass, resulting in a decrease in uptake rate (eqn. 3-A9). An increase in Q_{min} will also result in a decrease in both the amount of nitrogen that can be stored (eqn. 3-A1) and the growth rate (eqn. 3-A5). Effectively, a change in either Q_{min} or μ_{frond} offsets the effect that changing λ_R has on the model, which enables the output to be matched to observation. The two parameters Q_{min}, μ_{frond} are not linearly correlated (in the high-density scenario); however, their shared parameter space is constrained to the top right quadrant of the prior distribution, suggesting that their functions are complimentary within the model.

The change in the posterior of Q_{min}, which is seen across 3 sets of observations, is most likely a reflection of the true value of this parameter. If the three posteriors for Q_{min} were to show considerable differences dependent on the different initial densities (of sporelings), then this would bring to question how well the model parameterises internal nutrients and whether or not Q is density dependent. An increase in Q_{min} (with no change in Q_{max}) will result in a reduced internal storage capacity for *M. pyrifera*. Whether this is actually associated with an increase in the number of fronds is unknown. It could be that the smaller *M. pyrifera* individuals, associated here with the higher initial seeding density, have less storage capacity and there is an allometric relationship between size and storage capacity, but this is not modelled explicitly in equation (1).

The pairwise relationship between Q_{min} and K_C was expected. K_C is defined as a proportion of the internal storage capacity of *M. pyrifera* ($Q_{max} - Q_{min}$) (Solidoro et al. 1997), and therefore reduces as Q_{min} increases, provided that Q_{max}remains constant. The net effect of the change is to keep the nutrient-dependent growth rate constant (eqn. 3-A5), which is expected in a nutrient replete environment. Pairwise plots for (V_{NH_4}, K_{NH_4}) and (r_L, r_N) do not relay much information about the interaction between these parameters. In general nitrification (r_N) and remineralisation (r_L) are second order processes in the model, occurring on scales that should not impact the overall IMTA process. Together V_{NH_4} and K_{NH_4}(along with $[NH_4]$) control the uptake of ammonium, but this process is also dependent on biomass and internal N concentration, which are likely to have far more influence over this process in the model.

3.4.1.3 Parallel coordinate plots

There was little observable information gain in any of our three sets of marginal posterior distributions yet the KL divergence results indicate an order of magnitude contraction in the variance of the combined parameter space. Consequently, the

information contained in the parallel coordinate plots is very important. The high likelihood modes were, in some cases, constructed from conjugate sets of parameter values i.e. mode 1 had a high value for parameter A and a low value for parameter B whereas mode 2 had low A and high B. This highlights that the model can therefore achieve the same result using different mechanisms. Whether this variation is indicative of *M. pyrifera* growth in reality or is an artifice of the data assimilation process (in which parameter space is constrained in such a way that all sets chosen from the posterior would provide a reasonable approximation to observation) is not easily discerned from this approach, as both are possible conclusions. Macroalgae blades have been shown to vary their uptake of DIN, growth rate and photon harvesting capacity in response to environmental changes in PAR and nitrate (North et al. 1986; Gerard 1982), with variability occurring even between blades on the same frond (Kopczak 1994). Even if the environmental forcing of nutrients and PAR were held constant (as was the case here) or at least were the same for each *M. pyrifera* sporeling, the nutrient histories of the individual sporelings may differ. In this case individual sporeling may use available nitrogen in a different way; some may store N whilst others may use it to increase growth rate (Kopczak et al. 1991.) For farmed *M. pyrifera* there may even be significant variation in the PAR and nutrient environment between individual plants. The different modes presented in the parallel plots may capture this behaviour. In this approach it is the inference algorithm that chose between parameter sets in order to match the model output to the observations. However, it seems entirely acceptable to choose different parameter sets as long as they are physically realisable. In their approach Parslow et al. (2013) found some sets of parameter values chosen by the inference process were not possible in a realistic system. In this study no unrealistic parameter values or combinations were identified.

The different mechanisms, represented here as sets of parameters (modes), which allow the model to match output to observation may be obscured when each mode contains 17 parameters. What is interesting is that almost imperceptible changes in the marginals of the posteriors for most of the parameters results in such high variance in the sets of parameters the model uses to constrain the output to the observation. An interesting result, highlighting that marginals may not reflect the true learning obtained by this approach was observed for the parameter $\mathrm{K}_{\mathrm{NH}_4}$ conditioned on the low density data. Although there was no discernible change in the marginal of the posterior, for this parameter, the parallel plots showed that two of the high likelihood modes used values of $\mathrm{K}_{\mathrm{NH}_4}$ chosen from the tail of the prior distribution. All other modes included values for this parameter in a way that preserved the prior distribution.

3.4.2 General remarks

The great strength and value of this kind of BHM approach is how it accounts for model uncertainty. Three sources of possible uncertainty in the basic model structure (i.e. parameters, processes and data) were represented as probability distributions and stochastic processes, and creation of two new state variables (height and weight) introduced further uncertainty. It is encouraging that sparse data sets, such as in this example, can have such strong influence in constraining the response variables and particularly in constraining the unobserved state variables. In using uninformative priors and

allowing the data to inform the posterior, it is important to consider the times in the season that data are collected. For example, if all observations of macroalgae height were taken late in the season when growth had begun to asymptote then this would be reflected in the posteriors for the parameters, and these data would contain no information about nutrient uptake at low biomass. Although the observations in this study were sparse they covered the time period from initial growth up to the point where growth started to level off.

The BHM approach offered a rigorous analysis of the model's sensitivity to the parameters. In the original deterministic model each parameter was perturbed in turn (by $\pm 10\%$) to assess the sensitivity of the model to that parameter (Hadley et al. 2015.) In the current approach all parameters were perturbed simultaneously. The variance in the state variables (conditioned on the prior only), under that perturbation, provides a means to quantify the overall model sensitivity to parameters. The posteriors of the parameters when conditioned on the observations greatly reduced the model sensitivity for all state variables with the exception of detritus. If parameter learning were based solely on the marginal distributions then the high density data contained the most information as this resulted in the greatest observable difference between prior and posterior. In contrast, the results of the KL – divergence infer the medium density observations produce the most parameter learning. Unfortunately, the interpretation of the effect that density of initial seeding of sporelings has on the overall 17-D parameter space (as displayed in the parallel coordinate plots) is beyond the scope of this investigation.

For other density dependent behaviour, such as the eventual height and weight of individuals, the results concur with current understanding (based on experiments and observations) and show that densely seeded kelps will grow more slowly than those at lower densities, presumably reflecting the effects of increased light and nutrient limitation. Medium density seeding may allow less DIN (than lower density) for each individual *M. pyrifera* plant, but concentrations are still sufficient for these individuals to change their height and thereby reduce light limitation. Low density seeding provides the greatest DIN per individual but also less self-shading (than at medium density), yielding shorter but heavier plants compared with medium density seeding. Individuals grown in low density arrangements may be shorter compared to those in medium density because *M. pyrifera* is readily photoinhibited at high light, and therefore growing close to the surface is likely to inhibit growth, whereas at medium density there is more protection from this effect in the initial stages of growth. As a consequence of our results we can infer that DIN uptake is dependent on stocking density in such a way that an optimum density is found in the range between too sparse: where growth is biomass limited as DIN escapes through the gaps; and too dense where the plant growth is light and/or N limited (Figure 3-9).

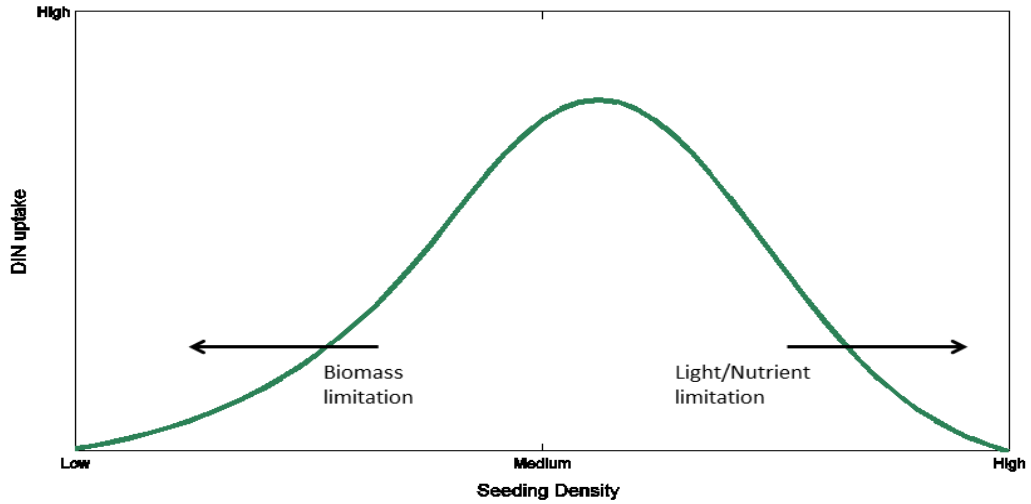

Figure 3-9: Conceptual model of the effect stocking density has on DIN uptake. Optimal uptake is in between a density that is too sparse, allowing DIN to escape the system, and too dense which inhibits growth due to limitation of light and nutrients.

3.4.3 Conclusion

Bayesian Hierarchical Modelling (BHM) provides a means to identify and quantify uncertainty in the state variables of deterministic models. Conditioning the results on observations can also considerably reduce this uncertainty which involves observed parameter learning, and which can help inform the model in other applications.

The results for the test model showed the existence of learning in 17-D parameter space and indicate a general contraction of the variance of the parameter distributions. The different models tested (based on three sets of observations from kelps seeded at different initial densities) resulted in different model outputs and demonstrated the potential for overall parameter learning. Although the test model did not reflect density dependence explicitly, the shift in several key parameters suggests it is capable of representing second order effects of this dependence by altering factors that affect uptake rate among other parameters.

Overall the model predicted that initiating sporelings at high-density provided the poorest bioremediation outcome, based on total uptake of DIN, and that sporelings initiated at medium (6 sporelings per metre) and low density (3 sporelings per metre) performed better.

3.5 Appendix 3-A

Table 3-A1: Biological intermediate processes.

Symbol no.	Eqn.	Description	Formula	Unit
f(N, Q)	3- A1	Uptake of external N source into internal reserve.	$\frac{V_M N}{K_{1/2}+N}\frac{Q_{max}-Q}{Q_{max}-Q_{min}}$	$mg\ N\ g^{-1}\ dw\ d^{-1}$
μg(E, Q, T)	3-A2	Growth function for macroalgae.	μg(E)g(Q)g(T)	d^{-1}
g(E)	3-A3	Growth limitation due to light.	$\frac{e}{k^*z}\left(e^{\frac{I_z e^{-kz}}{I_s}}-e^{\frac{I_z}{I_s}}\right)$	Dimensionless
g(T)	3-A4	Growth limitation due to temperature.	$\frac{1}{1+\exp[-\varsigma_p(T-T_p)]}\ \frac{1}{1+\exp(-(T-T_0)/T_r)}$	Dimensionless
g(Q)	3-A5	Growth limitation due to internal nutrient reserves.	$g\frac{Q-Q_{min}}{Q-k_c}$	Dimensionless
I_z	3-A6	Irradiance at top of macroalgal canopy.	$E_0 e^{-K_d(z-h_{MA})}$	μmol photons $m^{-2}\ s^{-1}$
K	3-A7	Extinction rate of light due to water and algae.	$k_w + k_{MA}$	m^{-1}
K_{MA}	3-A8	Extinction rate of light due to algae.	$N_f a_{cs}(\max\left(\frac{h_{MA}}{z},1\right))(\min(h_{MA},z)^{-1})$	m^{-1}
B	3-A9	Biomass of dry macroalgae.	$N_f Q_{min}^{-1}$	$g\ dw\ m^{-3}$
Q	3-A10	Internal nutrient quota of macroalgae	$Q_{min}\left(1+N_s N_f^{-1}\right)$	$mg\ N\ g^{-1}\ dw$
h_{MA}	3-A11	Height of *Macrocystis*	$(0.00174 N_f/\mu_{fronds})^{1.047}$	M

Table 3-A2*:* The priors on parameters used in the stochastic IMTA model are all log-normal with mean (μ) and standard (σ) deviation on the log-scale. The line separates the parameters that update the state variables from those updating the auto-regressive processes.

Parameter	Description	Mean (μ)	SD (σ)
V_{NH_4}	Max. Uptake Rate (Amm.)	8.0 $mg\ N\ g^{-1}\ dw\ d^{-1}$	0.5
V_{NO_3}	Max. Uptake Rate (Nit.)	10.3 $mgNgdw^{-1}d^{-1}$	0.5
K_{NH_4}	Half Sat. Const. (Amm.)	74.2 $mg\ N\ m^{-3}$	0.5
K_{NO_3}	Half Sat. Const. (Nit.)	182.0 $mg\ N\ m^{-3}$	0.5
Q_{max}	Max. Internal Nitrogen	25.0 $mg\ N\ g^{-1}\ dw$	0.5
Q_{min}	Min. internal Nitrogen	7.0 $mg\ N\ g^{-1}\ dw$	0.5
K_c	Half Growth Const.	6.0 $mg\ N\ g^{-1}\ dw$	0.5
T_0	Optimal Temp.	12.0 ℃	0.5
T_r	Range of Optimal Temp.	1.0 ℃	0.02
I_S	Saturation Irradiance	134.0 μmol photons $m^{-2}\ s^{-1}$	0.5
a_{cs}	Nitrogen Specific Shading	0.0001 $m^2\ mg^{-1}$ N	0.5
r_L	Remineralisation Rate	0.2 d^{-1}	0.5
r_N	Nitrification rate	0.1 d^{-1}	0.5
λ_R	Refresh rate	0.2 d^{-1}	0.5
K_d	Light attenuation coefficient	0.1 m^{-1}	0.5
μ_{Gmax}	Max. Growth Rate	0.2 d^{-1}	0.3
μ_{fronds}	Number of Fronds	4.0 Dimensionless	0.4
μ_{dM}	Mortality Rate	0.003 d^{-1}	0.3

Table 3-A3: Table of all the constants used in the model. All the constants update the state only.

Constant	Description	Value
T	Water temperature	12.0 ℃
NH_{4ref}	Background concentration NH_4 (Amm.)	30.0 mg N m^{-3}
NO_{3ref}	Background concentration NO_3 (Nit.)	154.0 mg N m^{-3}
D_{ref}	Background concentration Detritus	20.0 mg N m^{-3}
E_0	Average Irradiance	180 µmol photons m^{-2} s^{-1}
K_d	Light attenuation coefficient	0.1 m^{-1}
z	Cultivation depth	3 m

Table 3-A4: Initial conditions for *M. pyrifera*

Symbol	Mean (µ)	SD (σ)
N_f	0.1 g N m^{-3}	0.3
N_S	0.1 g N m^{-3}	0.3

3.6 Appendix 3-B: Kullback-Liebler (KL) Divergence Test

The KL divergence is a metric that assesses the change in density between two distributions P(x) and Q(x) using the following form if x is continuous,

$$DK_{KL}(P \parallel Q) = \int_{-\infty}^{\infty} p(x) log\left(\frac{p(x)}{q(x)}\right) dx \qquad \text{(3-B1)}$$

where p and q are the densities of P and Q. The metric (3-B1) is not symmetric and is not a distance function. We have the distribution for our parameter prior P which is multivariate normal given by,

$$P = N(\mu, \sigma) \qquad \text{(3-B2)}$$

where μ is the parameter mean and σ is the standard deviation. We do not have a parametric form for Q the probability density function (pdf) of our posterior; instead we use a kernel density function approach to estimate Q from a sample of the posterior distribution,

$$Q(x) = \frac{1}{n}\sum_{i=1}^{n} K_H(x - x_i) \qquad \text{(3-B3)}$$

K(.) is our kernel function; we assume this to be a Guassian mix. H is a bandwidth matrix and

$$K_H(x) = H^{-\frac{1}{2}} K(H^{-\frac{1}{2}} x) \qquad \text{(3-B4)}$$

For the optimal bandwidth selection of matrix H we use the Rule of Thumb approach,

$$\sqrt{H_{ii}} = \left(\frac{4}{d+2}\right)^{\frac{1}{d+4}} n^{\frac{-1}{d+4}} \sigma_i \qquad \text{(3-B5)}$$

here d is the sample size of points taken from the posterior.

Calibrating the KL Divergence

The Kullback-Liebler divergence test is an integrated information content metric that is used to assess the difference between two probability distributions. To interpret the results from this test we first need to calibrate the KL divergence results. This was achieved through comparing the results in this experiment with a known case. The parametric 17D prior constructed from [mean, variance] of our parameter set can change in three ways: 1.) a shift in the posterior mean; 2.) a reduction in the posterior variance; and 3.) a combination of both a shift in the posterior mean and a reduction in the posterior variance. In this study, we are interested in whether there is any evidence of learning in the posterior when compared with the prior, i.e. a contraction of posterior variance and thus reduction in uncertainty. To estimate the degree of learning (variance contraction) of the posterior distribution, a set of calibration tests were conducted by scaling the prior distribution. By multiplying the prior variances by a factor of 0.1, the resulting KL divergence between the prior and scaled prior was 58.2. This suggests that a KL divergence figure of approximately 58 corresponds with a 10 fold reduction in uncertainty.

CHAPTER 4
QUANTIFICATION OF THE IMPACTS OF FINFISH AQUACULTURE AND BIOREMEDIATION CAPACITY OF IMTA USING A 3D ESTUARY MODEL

Preface: IMTA is seen as a way forward for sustainable aquaculture. It provides both a method of bioremediation of the impacts of finfish aquaculture and a viable nutrient source to promote growth of macroalgae cultivated near the finfish farms. In this chapter the spatio-temporal variability of IMTA was examined using and idealised 3D test estuary

The response of an estuary to increased intensity in finfish farming was quantified. The capacity of IMTA to bioremediate those impacts was also examined. A strong spatial gradient was found whereby the success of IMTA depended on the location within the estuary relative to the river.

This work has been published in a refereed journal and is presented below in an identical form. The citation for the original publication is:

Hadley S, Wild-Allen K, Johnson CJ, Macleod CK (2015) Quantification of the impacts of finfish aquaculture and bioremediation capacity of integrated multi-trophic aquaculture using a 3D estuary model. J Appl Phycol DOI: 10.1007/s10811-015-0714-2.

Abstract

Reduced water quality is a potential outcome from intensive finfish aquaculture. Integrated Multi-Trophic Aquaculture (IMTA) can mitigate the negative effects of dissolved nutrients emanating from fish farms by harvesting species that extract nutrients grown at adjacent sites. In this study a coupled 3D hydrodynamic, sediment and biogeochemical model was used to simulate an idealised temperate test estuary. A macroalgal based IMTA model was applied within the estuarine model, to examine the spatial pattern of phytoplankton production arising from increasing levels of finfish aquaculture and the capacity of *Macrocystis pyrifera* to bioremediate the impacts of nutrification. Through increasing fish farm waste loads of dissolved inorganic nitrogen (DIN) the water quality in the estuarine model was forced into a 'poor water quality' classification determined by annual mean concentration of chlorophyll. Hydrodynamic conditions ensured the majority of increase in primary production was restricted to the northern section of the estuary. A non-linear increase in phytoplankton biomass was simulated as a result of the occurrence of an additional autumn phytoplankton bloom under elevated fish farm nutrient loads. To evaluate the potential of IMTA to mitigate the nutrification from finfish aquaculture, macroalgae farms were introduced to the estuary model on adjacent farm sites. The model results demonstrated a strong spatial variability in the capacity of *Macrocystis pyrifera* based IMTA to reduce chlorophyll concentration. Siting macroalgae farms next to those finfish farms situated in areas of high natural phytoplankton production resulted in a 'good water quality' classification for the whole system however this arrangement was not optimal for removing DIN from the system. This demonstration of the use of IMTA to improve system wide water quality is valuable for regional planners and managers as it provides an analysis and quantification of a method to retain estuarine health and economic benefit.

4.1 Introduction

Aquaculture provided 43% of the world's total fish supply in 2012, increasing from 25% in 2000 (FAO 2014). Global fish production is predicted to reach 181 million tonnes by 2030, with 60% being supplied by aquaculture (Lem et al. 2014). Over half of aquaculture by weight is currently provided by mariculture (Kapetsky 2013), and this sector is expected to increase accordingly. Mariculture is predominately practiced in coastal waters, including estuaries where conditions are calmer and shore-based infrastructure and markets are more accessible. Sites suitable for aquaculture in the coastal regions are limited by production requirements of depth/exposure and social considerations such as recreational and culturally significant areas (FAO 2013). With limited space for coastal mariculture to expand in to, any increase in global production will partly involve an increase in intensity of farming in existing sites, potentially increasing impacts on the marine environment. In the case of finfish aquaculture, impacts from nutrient rich waste products are of particular concern.

Marine based finfish aquaculture favours open cages which allow dissolved and particulate nutrient enriched waste to deposit in the surrounding water. Waste output

of nitrogen (N) from fish farms is estimated to range from 60% - 85% of total feed nitrogen (Islam et al 2005; Wang et al. 2009), dependent on the type of feed used and feeding procedures. Of the total N returned to the environment about 60% - 85% is in dissolved form (Wild-Allen et al. 2010; Wang et al. 2009). Finfish (salmon) is a major aquaculture industry in southeast Tasmania. Total feed in salmon aquaculture industry alone is predicted to rise to 4 million tonnes per annum by 2020 (Bostock et al. 2010). Understanding the mechanisms by which exogenous nutrients output from finfish aquaculture affect estuarine primary production is of global interest.

Estuaries generally are subject to high rates of input of nutrients and carbon from both natural and increasingly, anthropogenic sources. The potential for phytoplankton biomass is set by the nutrient supply rate (Howarth 1988); however, in an individual estuary, other attributes (e.g. depth, hydrodynamics, climate) will also influence the rate of conversion of nutrients to biomass (Cloern 2001). Within an estuary, annual phytoplankton primary production can vary up to 10-fold spatially and 5-fold from year to year due to sinking, advection, growth and mortality processes (Cloern 2014). Hydrodynamic conditions set by bathymetry, tidal currents and river flow determine whether the estuary is well-mixed or stratified, which in turn determines both the production cycles and magnitude within the estuary (Mann & Lazier, 1991). Empirical studies on estuaries where nutrients are not limiting have had found temperature, residence time and light limitation can result in high nutrient low chlorophyll conditions (Phinney et al. 2004; Muylaert et al. 2005; Yoshiyama and Sharp 2006).

There is little doubt that finfish aquaculture has the potential to alter natural patterns of production in the surrounding water. The major forms of dissolved inorganic nitrogen (DIN) output from finfish aquaculture are ammonium and nitrate and both of these nitrogen species are readily assimilated by phytoplankton. DIN released from finfish aquaculture may result in increased primary production (both pelagic and benthic), which may then lead to algal blooms and produce cascading effects on the trophic web (Buschmann et al. 2009; Bonsdorff et al. 1997) and in worst case, result in eutrophication (Anderson et al. 2002; Carmona et al. 2006). However, in some instances an increase in phytoplankton production around fish cages has gone undetected due to an increase in top down control from zooplankton (Pitta et al. 2009). Wang et al. (2009) showed that input of dissolved N from Norwegian salmon farms although considerable is still less than 15% of the natural loading from ocean upwelling. However, inputs of nutrients from finfish farms are potentially available in summer months when light is plentiful, unlike natural sources from upwelling events or periods of high river flow, which are more common in winter and spring in temperate regions. Furthermore fish farm nutrients are input into the euphotic surface layers and therefore are able to promote production even under growth limiting conditions such as stratification and turbidity.

One proposed solution to address nutrification from finfish aquaculture waste is Integrated Multi-Trophic Aquaculture (IMTA) in which nutrient-extracting species such as macroalgae (dissolved nutrients) or shellfish (particulate nutrients) are grown alongside

farmed finfish to bio-remediate the farm waste outputs (Troell et al., 2009). Currently the focus in IMTA is on farm implementation (FAO 2009) where biomass of extractive species is matched to the output of finfish waste. Empirical studies have shown macroalgae grown near finfish cages exhibit high growth rates (Sanderson et al. 2008; Buschmann et al. 2009). Numerical approaches have been aimed at either providing realistic growth estimates of macroalgae or comparing DIN uptake (of macroalgae) to farm output in order to optimize IMTA (Broch et al. 2013, Ren et al. 2012). What is beyond the scope of empirical studies, and has so far not been addressed in numerical approaches, is the application of macroalgae based IMTA in multiple sites within an estuary in order to bioremediate negative impacts of nutrification from multiple finfish aquaculture leases.

Ecosystem models are increasingly being employed to help understand aquaculture-environment interactions. Models like DEPOMOD are used by regulatory bodies and the aquaculture industry to manage benthic impacts from finfish aquaculture arising from particulate deposition (Cromey et al. 2002). However to date there have been few modeling studies into the impact of DIN waste. One such numerical study by Wild-Allen et al. (2010) on the impact of DIN released from salmon aquaculture on a southeast Tasmanian estuary, indicated a shift in trophic status from oligotrophic to mesotrophic for 12% of the estuary and predicted that this could extend to 53% under a proposed 3-fold increase in farm leases. Ecosystem models like the one used in that study, are extremely useful tools which provide the capacity to test hypotheses beyond the scope of observational methods.

In this study a coupled 3D hydrodynamic, sediment and biogeochemical (BGC) model is applied to investigate the effect of nitrogen output from finfish aquaculture on autotrophic production within a theoretical temperate test estuary. A Macroalgal growth model is then applied (within the test estuary) to simulate IMTA close to the finfish farms, using giant kelp (*Macrocystis pyrifera*), which occurs naturally in southeast Tasmania. *Macrocystis pyrifera* was chosen primarily because it was the most successful in a comparison study of possible species conducted using the same growth model (Hadley et al. 2015), but also because IMTA using this species may accrue important conservation benefits given significant decline of *Macrocystis pyrifera* in eastern Tasmania (Johnson et al. 2011). In this investigation we increase the output from finfish farms to force the test estuary into a state of 'poor' water quality, and then examine the capacity of large-scale farming of giant kelp to bioremediate the system.

4.2 Model setup and simulations

4.2.1 The model

Macroalgae growth model

The growth model for *M. pyrifera* used in this study has been applied previously (Hadley et al. 2015), and is summarized as follows. The model has 5 state variables:

- ammonium (NH_4; $mg\ N\ m^{-3}$), which is the major form of dissolved DIN output from the finfish farms and also exists in natural concentration in seawater;
- nitrate (NO_3; $mg\ N\ m^{-3}$), which is also output from the farms and exists in natural background concentrations;
- N_s ($mg\ N\ m^{-3}$), the internal reserve of nitrogen for the macroalgae;
- N_f ($mg\ N\ m^{-3}$), the nitrogen fixed by macroalgae; and
- D ($mg\ N\ m^{-3}$), describing detritus from the macroalgae.

The model contains an allometric term for converting kelp biomass to height, which increases both its access to photosynthetically active radiation (PAR) and its vertical distribution in the water column, and therefore its access to nutrients. Hadley et al. (2015) used a parameter describing the refresh rate as a proxy for hydrodynamic conditions but here a 3D hydrodynamic model replaces this element.

The macroalgae growth model describes uptake and assimilation of nitrogen by *M. pyrifera* based on species-specific parameters (Table 4-A4.) The model requires four environmental inputs, *viz.* PAR, sea temperature and ambient nutrient concentrations of ammonium and nitrate. We have modularized the growth model to implement it in an idealized estuary model developed using the CSIRO's Environmental Modeling Suite (EMS) platform (EMS; http://www.emg.cmar.csiro.au/).

3D estuary model

Hydrodynamic, sediment and BGC processes within the test estuary are simulated using EMS, a coupled 3D hydrodynamic, 1D sediment and BGC model. The model has been applied in numerous case studies and includes a library of biogeochemical processes for flexible application across diverse coastal and estuarine systems. In particular the EMS code has been used to investigate the impact of nutrient loads on existing estuaries (Skerratt et al. 2013; Wild-Allen et al. 2010, 2013) and general flow dynamics through application in a test estuary (Herzfeld and Gillibrand 2015).

Hydrodynamic and sediment model

The 3D hydrodynamic model SHOC (Sparse Hydrodynamic Ocean Code (Herzfeld 2006)) used in this study is a 3D finite difference model. It utilizes an Arakawa C grid, uses a free surface, mode splitting and partial bottom cells. The model is based on the equations of momentum, continuity and conservation of heat and salt, employing the hydrostatic and Boussinesq assumptions. An orthogonal curvilinear grid is used in the horizontal and wetting and drying 'z' in the vertical. The model outputs include salinity, density, velocity, mixing coefficients, temperature and passive tracers. Vertical water column and sediment transport processes including sinking and re-suspension are resolved using the 1D sediment model MECOSED (Margvelashvili 2008.)

A test domain consisting of a river emptying into a funnel shaped estuary (typical of southeast Tasmania) of 20m depth (fig. 1) was constructed. There were 9 fixed pelagic layers [0.0 -1.0 -2.0 -3.0 -4.0 -5.0 -10.0 -14.0 -20.0 m] throughout the grid with a horizontal resolution of 1000 m. Freshwater is input into the head of the river. Records for flow rate, salinity and dissolved nutrients were taken from Bureau of Meteorology records (BOM, http://www.bom.gov.au/tas/observations/) for the Huon River for the period June 2009 to July 2010. Flow ranged from 10 – 500 cumecs and was smoothed to a sinusoid shape with a peak in mid-winter (July 15). There was 1 offshore boundary to the east with a 1m semi diurnal tide (Southern Hemisphere). SHOC requires inputs that include forcing due to wind, atmospheric pressure gradients, surface heat and water fluxes and open boundary conditions (e.g. tides). The meteorological forcing for SHOC is taken from the Bureau of Meteorology (BOM) records for the D'Entrecasteaux Channel and Huon Estuary (the site of finfish aquaculture in SE Tasmania) for June 2009 to July 2010.

A test estuary with simplified boundary conditions was used in this study to make results more interpretable. The test domain with smoothed river flow and symmetric shape reduces the variability introduced by these factors in models of actual estuaries. The greater variability can act to obscure the features or processes being investigated; in this case the impact of river flow on primary production and IMTA. The emphasis in this study is placed on the features of interest in the model, which still exist when applied to models of actual estuaries and therefore results can be generalized to those applications (Herzfeld et al. 2010a).

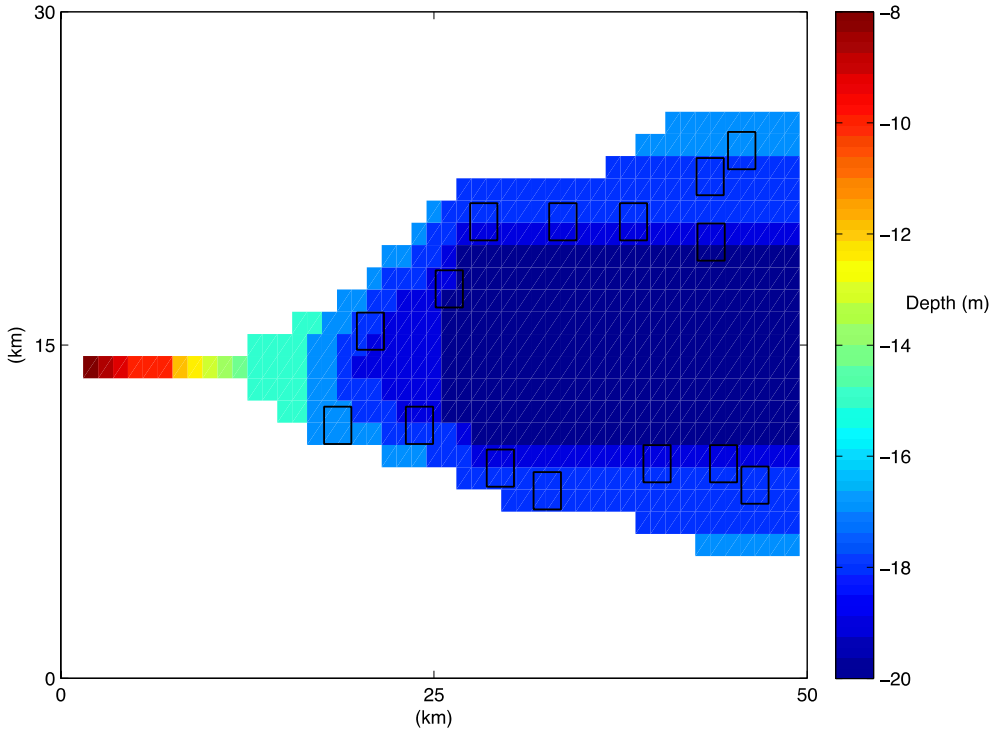

Figure 4.1: Theoretical 'test' estuary 50 km long and 20 km wide at the ocean boundary with a maximum depth of 20m. The model was forced with inputs from the river at one end and the ocean at the other. The black squares represent 15 sites where salmon farms operate within the estuary. The horizontal resolution was 1 km^2 for each grid cell. Waste N from finfish aquaculture was released at 0.5 - 15 metres depth. Farms located above/below the river line are referred to as being in the northern/southern section respectively.

BGC Model

The equations and parameters are given in appendix 4-A and a brief description is presented here. Biogeochemical tracers are advected and diffused, with sinking and re-suspension of particulates, and re-suspension and mixing of dissolved tracers, through the 3D model cells. Carbon, nitrogen, phosphorous and oxygen are cycled through both inorganic and organic phases comprising plankton, detritus, macrophytes and dissolved nutrients (Figure 4-2). The nitrogen, phosphorous and carbon stoichiometry is in the Redfield ratio 106:16:1 for plankton and the Atkinson ratio for macrophytes: 506:30:1 (C:N:P). Phytoplankton chlorophyll to nitrogen ratio is assumed fixed. The model includes large (diatoms) and small (flagellates) as the two functional groups of phytoplankton. These are predated upon by macro and micro zooplankton respectively. Of the three types of macrophytes modeled, seagrass and naturally occurring benthic macroalgae are grown in the epibenthic layer whereas farmed algae (*Macrocystis pyrifera*) is grown in the pelagic layers from 3 - 1 m depth. The maximum height of the macroalgae relative to the surface of the water is therefore 2m. The model also includes 4 types of particulate detritus (labile, pelagic, benthic and refractory), pools of dissolved organic carbon, nitrogen and phosphorous (DOC, DON and DOP) and dissolved inorganic carbon, nitrogen and phosphorous (DIC, DIN and DIP).

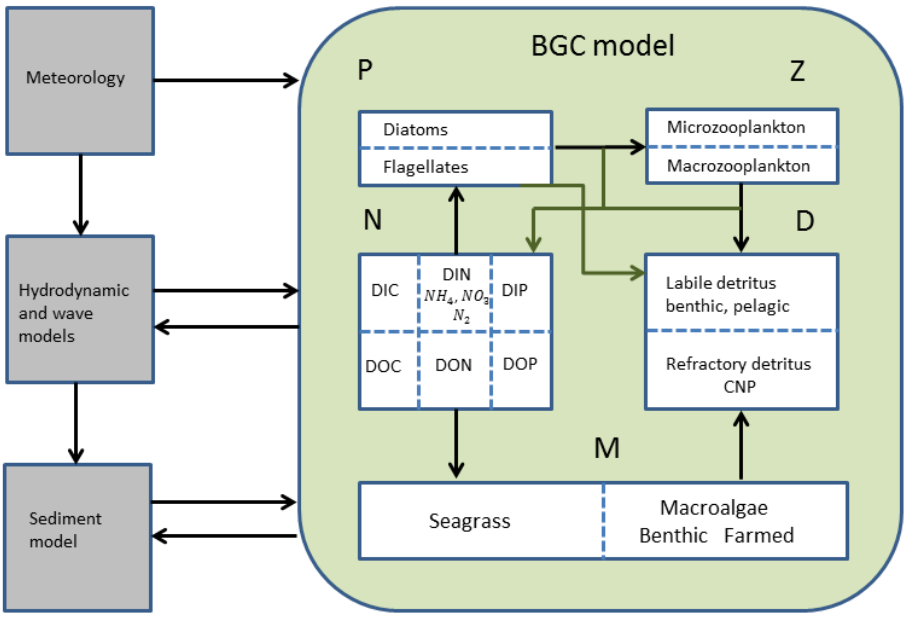

Figure 4-2: Hydrodynamic, sediment and biogeochemical model of estuarine processes. The macroalgal growth process model is nested in the 'biogeochemical' model. 5 compartments: nutrients (N); phytoplankton (P); zooplankton (Z); detritus (D) and macrophytes (M) are connected through processes such as uptake and mortality. Arrows show the direction of interaction between compartments.

DIN is available for autotrophic uptake and is modeled as ammonium and nitrate plus nitrite. Refractory detrital matter is remineralised to dissolved inorganic and organic matter over ~ 1 year. Dissolved organic material is considered highly refractory and remineralisation through breakdown by bacteria or chemical reaction takes ~ 2 years. Depending on oxygen availability, ammonium can then be converted into nitrate (nitrification) and nitrate can be denitrified to nitrogen gas (N_2 lost to the atmosphere). The ecological model updates tracer concentrations, which are returned to the hydrodynamic and sediment models at each ecological time step. The model was integrated with an adaptive 3D time step of 140 s for the hydrodynamic processes, and 1 hour for the biogeochemical processes.

4.2.2 Model Initialisation

The 'test' estuary was populated with 60 finfish farms each farm is 1 grid cell and is represented by a point source releasing DIN at a constant rate at depths between 0.5 - 15 m. We placed the finfish farms in groups of four (4 km^2 in total) in fifteen locations around the estuary (shown in Figure 4-1). The number of finfish farms was chosen so as to provide a major impact on the biogeochemistry of the 'test' estuary. Finfish farm waste discharge is simulated using point sources of nutrients (see Wild-Allen et al. 2010). The major nutrients released from the farms are detrital pelagic labile nitrogen, ammonium, nitrate, dissolved inorganic phosphorous and detrital refractory phosphorous. The ratio of these nutrients is kept constant and an increase in the intensity of finfish farming is modeled by an increase in the rate of each nutrient flowing in from the point source. The initial rate of discharge (from the finfish farms) was set at a value of 86.4 $\mathrm{kgN\ d}^{-1}$, as this value achieved a ratio of nitrogen input from aquaculture: river: ocean = 26:29:45; similar to that used in Wild-Allen et al. (2010) i.e. 20:20:60. The ratio of the forms of nitrogen input from each source varied between the three (Figure 4-3). The ocean and finfish input DIN only. The river output was ~75% refractory N and ~25% DIN. The river and ocean inputs were seasonally dependent whilst the finfish farms provided a constant supply.

DIN, temperature and salinity exit the ocean boundary at concentrations determined by the model, with concentrations flowing into the estuary set at seasonal averages for southeast Tasmania. Phytoplankton and zooplankton are modeled at the ocean boundary so that in flowing concentrations are the same as those exiting. The 'test' estuary is theoretical and so there are no historical records for spatially resolved tracer concentrations. Instead we use average concentrations typical of an estuary in SE Tasmania to initialize the model (Table 4-A5). For each scenario the model was run for 365 days, with the start date set to the 30th June 2009 (mid-winter).

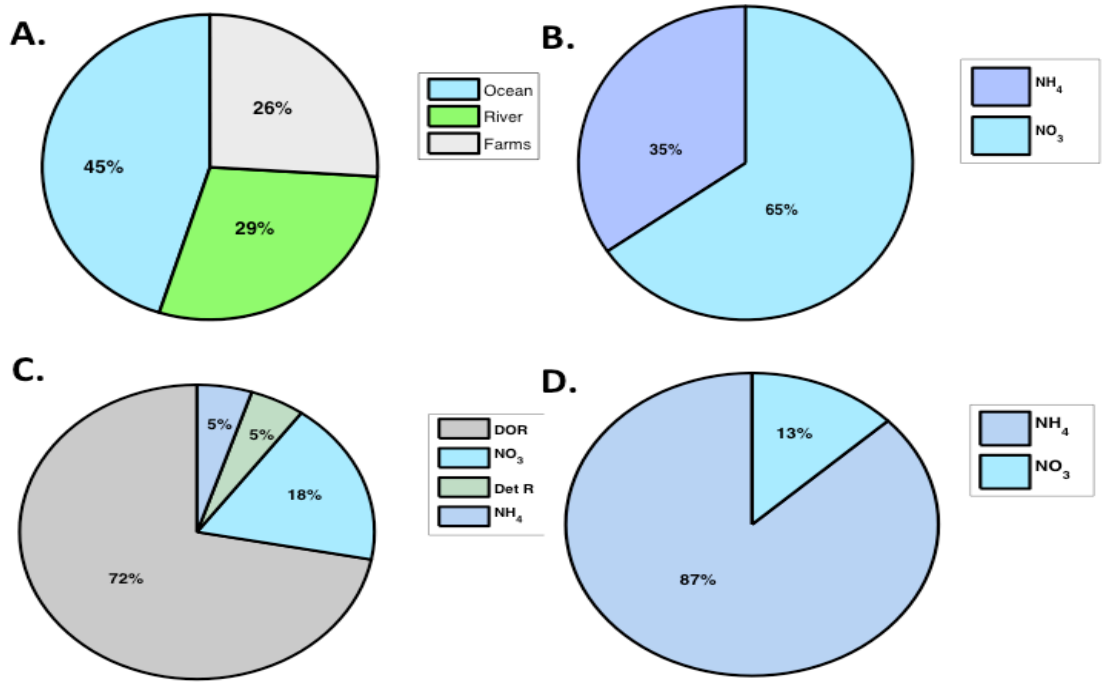

Figure 4-3: A. Ratio of annual input into the estuary from: ocean boundary ~3286 t N y^{-1}; river ~2106 t N y^{-1}; and fish farms ~1892 t N y^{-1} with the initial rate of finfish input set at 86.4 kg N d^{-1}. B. Ratio of the major sources of N from the ocean boundary. C. Ratio of major sources of N from the river. D. Ratio of major sources of N from the finfish aquaculture. The finfish aquaculture and ocean inputs are predominately DIN, which is readily taken up by autotrophs. River input is predominately in refractory form.

4.2.3 Model scenarios

4.2.3.1 Spatial pattern of phytoplankton primary production

Distribution of farm released tracers

An initial model run was used to establish the dispersal pattern of farm released 'tracers'. In this simulation a 'passive tracer' was introduced to track the path of farm-released tracers through the estuary subject to advection and diffusion only. This tracer was released from the farms at the same daily rate as NH_4 but was not taken up by the autotrophs. For this scenario boundary conditions stipulating no input of DIN from the ocean or river (although DIN was allowed to leave the estuary) were imposed. It is assumed autotrophic production will be predominately dependent on farm loads of DIN enabling a direct comparison between concentrations of the passive tracer, NH_4 and chlorophyll within the 'test' estuary.

Residence time of farm released tracers

An age tracer experiment (Mongin & Baird, 2014) was used to determine the residence time of water passing through the farm sites. The 'age' tracer τ was initialized to zero and a 'source' (S) tracer to 1 inside the farm grids and 0 elsewhere in the estuary.

The age tracer 'aged' at a rate of ψ = 1 day per day when inside the farm grids and decays (reduces in age) at a rate of $\theta = 0.1$ per day, when outside the farm grids according to

$\frac{d\tau}{dt} = \psi S$, inside the finfish farms,
$\frac{d\tau}{dt} = -\theta(1 - S)\tau$, outside the farms. (4-1)

From (4-1) it can be seen that when S=1 (inside the farm grids), the bottom equation = 0 and age tracer τ changes in value according to $\frac{d\tau}{dt} = \psi$ meaning that it ages (ψ is positive). Conversely when S=0 (outside farm grids), τ is determined by the equation $\frac{d\tau}{dt} = -\theta\tau$ and so reduces in value (grows younger as $-\theta$ is negative). As τ is advected and diffused like other dissolved tracers we can use this method to determine the fate of water that has passed through the farms. The decay represents processes such as advection and chemical reactions. Residence time has a strong influence of both phytoplankton and farmed macroalgae production.

Water quality

Water quality was defined in terms of chlorophyll concentration as per the ANZECC (2000) guidelines, which stipulate that 4 out of 5 water quality tests for chlorophyll, conducted within a period of a month, must exceed the threshold value in order for an estuary to receive 'poor' water quality classification. An ANZECC guideline value of 4 $\mathrm{mg\ Chl\ m^{-3}}$ was used to signify the point at which the test estuary displays poor water quality and is negatively impacted by finfish aquaculture. A series of model runs were conducted with finfish loading incrementally increased by 86.4 $\mathrm{kgN\ d^{-1}}$ (initial load) each time, to establish the relationship between nitrogen loading and phytoplankton primary production as determined by chlorophyll concentration; nitrogen is the limiting element for autotrophic growth in estuaries in the southeast Tasmanian region (Thompson et al. 2005). Nitrogen loads were increased until mean annual concentrations exceeded the ANZECC threshold for the top 10m of the whole estuary.

4.2.3.2 Bioremediation of water quality from IMTA

The 'water quality' scenarios were repeated with macroalgae farms included in the simulations. The algal farms were grown in the same grid cells as the finfish farms to simulate near field IMTA. The cultivation depth was between 1 - 3m, the optimal depth for *M. pyrifera* based on field IMTA studies (Buschmann et al. 2008). The initial concentrations of $\mathrm{N_f}$ and $\mathrm{N_s} = 0.1\ \mathrm{gN\ m^{-3}}$, for the *Macrocystis pyrifera,* giving an initial biomass of 140 $\mathrm{g\ m^{-3}}$ (wet weight). Both the end of season biomass of *M. pyrifera* and total remediated N ($= \mathrm{N_f} + \mathrm{N_s}$) was quantified for each site as finfish loading was increased along with the mean (annual and seasonal) chlorophyll concentration.

4.3 Model Results

4.3.1 Phytoplankton production within the estuary

Photosynthetically active radiation (PAR), temperature and salinity

The annual mean for PAR (top 1 m), water temperature (top 10 m) and salinity (top 1 m) were determined for the 'test' estuary from an initial model run (Figure 4-4). PAR was found to be lowest near the mouth of the river where the fresher water is high in colored dissolved organic matter (CDOM) with strong light attenuation. The average for PAR increases with distance from the river mouth and towards the ocean boundary. PAR (top 1 m) was higher at site B (near the ocean boundary) than at site A (near the river mouth) throughout the whole year, while mean temperature differed less than 1 °C between the two sites. There was a gradient in the temperature from the southern to the northern edge of the estuary; with a mean average difference of about 2 °C. Salinity displayed a similar pattern to PAR, which was not surprising given the link between fresh water and CDOM. Not surprisingly there was greater variation in salinity (in the top 1m layer) at site A (12-30 PSU) than at site B (25-30 PSU), however this variation was seasonally dependent. These results provided an indication of the variability of the conditions favoring autotrophic growth within the 'test' estuary.

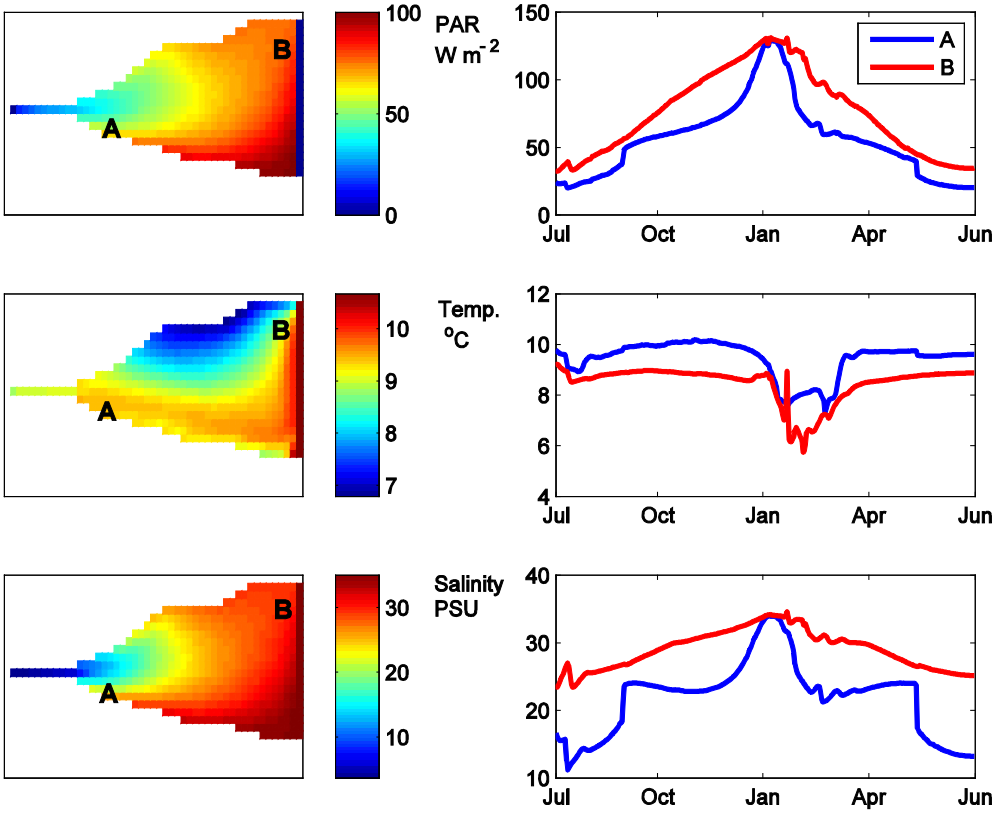

Figure 4-4: Top left: mean annual surface (averaged over the top 1 m) PAR (Wm^{-2}). Top right: seasonal variation in PAR (averaged over top 1 m) for two farm sites; A closest and B furthest from the mouth of the river (top). Middle left: mean annual sea (averaged over the top 10 m) temperature (°C). Middle

right: seasonal variation in temperature for sites A and B. Bottom left: mean annual (averaged over top 1 m) salinity (PSU). Bottom right: seasonal variation in salinity for sites A and B.

Water flow and exchange with the fish farms.

Mean annual residence times inside all fish farm sites ranged between 0.1-0.3 d. Instantaneous distributions of spatially resolved 'age tracer' at high and low river flow respectively, with 3D currents superimposed (Figure 4-5), clearly showed the relationship between residence time and water flow. Under high-river flow (Figure 4-5, left image) 'age tracer' released from the finfish farms in the southern section of the estuary travelled quickly towards the ocean boundary and out of the estuary with instantaneous residence times ranging from 0.1 – 0.3 d. The spatial distribution of the 'age tracer' showed streams of constant value travelling toward the ocean boundary. Changes in the values of the tracer aligned with current vectors i.e. faster currents produce lower residence time. Water travelling along the southern section passed through other farms en route to the ocean boundary and the 'age tracer' was reinforced.

In the northern section the residual flow was still directed towards the ocean but was slower. The residence time there ranged from 0.02 – 0.38 d. The two fish farms near the river mouth had low residence times due to a combination of high flow and no enrichment from other farms. The slower current through the rest of the salmon farms in the northern section resulted in higher residence times. The residual water motion (under high river flow) appeared to be moving in a circular pattern (eddy) around the farms in the northern section resulting in the observed spatial pattern, indicating farm released tracers reside in this region in elevated quantities.

The 'age tracer' was observed in very low concentrations in the center of the estuary indicating farm water did not reach there in significant quantities; for high and low flow. The dispersal pattern under low river flow showed the 'age tracer' was mainly concentrated within the salmon farms. The range of residence times was 0.28 – 0.55 d and 0.28 – 0.4 d for the northern and southern farms respectively. In effect, water parcels passing through the farms have high tracer concentrations only within or close to the farms. Once outside the farms the tracers have reduced 'naturally' to low levels.

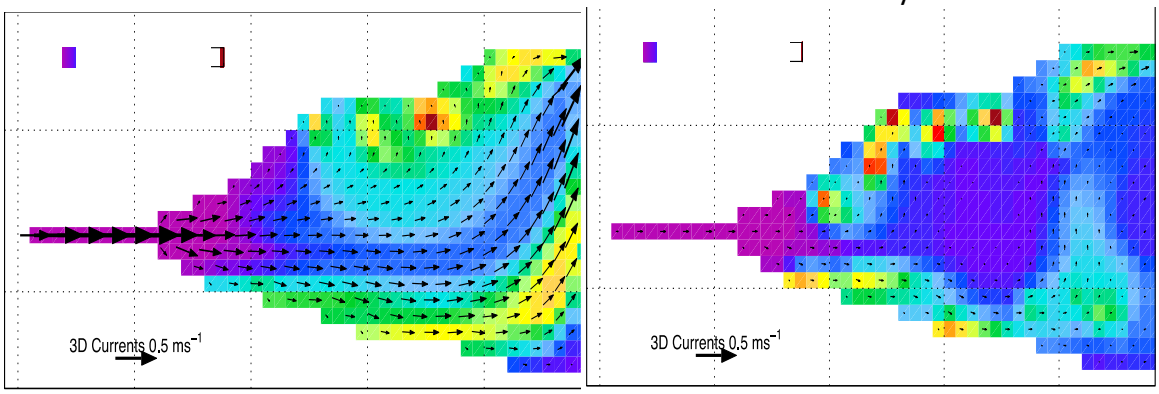

Figure 4-5: The instantaneous spatially resolved 'age' tracer with instantaneous 3D current overlaid. On the left are the results for high river flow (June 30th) and on the right are those for low flow conditions (January 1st).

Path of farm released tracers.

The 'passive tracer' released from the finfish farms accumulated in highest concentrations around the farm sites but reduced markedly towards the middle of the estuary (Figure 4-6). The pattern of dispersal was similar to that seen for the 'age tracer' under high flow. Farm released NH_4 accumulated around the salmon farms, but concentrations were much lower in those farms closest to the ocean boundary (particularly in the southern section). In contrast, chlorophyll concentration was highest around fish farms closest to the ocean but decreased considerably around farms near the river mouth. Although both tracers were released at the same rate 86.4 $kg\ d^{-1}$, the concentration of 'passive tracer' within the fish farms ranged from 8 – 20 $mg\ m^{-3}$, whereas for NH_4 the concentration ranged from 0 - 8 $mg\ m^{-3}$ due to local assimilation by biological and chemical filters.

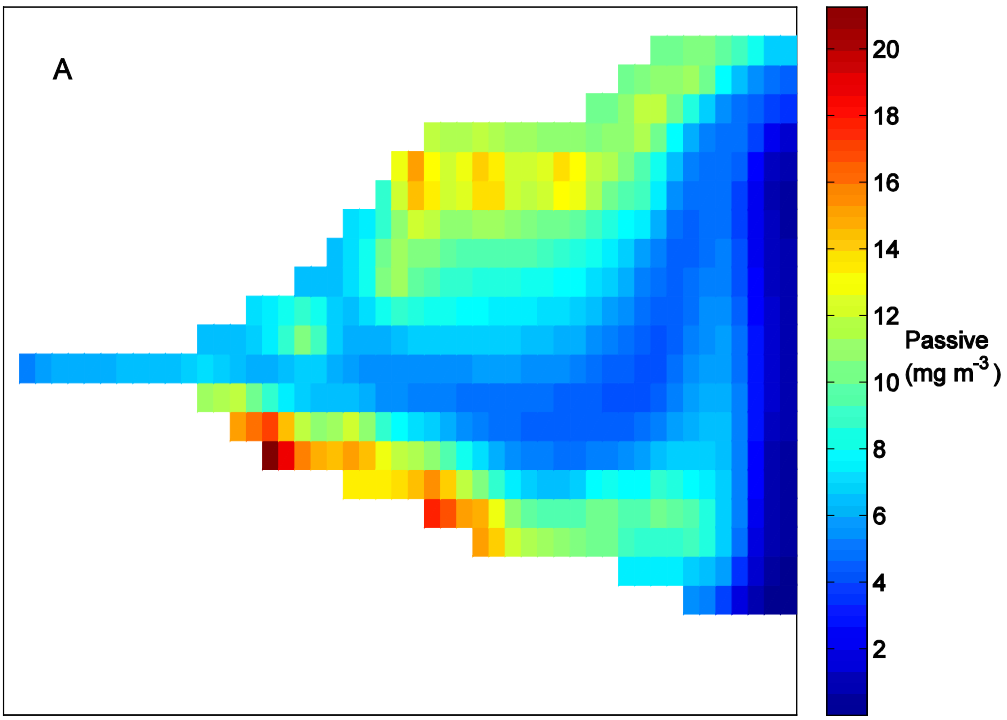

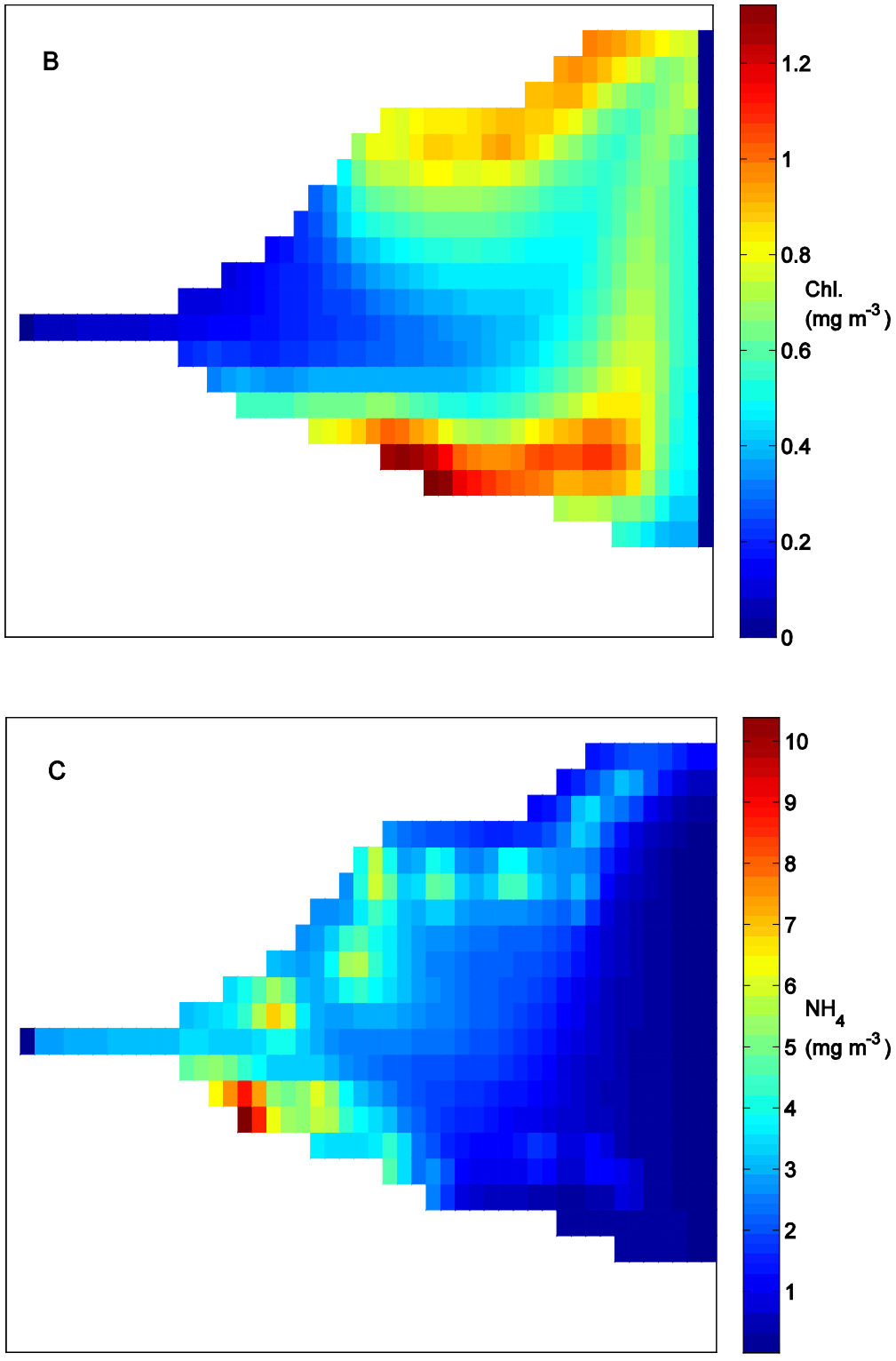

Figure 4-6: Annual mean concentration (top 10m) of the 'passive tracer' (A), ammonia (NH_4)(B) and chlorophyll (C). The 'passive tracer' accumulates around the farms in general with a greater pattern of dispersal in the northern section of the estuary. Ammonia is concentrated at the farms but is higher at

those near the mouth of the river in the southern section reducing significantly towards the ocean boundary. Chlorophyll is concentrated around the farms but is low around the mouth of the river and increases towards the ocean boundary.

Water quality

Mean annual chlorophyll showed a nonlinear relationship with increasing rates of fish farm loading (Figure 4-7). Depth integrated (10 m) mean chlorophyll concentrations increased from 1.07 – 2.75 mg chl m^{-3} as loadings increased from x1 - x20 initial loading (i.e. 86.4 $\mathrm{kgN\ d}^{-1}$), but jumped to 4.09 mg chl m^{-3} (> ANZECC value) when forcing was increased to x21 the initial loading. This equates to a 15-fold increase in production for the same incremental increase in load. That increase in production was due to a sustained autumn bloom. Chlorophyll concentrations in autumn jumped from a constant value of ~ 1 mg chl m^{-3} for all previous fish farm loads to over 4 mg chl m^{-3} at the critical load. In summer, mean chlorophyll concentrations were higher than the annual mean. Depth averaged (10 m) mean summer chlorophyll concentration for the estuary crossed the ANZECC threshold of 4 $\mathrm{mg\,chl\,m}^{-3}$ when fish farm loads were approximately x13 the baseline level.

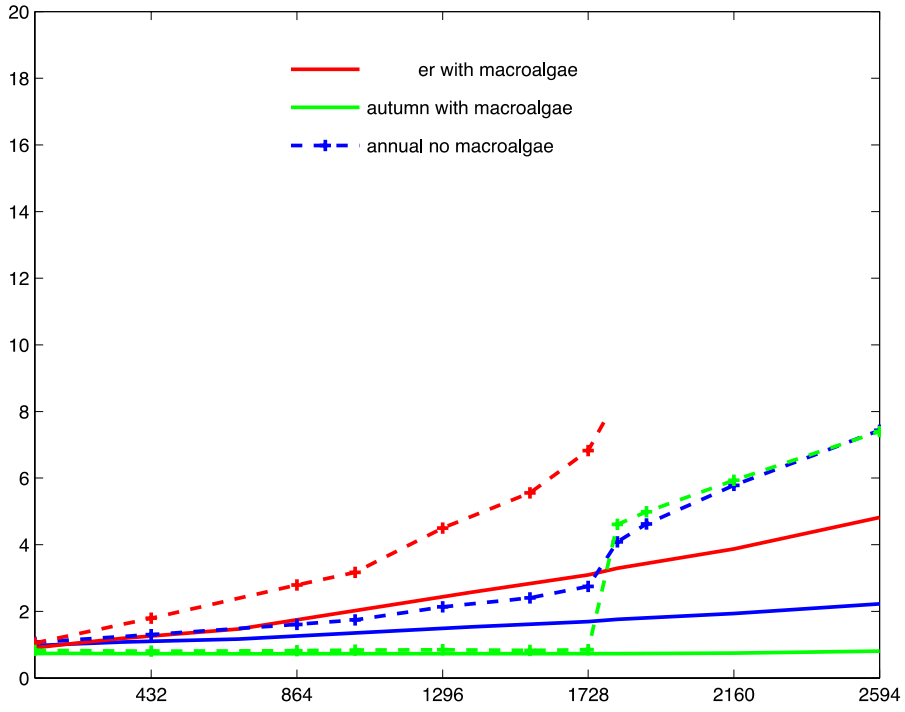

Figure 4-7: A comparison of the DIN loading from the salmon farms against the mean annual and mean summer concentrations of chlorophyll for the estuary. Key features are the strong non-linear response of Chl to farm loadings above 1730 kg N d^{-1} per farm, and the strongly mitigating effect of IMTA macroalgae.

The spatial distribution of chlorophyll showed that the majority of phytoplankton production is confined to the northern section of the estuary (Figure 4-8). As finfish

loading increased, mean chlorophyll concentration for the entire estuary was increasingly determined by the production in the northern section.

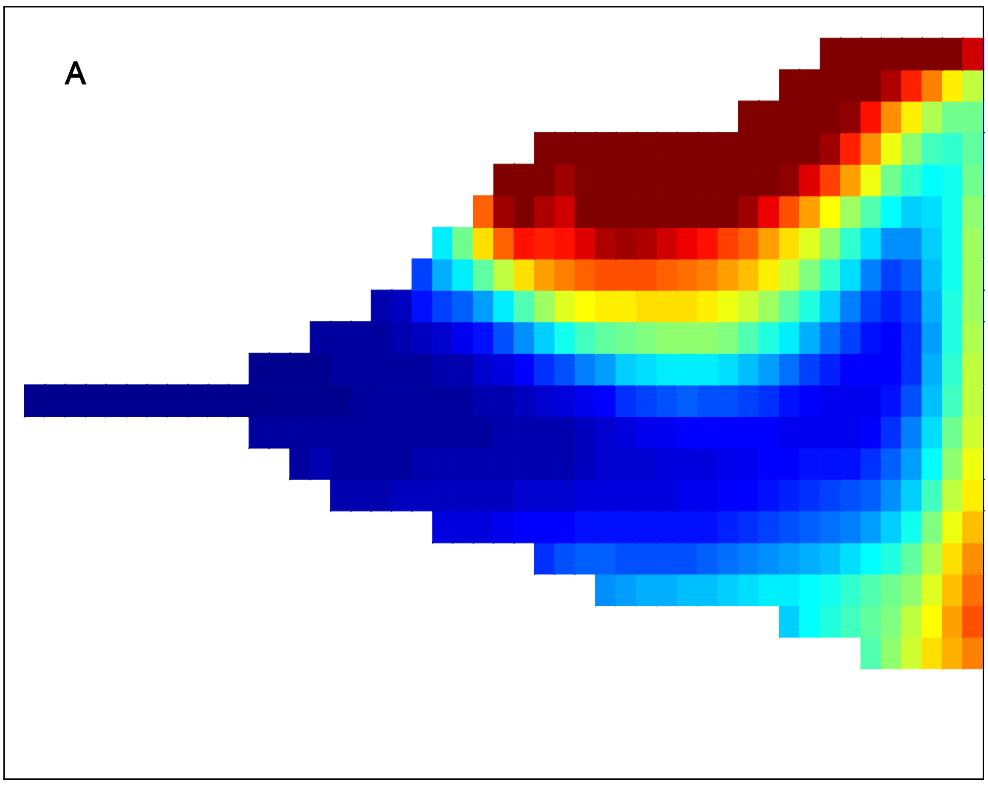

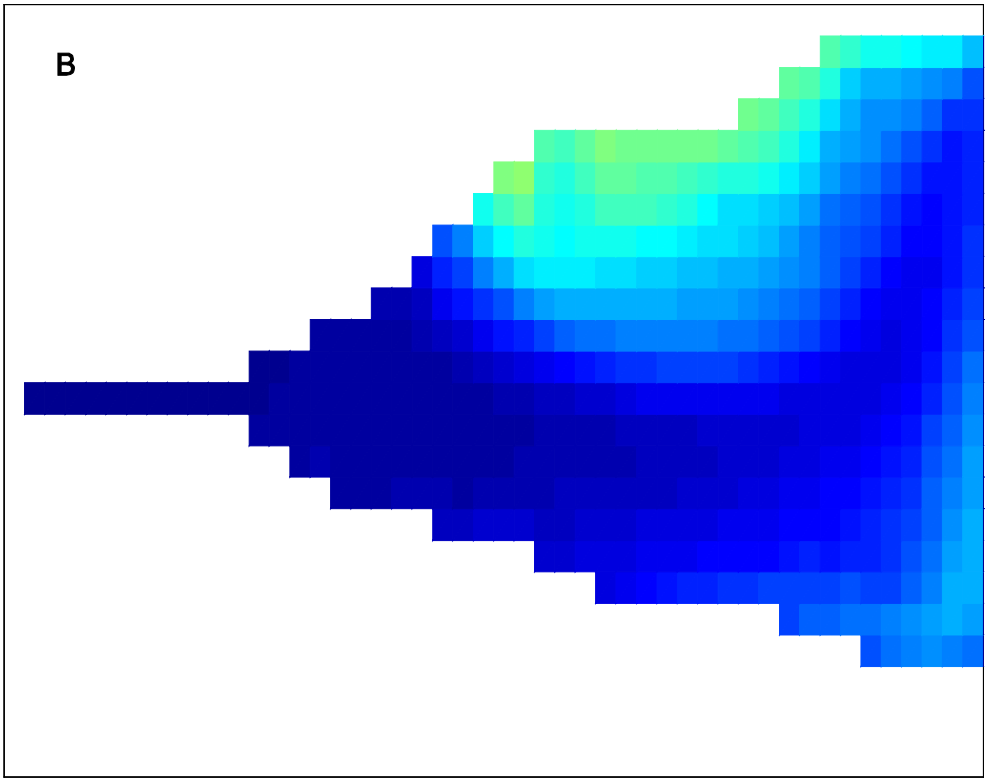
B

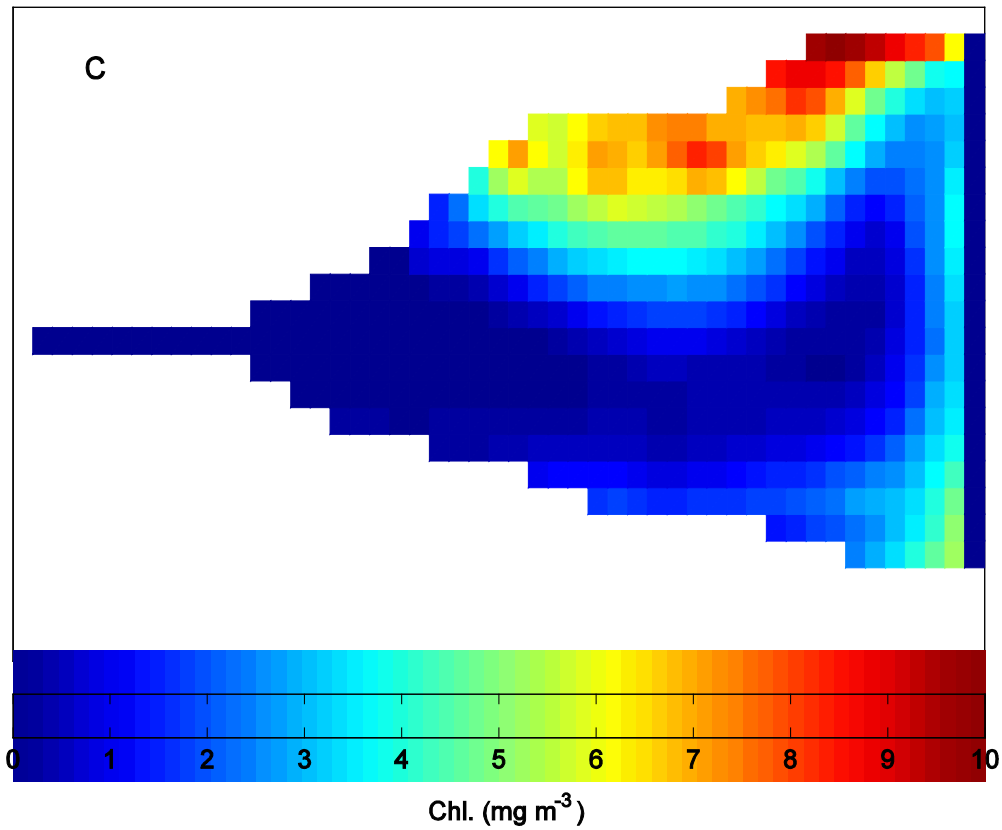

Figure 4-8: The depth averaged (10m) mean annual chlorophyll concentration for the estuary without macroalgae farms (A), with macroalgae farms (B) and the difference (C). The results are when the loading was at the critical level of 1728 kg N d^{-1}. Macroalgae based IMTA clearly reduces the chlorophyll build up attributed to the waste N from finfish farms.

4.3.2 Bioremediation of water quality using IMTA

When macroalgae farms were introduced into the estuary, the mean chlorophyll concentration only crossed the ANZECC threshold on one occasion; in summer when the load was at 2160 $\mathrm{kgN\ d^{-1}}$ or x25 the baseline loading. The loading versus chlorophyll concentration (Figure 4-7 solid line) remained linear (annually) with no autumn bloom, and phytoplankton primary production in the estuary is greatly reduced when macroalgal farms were operating. At the critical rate of fish farm loading 1814.4 $\mathrm{kg\ N\ d^{-1}}$(x21 baseline level), the mean annual chlorophyll concentration (from phytoplankton) was reduced from 4.09 (above the ANZECC threshold) to 1.76 (well below the threshold) mg chl $\mathrm{m^{-3}}$ with the introduction of the macroalgae farms into the test estuary. The spatial pattern for chlorophyll at the critical farm load (x21 initial loading) with and without IMTA gives a clear indication of the impact of IMTA in remediating water quality.

The spatial distribution for total macroalgal N ($= \mathrm{N_f} + \mathrm{N_s}$) associated with *M. pyrifera* production showed that locating algae farms in the southern section removed the most nitrogen (Figure 4-9) per farm. It is also apparent that in the southern section the total N removed by each algal farm reduces with proximity to the ocean boundary. Where macroalgae farms were located in the northern section the total N in the system was greatest near the ocean boundary and reduced with proximity to the river mouth. The modeled output suggested that a 20-fold increase in nutrient load from farms results in up to a 5-fold increase in the total N removed by macroalgae, from 10-50 to 50-250 $\mathrm{gN\ m^{-3}}$ dependent on where the macroalgae farms were located within the test estuary. Although algae farms in the southern section removed more N per farm, the farms in the northern section were almost solely responsible for bioremediation of the production increase resulting from the increase in finfish loading (shown in Figure 4-8).

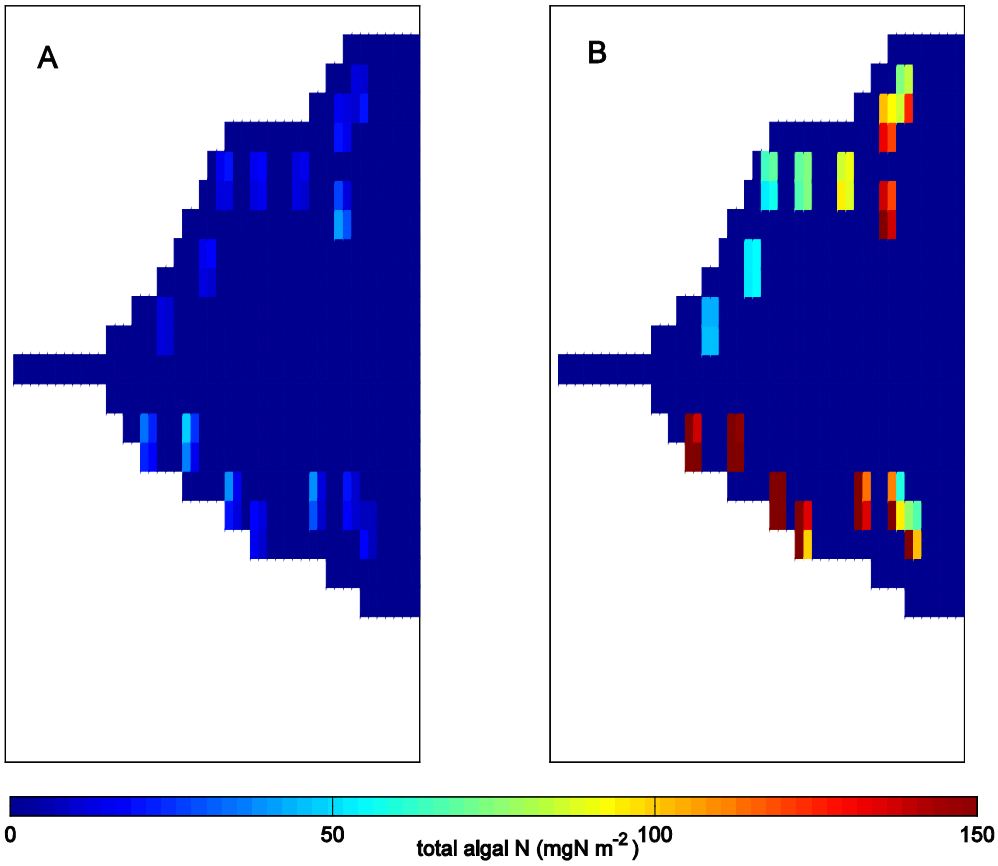

Figure 4-9: Mean annual end of season yield of total remediated nitrogen: stored + fixed ($= \mathrm{N_s} + \mathrm{N_f}$) at loadings of 86.4 (x1) (A) and 1814.4 $\mathrm{kg\ N\ d^{-1}}$ $(x21)$ (B).

At the critical finfish loading (x21), IMTA reduced the mean annual chlorophyll concentration in the estuary by: 57% in winter from 4.09 (i.e. above the ANZECC threshold) to 1.76 mg Chl $\mathrm{m^{-3}}$; and by 61% in summer from 8.41 to 3.29 mg Chl $\mathrm{m^{-3}}$ (Table 4-1). As loading was increased, the percentage of finfish released nitrogen removed by macroalgae (end of year) varied per site by as much as 15-fold at the lowest forcing used down to 8 times at the highest load, with the inter-site variation generally decreasing as loading increased. The %removal (average for estuary) of finfish DIN by farmed macroalgae ranged from 81% for the lowest finfish load to 30% for highest load; the ratio reduced monotonically with increasing loads.

Table 4-1: Effects of macroalgae in mitigating N loading from farms. Columns show chlorophyll concentrations at increasing farm loadings both with and without macroalgae cultivated for IMTA; Total DIN (stored and fixed) removed by macroalgae, showing the minimum, maximum and mean values for the sixty farm sites and the average annual percentage of farm nitrogen removed by IMTA macroalgae (annual farm DIN load – total macroalgae N)/(annual farm DIN load).

Load Released Per Farm	Mean Chlorophyll in Estuary $\mathrm{mg\ chl\ m^{-3}}$	Total removed N $\mathrm{gN\ m^{-2}\ y^{-1}}$	% finfish DIN removed

$kg\ N\ d^{-1}$

	No Macroalgae		Macroalgae		By site			
	Annual	Summer	Annual	Summer	Min.	Max.	Mean	Mean
86.4	1.07	1.06	0.97	0.91	6.4	100	25.8	81%
172.8	1.18	1.50	1.02	1.02	9.2	126	36.4	58%
345.6	1.30	1.80	1.08	1.20	15.6	158.0	55.2	44%
691.2	1.61	2.79	1.17	1.47	24.8	259.0	95.4	38%
1382.4	2.13	4.50	1.53	2.58	46.6	287.0	176.2	35%
1728.0	2.75	6.80	1.70	3.10	49.8	556.0	215.4	34%
1814.4	4.09	8.41	1.76	3.29	68.6	567.0	221.2	33%
2160.0	5.78	13.80	1.93	3.87	79.2	629.0	263.4	33%
2592.0	7.43	18.88	2.23	4.82	82.0	688.0	289.2	30%

4.3.3 Mass balance for the estuary

Mass balance for the system was calculated, including total net contributions from sediments, the river, ocean, farms and internal N sources, for 3 finfish farm loading rates of $86.4, 1296 \text{ and } 2160\ kg\ N\ d^{-1}$. The mass balance (Figure 4-10) showed that increasing farm loading increases the total N in the estuary. As the fish farm loading rate increases the ocean and river inputs became secondary sources for N input into the system (ocean and river sources shown are net inputs.) Moreover, increasing the fish farm loading results in a reduction in the relative net input from the ocean, meaning that a greater proportion of N in the estuary is lost across the ocean boundary. The total N from farmed macroalgae increases, as does natural production within the estuary as fish farm loading rates are increased. The ratio of N lost across the ocean boundary to that used in system production (including farmed algae) increased as loadings grew. Of the total N retained in the estuary, the percentage that is farmed macroalgae decreased from 45% to 41% at lowest and highest finfish aquaculture loads respectively.

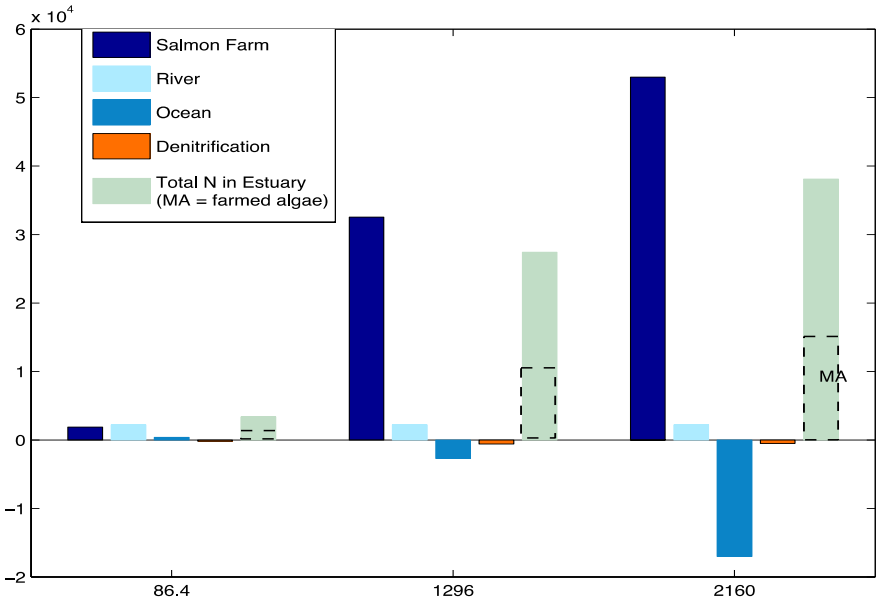

Figure 4-10: The nitrogen (N) mass budget for our system with each of our salmon farms forced at 86.4, 1296 and 2160 $\mathrm{kg\ N\ d^{-1}}$. Total N is for all sources in our estuary: phytoplankton, zooplankton, DIN, Refractory N, DON, and macrophytes including farmed macroalgae.

4.4 Discussion

4.4.1 Spatial pattern of phytoplankton primary production

The model results displayed a strong horizontal gradient in chlorophyll concentration in the test estuary. The combination of reduced PAR near the river mouth and low residence times, explains the pattern of production observed when DIN input was restricted to finfish aquaculture with no boundary inputs. This did not however, explain the increased concentration of primary production in the northern section of the estuary as N loading from the farms increased. Mean annual PAR was similar in the southern and northern sections and DIN was in high concentrations in the southern section also. The relative increase in chlorophyll concentration in the northern section compared to the south cannot be due to control of phytoplankton by zooplankton in the southern section, which has been observed in some oligotrophic aquaculture sites (Pitta et al 2009). In another numerical experiment the river was seeded with a slightly increased concentration of small phytoplankton resulting in increased phytoplankton production around the finfish farms in the southern section, including those at the river mouth. Transport processes were therefore driving the pattern of production.

In a numerical model of the D'Entrecasteaux Channel and Huon Estuary, Wild-Allen et al. (2010) found regions that were similarly sensitive to increasing loads of DIN from finfish aquaculture. These were areas categorized by high residence times and low CDOM where system DIN accumulated due to the residual flow in the system. A study by Saeck et al. (2013) on the impacts of flow events on phytoplankton production in an actual

river – estuary – bay system (Moreton Bay) also found that growth increased post flow in areas of nutrient accumulation and away from light limited zones. However, seasonal perturbations in hydrologic conditions (floods, drought etc.) make it difficult to predict the impact of anthropogenic nutrients on an estuarine ecosystem (Paerl et al. 2006). Using a range of forcing for river-flow could help examine production under extreme events. This study however, was primarily used to describe the seasonal influence of the river input on production. In general, studies on estuaries where nutrients were not limiting production found residence time, light and temperature to be defining factors in the spatio-temporal patterns of production (Saeck et al. 2013; Muylaert et al. 2005; Paerl et al. 2006).

In the test estuary, river flow flushed phytoplankton out of the southern section of the estuary for large parts of the year, accounting for the low mean annual chlorophyll concentrations in this area. At times of high-river flow a region of freshwater influence (Simpson 1997) was simulated in the northern section, which created a residual circular (eddy) current. Eddy circulations due to buoyancy driven currents have been observed in estuaries and bays (Fujiwara 2003; Ott and Garrett 1998) including the D'Entrecastaux Channel and Huon Estuary (Herzfeld et al. 2010). Tracers including nutrients and phytoplankton were recycled around the northern section of the test estuary in effect increasing their residence time. Oceanic phytoplankton was brought into this section of the estuary and then retained in the rotational flow, thus supporting high production rates. Import of ocean-derived phytoplankton is an important component of high production rates in estuaries (Cloern 2014.)

The circulation pattern in the northern section was partly responsible for the spatial asymmetry observed in phytoplankton production as finfish loading increased. River flow also acted to suppress this production in the southern section through flushing. In a study of a eutrophic tidal estuary, Maier et al. (2012) found blooms were strongly positively correlated with long residence times and ocean water influence and negatively correlated with increased river flow. In fact production has been shown not to increase in estuaries, even those impacted by heavy nutrification, if the dilution rate exceeds the growth rate of phytoplankton (Dugdale et al. 2012; Glibert et al. 2014). Primary production was relatively constant in the southern section as loading increased, which would lead to the assumption that the phytoplankton concentrations are being diluted.

The test estuary described in this model was naturally oligotrophic, with river and ocean N inputs and environmental forcing based on the Huon River and D'Entrecasteaux Channel system in Southern Tasmania. The Huon river discharge was high in CDOM, which rapidly attenuated PAR (Clementson et al. 2004) and could therefore act to suppress phytoplankton along a gradient emanating from the river mouth. In general though, phytoplankton production in a shallow estuary is unlikely to be light limited. Factors such as wind shear, bottom stress and tidal currents can work to increase mixing and bring phytoplankton into the photic zone (Cloern et al. 2014). It is important to note that the finfish farms deposit DIN at relatively shallow depths in the water column and at

a constant rate, increasing the likelihood that these nutrients are available for photosynthesis, particularly in close proximity to the farms. This is important for estuaries with high concentrations of light attenuating particles. PAR was heavily attenuated in the test estuary to the extent that it is virtually extinguished at depths greater than 2.5 m near the river mouth and 5 m near the coast in winter (10 m and 15 m respectively in summer). If thermal stratification were to occur the nutrients would still be available in the top layers, enabling production to occur. In any event production would not be nutrient limited, nor light limited in the upper layers. Under such conditions phytoplankton resupply into the surface layer, would most likely have an increasing influence on production in the estuary.

4.4.2 Bioremediation of water quality

At high nutrient loads the simulated autumn bloom resulted in the mean annual chlorophyll concentration exceeding the ANZECC threshold, resulting in a categorization of 'poor' water quality. Blooms occur when phytoplankton growth exceeds losses to advection or zooplankton grazing (Thompson et al. 2008). Plankton models of the type used in this study can exhibit constant bloom behavior when timescales associated with fluid stirring become slower than those associated with growth (Hernandez-Garcia and Lopez 2004). Modeling different species or including more species may alter the bloom dynamics. Similarly altering the river flow and thus residence time would similarly affect those dynamics. The study by Pitta et al. (2009) showed top down control to be responsible for the absence of increased production around salmon leases in oligotrophic waters in the Mediterranean. However, it was noted that small sized primary producers, which were easily grazed, dominated the phytoplankton community structure. Other work has shown that early growth of copepods resulting from a warmer winter can suppress spring blooms (Cloern et al. 2014.) In the test estuary a point was reached at which 'bottom up' stimulation of phytoplankton overcame 'top down' control from grazing. Fortunately the aquaculture industry also have a vested interest in avoiding this situation as phytoplankton blooms have the potential to cause stock losses in aquaculture farms as a result of oxygen depletion and poisoning from toxic species (Lansberg 2002). It is worth noting is that sustained blooms lasting several months have been observed in nature and these events were driven by extreme conditions involving high temperatures, high winds driving mixing and floods transporting large quantities of nutrients into an estuary (Nixon et al. 2008). In estuaries where finfish aquaculture is practiced and there is potential for environmental extremes, it would be worth investigating the impact of such events on primary production.

The focus in this study was on annual and seasonal changes in mean estuarine chlorophyll concentrations; however, the ANZECC threshold only needs to be exceeded

for 4 out of 5 tests conducted within the timeframe of one month for a system to be considered to exhibit 'poor' water quality. In summer the threshold was exceeded at loads x16 the initial value, which is much lower than the x21 loading required for the mean annual concentration to exceed the threshold. If the analysis were restricted to the northern section of the estuary only, and in summer, then the threshold would be exceeded at even lower loads. In summary, dependent on the location of sampling, 'poor' water quality may be designated at a relatively low intensity of aquaculture.

The introduction of macroalgae farms had a clear impact on water quality at all finfish loads whereby ANZECC guidelines were only exceeded at the highest load for summer. This was in effect a large bioremediation potential attributed to macroalgae farms; however, this was a theoretical exercise and the results cannot be validated with empirical data. It has been shown in field based studies that DIN waste from finfish aquaculture enhances the growth of macroalgae cultivated in close proximity to the cages (Sanderson et al. 2008; Buschmann et al. 2008). What this study shows is that removing waste DIN does not equate to reducing primary production. IMTA conducted in the southern section had little impact on primary production in the test estuary even if the macroalgae in those farms clearly benefitted from the finfish waste. In a study conducted in a high nutrient/low chlorophyll estuary it was shown that whilst residence time limited growth of suspended algae, attached micro and macroalgae were highly productive due to the fact for those species residence time is ostensibly unlimited (Phinney et al. 2004).

If macroalgae farming were concentrated only in the northern section of the estuary this would improve the water quality as much as if algae were farmed in both sections. Therefore successful bioremediation of the system could be achieved using only half the amount of algal farms, significantly reducing operational costs. Conversely, macroalgae farmed in the southern section returned the greatest biomass. If the purpose is to grow algae for profit then it would make sense to grow *M. pyrifera* in the south, or at selected sites elsewhere that returned the highest biomass yields, while growing *M. pyrifera* in the northern part of the estuary would optimize water quality.

4.4.3 Other considerations

The model results for algal biomass (table 1) were comparable to literature values at the lower rates of finfish forcing**.** A model of growth in *Saccharina latissima* (Broch et al., 2013) proposed that about 170 t fresh weight algae ha^{-1} could be achieved with 120 tN $y^{-1}$of nutrient waste released from fish farming. This study calculated an output of 200 t fresh weight algae could be achieved for the same forcing (assuming dry weight to be 10% of wet weight, and using *Macrocystis pyrifera* in the model and not *Saccharina latissima*). *Macrocystis pyrifera* grown in IMTA arrangements in Chile have returned biomasses ranging from 14.4 kg m^{-1} wet weight in 8 months (Gutierrez et al. 2006) to 66 kg m^{-1} wet weight in 5 months (Westermeier et al. 2011). These are similar to the mean biomass returned at the low to medium finfish loads respectively. Whilst it is important

that the model returned reasonable values for macroalgal biomass, the key aim of this study was to investigate system variability in IMTA yields and bioremediation potential.

In this study the DIN removal ranged (average over all sites) from 30% to 81% dependent on loading. Empirical studies such as that conducted by Abreu et al. (2009) put this figure more conservatively at around 10%. Once again the spatial variability found for this value was the important finding in the present study. Studies such as those by Abreu et al. (2009) extrapolate the results from small-scale experiments to estimate the quantity of biomass required to remove DIN waste from a full-scale finfish farm. It is not clear that there exists such a linear relationship in IMTA. Furthermore, estuarine dynamics may allow the DIN to cycle around the macroalgae farms enabling higher removal rates than if finfish released N passes once through a macroalgae field. In an estuary with many macroalgae fields in close proximity, farm waste may pass through several fields (as seen in the age tracer results) of macroalgae, which would in all likelihood increase the amount of N stripped from the water. It must also be acknowledged that in our study the horizontal resolution was $1km^2$ for each grid cell. This obviously influenced the amount of macroalgal biomass and subsequent DIN removal calculated by the model. However, the purpose of the investigation and overall findings were not affected by the grid size.

The highest finfish loadings used in this study were most likely unrealistic but were necessary to force the estuary into 'poor' water quality. In the D'Entrecasteaux Channel and Huon Estuary, finfish aquaculture outputs approximately 1784 tN/yr (Ross and Macleod 2012) and for the test estuary this value was 1892 tN/yr at initial loads. The estuaries are comparable in size and a x21 increase in farm loads would be excessive. However as mentioned previously, if finfish farms were confined to the southern section of the test estuary then it may not be possible to force the estuary into 'poor' water quality at any load. Conversely, if the entire exercise were restricted to northern section and for summer only, then the ANZECC threshold would have been exceeded at much lower loads.

4.4.4 Improvements to the model

Our test estuary is a theoretical model and this limits any assessment of its performance against observation. If, however, we were to base our model an actual estuary i.e. the site of large scale IMTA, it would still not be possible to validate simulations in which the forcing from finfish-derived N is increased beyond existing farming levels. This is an inherent problem in simulation modelling. The upper end of finfish loads used in the present study could be viewed as excessive; however, we have outlined the purpose and context for this level of forcing. One consideration however is the highest biomasses returned in the most productive farms (at highest loads) were approximately 3-fold that recorded by Westermeier et al. (2011) indicating that our self-shading algorithm may need to be re-examined in the underlying growth model (Hadley et al. 2015).

The model used a constant mortality term for the farmed algae; however, more realistic loss terms could be determined to account for distal erosion and frond loss caused by hydrodynamic forces which can account for up to 10% of the seasonal standing biomass in kelp farms (Zhang et al., 2012). This could impact on spatial variability of the standing biomass found in this study, which grew best in the areas of highest flow. The macroalgae model could also be extended to include carbon uptake, providing a more realistic growth estimates (Broch et al. 2013). Carbon ratios used in the model were constrained to the Atkinson ratio for parsimony however these ratios are known to vary which may affect growth estimates.

4.4.5 Conclusions and implications for IMTA

In the idealized estuary described in this study, we found the hydrodynamic conditions controlled the spatial and temporal pattern of natural phytoplankton production. Phytoplankton production peaked in the northern section despite the south having suitable conditions to support high phytoplankton growth rates. This was also important for locating macroalgae farms for bioremediation purposes, where it was more important to find areas of high natural phytoplankton production than areas with high levels of ambient DIN per se. If the purpose of IMTA is to maximize macroalgal biomass for economic purposes, then areas of lower natural production combined with higher DIN would appear more suitable. Most importantly, the choice of the macroalgae farm site determined whether or not bioremediation was successful. It is important to note that bioremediation is not simply the process of removing excess DIN output from the finfish farms. Bioremediation should mitigate the potential harmful effects of nitrification, which in this study was to avoid causing poor water quality as a direct result of excessive phytoplankton production and accumulation.

4.5 Appendix 4-A – Biogeochemical model equations and parameters

For each layer and grid location the time evolution of each model substance (**Y**) is the sum of conservative advection, diffusion and sinking processes (φ**Y**) and non-conservative biogeochemical rate processes (**βY**):

$$\partial Y/\partial t = -\varphi Y + \beta Y \qquad (1)$$

where $\varphi Y = (u\Delta Y + \Delta_H K_H \Delta Y) - (\partial/\partial z)K_Z(\partial Y/\partial z) + (\partial w_S Y/\partial z)$

and $\Delta = (\partial/\partial x) + (\partial/\partial y) + (\partial/\partial z)$; $\Delta_H = (\partial/\partial x) + (\partial/\partial y)$

[Here u is the velocity vector; K_H and K_z are the horizontal and vertical diffusion coefficients and w_S is the settling velocity.]

Table 4-A1: Non-conservative β terms for each biogeochemical model state variable (some at Redfield 106C:16N:1P or Atkinson ratio 550C:30N:1P)

Symbol	State Variable (Ratio)	Processes	β term
Nitrogen (mg N m^{-3})			
B_1	Small phytoplankton (R)	net growth, grazing, mortality	$\beta_{B1} = (\mu_{B1} - m_B)B_1 - g_1$
B_2	Large phytoplankton (R)	net growth, grazing, mortality	$\beta_{B2} = (\mu_{B2} - m_B)B_2 - g_2\phi_2 / r_{enc}$
B_3	Microphytobenthos (R)	growth, grazing, mortality	$\beta_{B3} = (\mu_{B3} - m_{B3}B_3)B_3 - g_2\phi_4 / r_{enc}$
N_s	Stored N (*M. pyrifera*) (-)	Net uptake, fixation, loss	$\beta_{Ns} = (u_{NsN1} + u_{NsN2})Q_{\min} / N_f - g_{ma}N_s - d_M N_s$
N_f	Fixed N (*M. pyrifera*) (A)	Net fixation, mortality	$\beta_{Nf} = g_{ma}N_s - d_M N_f$
M	Benthic Macroalgae (A)	net growth, mortality	$\beta_M = (\mu_M - m_M)M$

S	Seagrass (A)	net growth, mortality	$\beta_S = (\mu_S - m_S)S$
Z_1	Small zooplankton (R)	growth, mortality	$\beta_{Z1} = g_1 e - m_{Z1} Z_1^2$
Z_2	Large zooplankton (R)	growth, mortality	$\beta_{Z2} = g_2 e - m_{Z2} Z_2^2$
N_1	Nitrate (-)	uptake, nitrification(wc+sed), denitrification(sed)	$\beta_{N1} = -(\mu_{B1}B_1 + \mu_{B2}B_2 + \mu_{B3}B_3 + \mu_S S + \mu_M M + \mu_{BA})N_1/(N_1+N_2)$ $- u_{NsN1} Q_{\min}/N_f + r_N N_2 O/(K_O + O)$ $+ (1 - K_{OD}/(K_{OD}+O)) r_{Nsed} O^2 N_2/(K_O^2 + O^2)$
N_2	Ammonium (-)	uptake, mortality, defecation, remineralisation, nitrification(wc+sed)	$\beta_{N2} = -(\mu_{B1}B_1 + \mu_{B2}B_2 + \mu_{B4}B_3 + \mu_S S + \mu_M M + \mu_{BA})N_2/(N_1+N_2)$ $- u_{NsN2} Q_{\min}/N_f + d_M N_s + (1-\gamma)(m_{Z1}Z_1^2 + m_{Z2}Z_2^2) + (g_1+g_2)(1-e-\varsigma)$ $+ r_L(D_1+D_2)(1-\xi-\vartheta) + r_R D_3(1-\vartheta_3)$ $+ r_D N_3 - r_N N_2 O/(K_O+O) - r_{Nsed} O^2 N_2/(K_O^2+O^2)$
N_3	Dissolved organic N (-)	remineralisation	$\beta_{N3} = \vartheta r_L(D_1+D_2) + \vartheta_3 r_R D_3 - r_D N_3$
D_1	Pelagic labile detritus (R)	mortality, defecation, remineralisation	$\beta_{D1} = m_B(B_1+B_2) + m_{B3}B_3^2 + \gamma(m_{Z1}Z_1^2 + m_{Z2}Z_2^2)$ $+ \varsigma(g_1+g_2)(1-e) + d_M N_f - r_L D_1 + \mu_{BA}$
D_2	Benthic labile detritus (A)	mortality, remineralisation	$\beta_{D2} = m_S S + m_M M - r_L D_2$
D_3	Refractory detrital N (-)	remineralisation	$\beta_{D2} = \xi r_L(D_1+D_2) - r_R D_3$
Phosphorous (mg P m^{-3})			
P_1	Dissolved inorganic P (-)	uptake, mortality, defecation, remineralisation, desorption	$\beta_{P1} = -((\mu_{B1}B_1 + \mu_{B2}B_2 + \mu_{B3}B_3)R_{WP} + (\mu_S S + \mu_M M)A_{WP})$ $+ (1-\gamma)(m_{Z1}Z_1^2 + m_{Z2}Z_2^2)R_{WP} + (g_1+g_2)(1-e-\varsigma)R_{WP} - \mu_{BA}R_{WP}$ $+ r_L(D_1 R_{WP} + D_2 A_{WP})(1-\xi-\vartheta) + r_R E_1(1-\vartheta_3) + r_D P_2 + d_2 + d_3$
P_2	Dissolved organic P (-)	remineralisation	$\beta_{P2} = \vartheta r_L(D_1 R_{WP} + D_2 A_{WP}) + \vartheta_3 r_R E_1 - r_D P_2 + d_2 + d_3$
E_1	Refractory detrital P (-)	remineralisation	$\beta_{E1} = \xi r_L(D_1 R_{WP} + D_2 A_{WP}) - r_R E_1$

E_2	Unflocculated particulate inorganic P (-)	desorption, flocculation, immobilization	$\beta_{E2} = -d_2 - r_F E_2$ $\beta_{E2} = -d_2 - r_F E_2 - r_I E_2$ sediment
E_3	Flocculated particulate inorganic P (-)	desorption, flocculation, immobilization	$\beta_{E3} = -d_3 + r_F E_2$ $\beta_{E3} = -d_3 + r_I E_2 - r_I E_3$ sediment
E_4	Immobilized particulate inorganic P (-)	immobilization	$\beta_{E3} = r_4 E_2 + r_{E4} E_3$
Carbon (mg C m^{-3})			
C_1	Dissolved inorganic C (-)	uptake, mortality, defecation, remineralisation	$\beta_{C1} = -\left(\left(\mu_{B1}B_1 + \mu_{B2}B_2 + \mu_{B3}B_3\right)R_{WC} + \left(\mu_S S + \mu_M M\right)A_{WC}\right)$ $+\left(1-\gamma\right)\left(m_{Z1}Z_1^2 + m_{Z2}Z_2^2\right)R_{WC}$ $+\left(1-e-\varsigma\right)\left(\left(g_1 + \left(g_2 / r_{enc}\right)\left(\phi_2 + \phi_4\right)\right)R_{WC}\right)$ $+ r_L\left(D_1 R_{WC} + D_2 A_{WC}\right)\left(1-\xi-\vartheta\right) + r_R F_1\left(1-\vartheta_3\right) + r_D C_2$ $-\mu_{BA} R_{WC}$
C_2	Dissolved organic C (-)	remineralisation	$\beta_{C2} = \vartheta r_L\left(D_1 R_{WC} + D_2 A_{WC}\right) + \vartheta_3 r_R F_1 - r_D C_2$
F_1	Refractory detrital C (-)	remineralisation	$\beta_{F1} = \xi r_L\left(D_1 R_{WC} + D_2 A_{WC}\right) - r_R F_1$
Oxygen (mg O m^{-3})			
O	Dissolved oxygen (-)	growth, mortality, defecation, remineralisation	$\beta_{P1} = \left(\left(\mu_{B1}B_1 + \mu_{B2}B_2 + \mu_{B3}B_3\right)R_{WO} + \left(\mu_S S + \mu_M M\right)A_{WO}\right)$ $+\left(\left(1-\gamma\right)\left(m_{Z1}Z_1^2 + m_{Z2}Z_2^2\right)R_{WO}\right)O/\left(K_{OA}+O\right)$ $+\left(\left(1-e-\varsigma\right)\left(\left(g_1 + \left(g_2 / r_{enc}\right)\left(\phi_2 + \phi_4\right)\right)R_{WO}\right)\right)O/\left(K_{OA}+O\right)$ $-\left(r_L\left(D_1 R_{WC} + D_2 A_{WO}\right)\left(1-\xi-\vartheta\right) + \left(r_R D_3\left(1-\vartheta_3\right) + r_D N_3 + \mu_{BA}\right)R_{WO}\right)O/\left(K_{OA}+O\right)$
Mineral Suspended Solids (kg TSS m^{-3})			
T_1	Unflocculated solids (-)	flocculation, burial	$\beta_{T1} = -r_F T_1$ $\beta_{T1} = -\left(r_F + r_b\right)T_1$ for sediment

T_2	Flocculated solids (-)	flocculation, burial	$\beta_{T2} = +r_F T_1$	
			$\beta_{T2} = r_F T_1 - r_b T_2$	for sediment

Table 4-A2: Rate processes included in the state variable equations

Symbol	Process	Equation
$u_{NB1,2,3}$	Maximum phytoplankton uptake of N (mg N $s^{-1}cell^{-1}$)	$u_{NB} = \psi(\varepsilon_{N1} N_1 + \varepsilon_{N2} N_2)$
$u_{PB1,2,3}$	Maximum phytoplankton uptake of P (mg P $s^{-1}cell^{-1}$)	$u_{PB} = \psi \varepsilon_{P1} P_1$
$u_{IB1,2,3}$	Maximum supply of light to phytoplankton - portion respired (E $s^{-1}cell^{-1}$)	$u_{IB} = I_{av} k_a m_N - r\mu_B^{\max} m_{IB}$
u_{IB3}	Maximum supply of light to benthic algae – Portion respired (E $s^{-1}cell^{-1}$)	$u_{IB3} = \left(I_{botS} m_{NB}\left(1 - e^{-k_{a4} B3 dz}\right)/ B_3 dz\right) - r\mu_B^{\max} m_{IB}$
u_{NM}	Maximum benthic macroalgae uptake of N (mg N $s^{-1}m^{-2}$)	$u_{NM} = (\varepsilon_{N1} N_1 + \varepsilon_{N2} N_2)/\delta$
u_{PM}	Maximum benthic macroalgae uptake of P (mg P $s^{-1}m^{-2}$)	$u_{PM} = \varepsilon_{P1} P_1 / \delta$

u_{NsN1}	M. pyrifera uptake of nitrate (mg N g^{-1} dw d^{-1})	$u_{NsN1} = (V_{NO3}N_1/(K_{NO3}+N_1))((Q_{max}-Q)/(Q_{\max}-Q_{\min}))$
u_{NsN2}	M. pyrifera uptake of Ammonium (mg N g^{-1} dw d^{-1})	$u_{NsN2} = (V_{NH4}N_2/(K_{NH4}+N_2))((Q_{max}-Q)/(Q_{\max}-Q_{\min}))$
u_{IM}	Maximum supply of light to benthic macroalgae – portion respired (E $s^{-1}m^{-2}$)	$u_{IB} = I_{bot}\left(1-e^{-k_M M}\right)-r\mu_M^{\max}m_{IM}$
u_{NS}	Maximum seagrass uptake of N (mg N $s^{-1}m^{-2}$)	$u_{NS} = S\mu_S^{\max}\left(N_1+N_2\right)/K_N$
u_{PS}	Maximum seagrass uptake of P (mg P $s^{-1}m^{-2}$)	$u_{PS} = S\mu_S^{\max}P_1/K_P$
u_{IS}	Maximum supply of light to seagrass – portion respired (E $s^{-1}m^{-2}$)	$u_{IS} = I_{botM}\left(1-e^{-k_S S}\right)-r\mu_S^{\max}m_{IS}$
μ	Autotroph growth (d^{-1})	$\mu = \mu^{\max}R_N R_P R_I$ found in a look-up table of solutions to 3 simultaneous equations equating uptake and growth (to avoid explicitly modelling relative resources R_N R_P R_I for each autotroph): $u_N(1-R_N) = \mu_{\max}R_N R_P R_I m_N$ $u_P(1-R_P) = \mu_{\max}R_N R_P R_I m_P$ $u_I(1-R_I) = \mu_{\max}R_N R_P R_I m_I$
g_{mp}	*M. pyrifera* growth (d^{-1})	$g_{\max}l_L l_T l_Q$ maximum growth multiplied by limitation due to irradiance, temperature and N
l_I	Light limitation for *M. pyrifera* (-)	$\frac{e}{k*h}\left(e^{-\frac{I_z e^{-kh}}{I_s}}-e^{-\frac{I_z}{I_s}}\right)$
l_T	Temperature limitation for *M. pyrifera* (-)	$\frac{1}{1+\exp[-\varsigma_p(T-T_p)]}$

l_Q	Nutrient limitation for *M. pyrifera* (-)	$g\frac{\text{Q-Q}_{\min}}{\text{Q-k}_c}$
Q	Internal quotient of N For *M. pyrifera* (mg N g^{-1} dw)	$Q_{min}(1 + N_s N_f^{-1})$
h	Height of *M. pyrifera* (m)	$\max((0.00174\text{N}_f/\text{num\_fronds})^{1.047}, 1)$
μ_{BA}	Bacterial growth (d^{-1})	$\mu_{BA} = \mu_{BA\max}(\min\{u_{NBA}, u_{PBA}, u_{CBA}\})$ $u_{NBA} = (N_1 + N_2)^2/(K_{NBA} + N_1 + N_2)$ $u_{PBA} = P^2/(K_{PBA} + P)R_{WP}$ $u_{CBA} = r_{LM}(C_3 + F_2)/R_{WC}$
g_1	Small zooplankton grazing (mg N s^{-1}) (cell P cell Z^{-1} s^{-1}) (cell P cell Z^{-1} s^{-1})	$g_1 = (\min\{r_{ing}, r_{enc}\})(Z_1/Z_{1m})(B_1/B_{1m})$ where: $r_{ing} = \mu_{Z1}^{\max} e(Z_{1m}/B_{1m})$ $r_{enc} = (B_1/B_{1m})(\phi_{diff1} + \phi_{rmot1} + \phi_{shear1})$
g_2	Large zooplankton grazing (mg N s^{-1}) (cell P cell Z^{-1} s^{-1}) (cell P cell Z^{-1} s^{-1})	$g_2 = (\min\{r_{ing}, r_{enc}\})(Z_2/Z_{2m})((B_2/B_{2m}) + (B_4/B_{4m}))$ where: $r_{ing} = \mu_{Z2}^{\max} e((Z_2/B_{2m}) + (Z_2/B_{4m}))$ $r_{enc} = (B_2/B_{2m})(\phi_{diff2} + \phi_{rmot2} + \phi_{shear2}) + (B_4/B_{4m})(\phi_{diff4} + \phi_{rmot4} + \phi_{shear4})$
ϕ_{diff}	Diffusive encounter rate ($m^3 s^{-1}$cell Z^{-1})	$\phi_{diff} = (2BB.T/3\sigma\upsilon_K)(2 + r_B/r_Z + r_Z/r_B)$
ϕ_{rmot}	Relative motion encounter rate ($m^3 s^{-1}$cell Z^{-1})	$\phi_{rmot} = \pi(r_B + r_Z)^2(-w_S^2/(3U_P^2/3U_Z + U_Z) + (U_P^2/3U_Z + U_Z))$
ϕ_{shear}	Fluid shear encounter rate ($m^3 s^{-1}$cell Z^{-1})	$\phi_{shear} = 1.3(K_Z/\nu_K)^{0.5}(r_B + r_Z)^3$
r_F	Flocculation rate (s^{-1})	$r_F = r_{F10}$ for SS > 10 psu $r_F = r_{F10}(SS - 6)/4$ for 6 < SS < 10 psu

$d_{2,3}$	Desorption of P (mg P $m^{-3}s^{-1}$)	$d_2 = pT_2 p_{ak}\left(E_2 / T_2 p_{ak} - P_1 O/\left(K_{PA} + O\right)\right)$ $d_3 = p_a T_2 p_{ak}\left(E_3 / T_2 p_{ak} - P_1 O/\left(K_{PA} + O\right)\right)$

Table 4-A3: Derived model variables

Symbol	Derived Variable	Equation
X	Phytoplankton chlorophyll (mg Chl m^{-3})	$X = \left(B_1 + B_2 + B_4\right) Q_{XN}$
Kd	Attenuation coefficient (m^{-1})	$Kd = k_w + k_{fw}\left(35 - SS\right)/35 + k_{a1}B_1 + k_{a2}B_2 + k_{a4}B_4$ $+k_{dt}\left(D_1 + D_2 + D_3\right) + k_n N_3 + k_t\left(T_1 + T_2\right) + k_m M + a_{cs}N_f$
I_{av}	Layer mean PAR (E m^{-2} s^{-1})	$I_{av} = \left(Q_{QW} / AV\right)\left(I_{top} - I_{bot}\right)/ Kd.dz$ where $I_{bot} = I_{top} e^{-Kd.dz}$
I_{botM}	PAR below macroalgae (E m^{-2} s^{-1})	$I_{botM} = \left(Q_{QW} / AV\right) I_{bot} e^{-k_M M}$
I_{botS}	PAR below seagrass (E m^{-2} s^{-1})	$I_{botS} = \left(Q_{QW} / AV\right) I_{botM} e^{-k_S S}$
I_{botB4}	PAR below microphytobenthos (E m^{-2} s^{-1})	$I_{botB4} = \left(Q_{QW} / AV\right) I_{botS} e^{-k_{a4} B_4 dz}$

Table 4-A4: Model parameters.

Symbol	Autotroph Parameters	Large Phyto-plankton B_2	Small Phyto-plankton B_1	Micro-phyto-benthos B_4	Sea Grass S	Macro-algae M
r_B	Radius (m)	1.0E-5	2.5E-6	1.0E-5	N/A	N/A
μ_{max}	Max growth rate (d^{-1})	1.25	1.25	1.35	0.1	0.02
r	Respired fraction of μ_{max} (-)	0.025	0.025	0.025	0.025	0.025
k	Specific absorption cross section ($m^2 mg\ N^{-1}$)	0.0018	0.0024	0.0018	1.0E-5	0.001
m_B	Mortality term (d^{-1})	0.14	0.14	0.0001 ($d^{-1}(mgN\ m^{-3})^{-1}$)	0.00275	0.01
K_N	Half saturation constant for N uptake in sediment (mg N m^{-3})	N/A	N/A	N/A	15.0	N/A
K_P	Half saturation constant for P uptake in sediment (mg P m^{-3})	N/A	N/A	N/A	15.0	N/A
Symbol	**Zooplankton Parameters**	**Large Zoo-plankton Z_2**	**Small Zoo-plankton Z_1**	**Optical Parameters**		**Value**
r_Z	Radius (m)	$5.0E^{-4}$	$12.5E^{-6}$	Background attenuation of sea water		0.1
e	Growth efficiency (-)	0.38	0.38	CDOM attenuation coefficient of fresh water (m^{-1})		2.2
μ_{max}	Maximum growth rate at 15˚C (d^{-1})	0.6	3.0	Detrital specific attenuation coefficient (m^{-1})		0.0038
U_Z	Swimming velocity (m)	$1.5E^{-3}$	$2.0E^{-4}$	TSS specific attenuation coefficient ($m^{-1}kg^{-1}\ m^{-3}$)		30

ζ	Fraction of growth inefficiency lost to detritus (-)	0.5	0.5	Dissolved organic nitrogen specific attenuation coefficient ($m^{-1}mgN^{-1}m^{-3}$)	0.0009
m_Z	Mortality (quadratic) rate ($d^{-1}(mgN\ m^{-3})^{-1}$)	0.004	0.02		
γ	Fraction of mortality lost to detritus (-)	0.5	0.5		
Symbol	**Detritus & Remineralisation Parameters**	**Value**	**Symbol**	***M. pyrifera* Parameters**	**Value**
r_L	Pelagic labile detritus breakdown rate (d^{-1})	0.1	g_{mp}	Maximum growth rate (d^{-1})	0.2
r_R	Refractory detritus breakdown rate (d^{-1})	0.0036	V_{NH_4}	Maximum uptake rate (NH_4) ($mg\ N\ gdw^{-1}d^{-1}$)	8.0
r_D	Dissolved organic matter breakdown rate (d^{-1})	0.00176	V_{NO_3}	Maximum uptake rate (NO_3) ($mg\ N\ gdw^{-1}d^{-1}$)	10.3
ϑ_L	Fraction of labile detritus converted to DOM (-)	0.01	K_{NH_4}	Half saturation constant (NH_4) ($mg\ N\ m^{-3}$)	74.2
ξ	Fraction of labile detritus converted to refractory detritus (-)	0.19	K_{NO_3}	Half saturation constant (NO_3) ($mg\ N\ m^{-3}$)	182.0
ϑ_R	Fraction of refractory detritus converted to DOM (-)	0.01	Q_{max}	Max internal nitrogen ($mg\ N\ m^{-3}$)	25.0
r_N	Maximum water column nitrification rate (d^{-1})	0.1	Q_{min}	Minimum internal nitrogen ($mg\ N\ gdw^{-1}$)	7.0
r_{Nsed}	Maximum sediment nitrification rate (d^{-1})	20.0	K_c	Half growth constant ($mg\ N\ gdw^{-1}$)	6.0

K_O	O2 half saturation rate for nitrification (mg O m^{-3})	500.0	T_0	Optimal Temperature (°C)	12.0
K_{OD}	O2 half saturation rate for denitrification (mg O m^{-3})	10000.0	T_r	Range of Optimal Temperature (°C)	1.0
K_{OA}	O2 half saturation rate for aerobic respiration (mg O m^{-3})	500.0	I_S	Saturation irradiance ($E\ m^{-2}s^{-1}$)	0.000134
			a_{cs}	Nitrogen Specific Shading ($m^2\ mg\ N^{-1}$)	0.0001
			d_m	Mortality Rate (d^{-1})	0.003
			Num_fronds	Number of Fronds (-)	7.0

Table 4-A5: Initial concentrations of autotrophs and zooplankton

Symbol	State Variable (*mg m^{-3}*) (**g m^3*)	Value (Water column, sediment)	Symbol	State Variable (*mg m^{-3}*)	Value (Water column, sediment)
B_1	Small phytoplankton	(0.1, 0.01)	M	Benthic Macroalgae	(10.0, N/A)
B_2	Large phytoplankton	(1, 0.01)	S	Seagrass	(10.0, N/A)
B_3	Microphytobenthos	(0.01, 100.0)	Z_1	Small zooplankton	(0.5, 0.001)
N_s	Stored N (*M. pyrifera*) *	(0.1, N/A)	Z_2	Large zooplankton	(0.5, 0.001)
N_f	Fixed N (*M. pyrifera*) *	(0.1, N/A)			

CHAPTER 5
INVESTIGATION OF BROAD SCALE IMPLEMENTATION OF IMTA IN A TEMPERATE ESTUARY USING A 3D MODEL

Preface: The final objective of this thesis was to provide a quantification of the capacity of IMTA to reduce the impacts of finfish aquaculture on the D'Entrecasteaux Channel and Huon Estuary in southeast Tasmania. A 3D estuarine model was used to quantify these impacts in the original study. This chapter similarly uses a similar estuarine model to examine IMTA.

IMTA is able reduce phytoplankton production increases under a range of finfish loads; however this reduction decreased with loading. The effect of harvesting, farm size and cultivation period was also examined. These strategies are shown to both increase bioremediation capacity of IMTA in general and also allow some control over the seasons in which IMTA is most effective.

At the time of thesis submission, this work was due to be submitted to a refereed journal and is presented below in pre-submission form. The citation for the intended publication is:

Hadley S, Wild-Allen K, Johnson CJ, Macleod CK (2015) Investigation of broad scale implementation of IMTA in a temperate estuary using a 3D model.

Abstract

Results from a coupled physical-biogeochemical model simulation of a temperate Australian estuary and marine channel demonstrate that macroalgae-based Integrated Multi-Trophic Aquaculture (IMTA) can achieve up to 30% reduction in the excess water column chlorophyll concentration resulting from low and high intensity finfish aquaculture. Finfish aquaculture is increasingly recognized as an important solution to the issue of food security in future planning. There is however a need to understand the ecosystem effects of additional inputs of dissolved inorganic nutrients as a result of finfish aquaculture and to provide management solutions for any potential risks associated with increased production. A fully coupled 3D hydrodynamic, sediment and biogeochemical model was used to investigate changes in water quality brought about by salmon aquaculture in the D'Entrecasteaux Channel and Huon Estuary in southeast Tasmania. Macroalgae based IMTA was simulated in a range of scenarios and the efficacy of this method for mitigation of environmental responses to dissolved inorganic nutrient loading from salmon aquaculture was investigated. We found that an increase in finfish farm inputs resulted in an increase in primary production, trending this naturally oligotrophic region to mesotrophic. In our simulated estuary, macroalgae grew best around the finfish aquaculture sites, and IMTA with macroalgae was successful in reducing water column chlorophyll concentration. Simple optimization strategies formulated around cultivation period, farm area and harvesting increased the chlorophyll reducing capacity of IMTA, with reductions in excess of 30% of excess chlorophyll under low aquaculture loads. Our findings suggest that IMTA could have an important impact on reducing negative effects of finfish aquaculture on water quality, and we recommend further empirical studies to confirm the potential of near field bioremediation.

5.1 Introduction

Recent studies into the effects of waste output from finfish aquaculture have demonstrated that nutrient enrichment of the surrounding water can to lead to ecosystem changes (Buschmann et al. 2008; Jiang et al. 2010; Wild-Allen et al. 2010). Aquaculture is a growing industry with global production in 2012 at 66 million tonnes of foodfish, including a contribution from Australia of 80 thousand tonnes (FAO 2014). Coastal finfish aquaculture uses open cages as they are easily assembled and allow waste dispersal into surrounding water, thus reducing costs (Bostock et al. 2010). Inshore aquaculture operations are often sited in sheltered waterways and estuaries, which are areas of high ecological diversity. Cloern et al. (2001) highlighted the variability in the responses of coastal ecosystems to nutrification, where biological and chemical 'filters', flow regimes, bathymetry, light conditions and optical properties of the water column interact to determine system response to nutrification from anthropogenic inputs. Without knowledge of the system response it is particularly difficult to manage industries that introduce bio reactive nutrient

rich waste as a byproduct. For dissolved nutrients subject to advection and diffusion, the system wide effects can be particularly difficult to quantify without the use of longitudinal studies from purpose designed monitoring systems. Several studies have recommended that further research is needed to determine the risk of adverse interactions between finfish aquaculture farms and the environment and to identify potential management responses (Buschmann et al. 2009; Eng et al. 1989; Wu 1995.)

Whilst it makes good economic sense for farmers to minimize waste feed output, finfish respire ammonium and excrete faeces and so in an open cage system waste nutrient outputs are unavoidable. Consequently the ability of an ecosystem to assimilate wastes will be the primary determinant of the carrying capacity of the water body. Models for waste output of dissolved inorganic nitrogen (DIN) (Islam et al. 2005; Wang et al. 2012) suggest that as much as 65% of total feed derived nitrogen can be returned to the water column, with up to 45% of this quantity in dissolved form. Consequently integrated multitrophic aquaculture (IMTA) has been proposed as a significant new approach for remediation of the effects of the dissolved nutrients (Troell et al. 2009, Buschmann et al. 2009).

In IMTA, extractive species (e.g. macroalgae to take up DIN waste) are grown next to the fed 'primary' species (e.g. finfish). In addition to mitigating nutrification there is potential for economic benefit from the sale of the macroalgae. Field studies have shown the benefit of growing macroalgae species near fish farms for both algal growth and nutrient removal (Abreu et al. 2009; Buschmann et al. 2008; Sanderson et al. 2008; Westermeier et al. 2011). Much of the current focus for modeling macroalgal based IMTA has been on the optimisation of ratios of fed to extractive species, with the approach combining empirical data with process models to establish a realistic DIN sequestering potential for selected species of algae (Broch et al. 2013; Ren et al. 2012). The FAO (2009) have highlighted the need for research into the technical implementation of integrated mariculture at the farm level. However, an equally important consideration is to determine how the spatial distribution of finfish aquaculture within an estuary affects the impact of waste DIN as this can inform the implementation of IMTA. Annual phytoplankton primary production within estuaries can vary up to 10-fold spatially and 5-fold from year to year due to sinking, advection, growth and mortality processes (Cloern 2014). Modelling at the estuarine level is therefore essential to realistically assess and optimize IMTA activity.

Wild-Allen et al. (2010) used a fully coupled hydrodynamic, sediment and biogeochemical model to examine the effects of salmon aquaculture on a temperate estuary in southeast Tasmania. Their results suggested that a proposed increase in salmonid aquaculture would result in large areas of the estuary shifting from oligotrophic to mesotrophic classification in terms of mean chlorophyll concentration. An IMTA process model developed by Hadley et al. (2015) was used to compare the bioremediation capacity of three functionally different species of macroalgae, with the giant kelp *Macrocystis pyrifera* clearly showing greatest

potential (the other species were *Ulva lactuca* and *Porphyra umbilicalis*). In the present study we use a simulation of the southeast Tasmanian estuary studied by Wild-Allen et al. (2010) to quantify the bioremediation potential of *Macrocystis pyrifera*. Primary phytoplankton production in the estuary is investigated under low and high aquaculture-derived nitrogen loads, with and without farmed *Macrocystis pyrifera*, to quantify the magnitude of the IMTA effect.

5.2 Methods

5.2.1 Model location

Although the model used in this study includes the Derwent Estuary we only consider results in the D'Entrecasteaux Channel and Huon Estuary, which contain finfish aquaculture in southeast Tasmania. The D'Entrecasteaux Channel and Huon Estuary (DCHE) form a connected water body in southeast Tasmania (Figure 5-1), characterized by a cool temperate maritime climate dominated by zonal westerly winds with seasonally driven rainfall. The Huon Estuary is a drowned river valley with a strongly stratified (salt wedge) water column at the head, partially mixed at the mouth, and is intermediate between wave- and tide-dominated (Butler 2006). The D'Entrecasteaux Channel lies between Bruny Island to the east and the main island of Tasmania, with the mouth of the Huon Estuary bisecting it. The 'Channel' connects to the Derwent Estuary through a narrow passage in the north section and opens to the Tasman Sea in the south. The region supports a thriving salmon aquaculture industry, has a relatively low population and shows relatively minor impacts from anthropogenic sources (Parsons 2012).

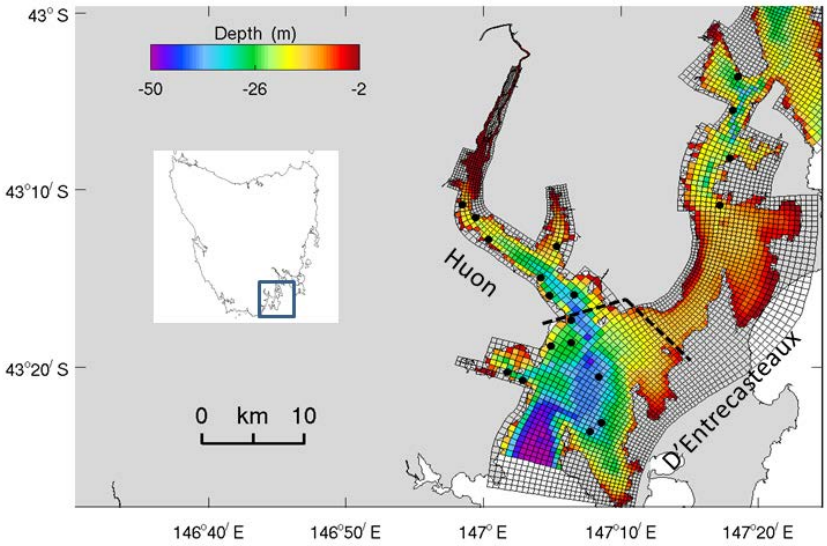

Figure 5-1: Schematic of the D'Entrecasteaux Channel and Huon Estuary showing the model grid, with water depth shown in color. The salmon farms are shown as black dots in the estuary.

5.2.2 Model Description

The biogeochemical model applied on the Derwent Huon D'Entrecasteaux (DHD) grid has evolved through a series of case studies in the area including the Derwent Estuary Ecological Risk Assessment (Parslow et al. 2001), the Aquafin CRC study of the D'Entrecasteaux Channel (Wild-Allen et al. 2005), the Huon Estuary study (CSIRO Huon Estuary Study Team 2000) and the Derwent Estuary modelling study (Herzfeld et al. 2005a; Margvelashvili 2005; Wild-Allen et al. 2013; Skerratt et al. 2013). Each study has addressed specific environments and ecological questions resulting in the development, implementation and testing of a diverse range of model components, which have been synthesised into the CSIRO environmental modelling suite (EMS). The DHD model is similar in design to both the Derwent and D'Entrecasteaux - Huon models (Wild-Allen et al. 2010, 2013) however the grid now fully connects these 2 large estuarine systems. The DHD model is implemented on a fine model grid with fully coupled hydrodynamic, sediment and biogeochemical model components.

Hydrodynamic model

The 3D finite difference hydrodynamic model SHOC (Sparse Hydrodynamic Ocean Code; Herzfeld 2006) advects and diffuses physical tracers (e.g. temperature and salinity) through cells in the model grid. The horizontal coordinates are provided using an orthogonal curvilinear grid with resolution ranging from <100 m in the upper Derwent and Huon estuaries and coastal cells to a maximum ~1 km in the deeper waters at the ocean boundaries. For computational efficiency the upper parts of the Huon and Derwent rivers were resolved in 2D surface cells. The vertical grid was comprised of 25 z coordinates (layers) plus the surface (air-water) and

epibenthic (sediment-water) layers which vary dynamically in thickness (m) (-60.0 -50.0 -40.0 -30.0 -25.0 -21.0 -17.0 -14.0 -12.0 -10.2 -9.0 -8.0 -7.1 -6.3 -5.6 -5.0 -4.5 -4.0 -3.5 -3.0 -2.5 -2.0 -1.5 -1.0 -0.5 0.0). Inputs to SHOC include the meteorological forcing for wind speed and direction, cloud cover, pressure and humidity, which were provided from the Bureau of Meteorology operational meteorological product ACCESS (2014). The hydrodynamic model is nested within regional and local scale ocean models, which provide temperature, salinity, sea level, tide and velocity conditions to the local model at the open boundaries. There was forcing for flow from the Huon, Derwent and 3 smaller rivers (Jordan, North-West Bay and Esperance). The local hydrodynamic model was integrated with an adaptive 3D time step of 30s and 2D time step of 3.75s (small time steps are necessary for numerical stability in high-resolution parts of the grid). The vertical transport processes for the water column and sediment, including advection, diffusion, re-suspension and sinking, are resolved using the sediment model MECOSED (Margvelashvili 2008.) The model runtime ratio in fully coupled mode was approximately 60:1 (i.e. 60 simulated days achieved in 1 day of simulation), which permits simulation of a seasonal hindcast.

Biogeochemical Model

Carbon, nitrogen, phosphorous and oxygen are cycled through both inorganic and organic phases comprising plankton, detritus, macrophytes and dissolved nutrients (Figure 5-2). Dissolved inorganic nitrogen (DIN) is available for autotrophic uptake and is modeled as ammonium, nitrate and nitrite. Dissolved inorganic carbon and phosphorous (DIC and DIP) are taken up by autotrophs in quantities that satisfy the Redfield (C:N:P = 106:16:1) and Atkinson (506:30:1) ratios for phytoplankton and macrophytes respectively. The model includes 3 types of particulate detritus (labile pelagic, labile benthic and refractory) and pools of dissolved organic carbon, nitrogen and phosphorous (DOC, DON and DOP). Detrital matter is remineralised to dissolved inorganic and more refractory organic matter. Dissolved organic material is considered highly refractory and remineralisation occurs through slow breakdown by bacteria or chemical reaction. Dependent on oxygen availability, ammonium is converted into nitrate (nitrification) and nitrate can be denitrified (in the sediment layer) to nitrogen gas (N_2 lost to the atmosphere).

The model includes 4 types of phytoplankton and 3 types of macrophytes including farmed macroalgae (*Macrocystis pyrifera*.) Phytoplankton chlorophyll to nitrogen ratio is assumed fixed at $7\ \mathrm{mg\ N\ mg\ Chl^{-1}}$. Modeled autotroph growth is determined by access to nutrients (nitrogen and phosphorous) and diurnally variable photosynthetically active radiation (PAR) which is calculated from hourly incident surface PAR. Surface PAR is attenuated through the water column by seawater, coloured dissolved organic substances (CDOM), and organic and inorganic particles. Phytoplankton is predated upon by macro and micro zooplankton with C:N:P composition at the Redfield ratio. Plankton that sink to the bottom are considered deceased and returned to detrital pools in the sediment. Biogeochemical dissolved

nutrients are advected and diffused, while particulate matter also sinks and is re-suspended. There are 3 zones, *viz.* pelagic, epi-benthic and sediment. At each ecological time step (1 hr in this study) the conservative ecological processes are integrated (using an adaptive time-step) and updated tracer concentrations are returned to the hydrodynamic and sediment models. The model equations and parameters are given in Appendix 5-A.

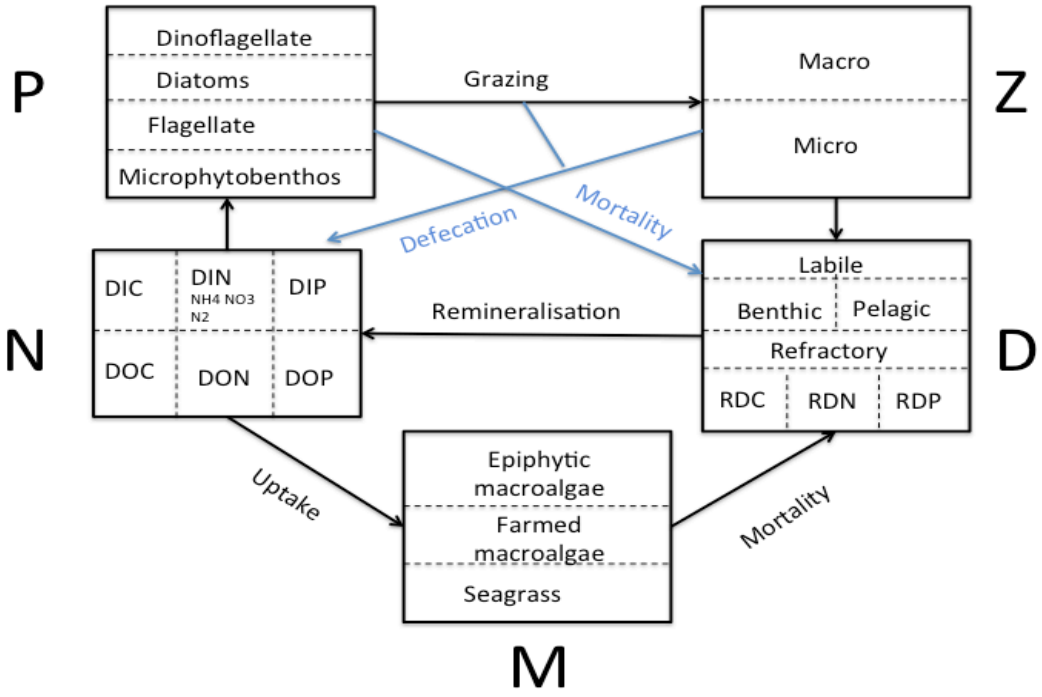

Figure 5-2: Schematic of biogeochemical cycle used in the EMS model. 5 compartments: nutrients (N); Phytoplankton (P); Zooplankton (Z); Detritus (D) and Macrophytes (M). The arrows represent a transfer (with direction) between compartments.

Farmed macroalgae growth model

The growth model for farmed macroalgae (*Macrocystis pyrifera*) used in this study has been applied previously by Hadley et al. (2015), and is summarized here. The uptake and assimilation of nitrogen by *Macrocystis pyrifera* is based on species-specific parameters (Table A4) and requires the environmental inputs of PAR, sea temperature, ammonium (NH_4) and nitrate (NO_3). NH_4 is output as waste from salmon aquaculture and along with NO_3 is present in natural concentrations in seawater. These two forms of DIN are taken up by *Macrocystis pyrifera* into intracellular pools and subsequently fixed into the cellular structure to create more biomass, with a small fraction (Q_{min}) being used to support basic cellular functions. The intracellular N is thus modeled in two forms, stored and fixed nitrogen, N_s and N_f respectively. Uptake rate is dependent on the ambient concentration of DIN, the internal quota of macroalgal N (Q, proportional to the ratio N_s: N_f) and the biomass of macroalgae. N_s is fixed at a rate controlled by PAR, temperature and Q.

Carbon and phosphorous are also fixed so that C:N:P for *M. pyrifera* is in the Atkinson ratio. Kelp mortality is set at a constant rate, which accounts for all causes including partial mortality such as distal erosion, predation and natural senescence. N_s is returned to the water as labile detrital N, C and P and N_s is returned as NH_4. An allometric term is used to convert *M. pyrifera* biomass to height, which increases the access to photosynthetically active radiation (PAR). Hadley et al. (2015) used a refresh rate parameter as a proxy for hydrodynamic conditions, which in this study is replaced by the 3D hydrodynamic model. We have modularized the growth model to implement it within the CSIRO EMS model.

5.2.3 Initialisation of Biogeochemical model

Loads of carbon, nitrogen and phosphorous enter at the Derwent Estuary across the marine boundary, from the Derwent River and from a number of point source discharge locations throughout the region. For the Huon Estuary and D'Entrecasteaux Channel the nutrient sources are the marine boundary, Huon River and point source discharges (including sites of finfish aquaculture). Fluxes from marine and river sources are modeled as boundary conditions to the model. Loads from industry, sewage treatment plants (STPs) and fish farms are included as point source loads delivered at specific locations and depths into the model domain.

At the marine boundaries all tracer concentrations were specified with the 'upstream condition', a conservative scheme where the model determines out-flowing concentrations but in-flowing concentrations are specified. Inflowing nitrate and dissolved oxygen concentrations were derived from regression analysis on observed concentrations of temperature and salinity (Wild-Allen and Rayner 2014); phosphorous was estimated using the molar Redfield ratio of 102C:16N:1C on nitrate. Climatology's of in-situ observations of phytoplankton were constructed for the mouth of the Derwent and south D'Entrecasteaux area, and this chlorophyll data was partitioned between plankton groups based on historical observations of species composition and by assuming a fixed nitrogen:chlorophyll ratio of 7 mgN: 1mgChl. (Crawford et al. 2009). Zooplankton was estimated as half of the corresponding phytoplankton biomass.

The model was forced at the head of the Huon estuary with Huon River flow and sediment and biogeochemical tracers (nitrate, ammonium, DIP, labile and refractory detritus, suspended particulate matter, DON, oxygen and plankton biomass) estimated from sediment and nutrient loads and flow rates similar to those reported in Wild-Allen et al. (2010) using an 'upstream condition'. The minor rivers (i.e. Northwest Bay rivulet and Esperance River) were specified as point source loads. The adjacent Derwent Estuary was forced similarly with Derwent River data and the minor Jordan River as a point source load.

Point source loads from sewage treatment plants (STP) and industry were collated from local councils and major industries in the model domain as well as the Department of Primary Industries, Parks, Water and Environment (DPIPWE.)
There were 19 active fish farm leases located in Huon and D'Entrecasteaux (Figure 5-1). Data (collected from DPIPWE) describing monthly feed load to each lease was converted to estimated dissolved and particulate waste load assuming full consumption of feed pellets; based on a Food Conversion Ratio (FCR) for the Tasmanian industry of 1.35 (i.e. 1.35 kg of dry feed produces 1 kg of fish), a digestibility co-efficient of 90%, the nitrogen content of feed (7.2%N) and the nitrogen content of the fish produced (3% N). Of the total feed 5% and 0.8% were assumed to be discharged by the fish as waste nitrogen and phosphorous respectively, with 85% estimated to be in dissolved form (ammonium) (Wild-Allen et al. 2010). The fish farms deposit waste at depths of 0.5-15m. There were six STP's operational in the D'Entrecasteaux Channel and Huon Estuary (13 in the Derwent Estuary.) Annual loads for point sources, rivers and marine boundaries for DCHE are shown in table 5-1. Inputs from the marine boundaries and rivers followed a seasonal pattern, whereas the STP's and fish farms were more uniform throughout the year.

Table 5-1: Shows the inputs of nitrogen into the DCHE. Input of rivers is Huon (90%) and two smaller North West Bay Rivulet (1%) and Esperance River (9%).
There were 6 STP's inputs represented as point sources. Fish farms were 85% DIN and 15% labile N with 30% in the Huon, 20% upper D'Entrecasteaux and 50% lower D'Entrecasteaux.

STP's	Rivers	Fish farms	Ocean
	(tNyr^{-1})		
21.3	801	1754	-1406

The biogeochemical model was initialized with nutrient, chlorophyll and sediment concentrations derived using data from the Derwent Estuary Program (DEP) for the Derwent and via the Salmon Farming Industry's published report (Ross and McLeod 2013) for the Huon Estuary and D'Entrecasteaux Channel. Observed chlorophyll concentrations were partitioned between the relative fractions of each algal group and translated to N biomass assuming a fixed nitrogen: chlorophyll ratio of 7 mgN: 1mgChl. For the dinoflagellate compartment the carbon concentration was calculated by assuming a fixed ratio of 106C:16N:1P (Redfield ratio). The whole model grid was initialised with a small uniform biomass of macrophytes. The model was run forward for one year from September 2008 – August 2009 with the model output at the end of the run used to initialize subsequent model runs.

5.2.4 Model Validation

Model validation was achieved by evaluating the performance of the model against specific validation criteria (Rykiel 1996). If these criteria were met, the model was designated as 'fit for purpose'. The first criteria was the model must conserve mass of carbon, nitrogen and phosphorous. At the start of each time step the total

mass of carbon, nitrogen and phosphorus in the water column, epi-benthos and sediment across all biogeochemical model tracers were summed. Computations then proceeded for the uptake and transformation of substances within the biogeochemical model. At the end of the biogeochemical model time step the mass of all tracers were summed and checked against their initial value to confirm conservation of mass for all biogeochemical model processes.

The next criterion was the model must reproduce the correct timing of the seasonal cycle in, and simulate the correct magnitude of, dissolved nutrients (nitrate, ammonium, dissolved inorganic phosphate), phytoplankton and dissolved oxygen over a year. Model predictions were compared with empirical observations made at stations throughout the estuary. The skill assessment results were restricted to the surface water observations of the D'Entrecasteaux Channel and Huon Estuary, which was the focus of this investigation, and simulations were compared to empirical patterns from monitoring at 15 sites (Ross and McLeod 2013).

In the north D'Entrecasteaux Channel (Figure 5-3) simulated DIN and phosphate concentrations were lower than observed particularly in winter when concentrations were underestimated by ~10 µM for DIP and ~40µM for DIN. Concurrent with the reduced winter nutrients simulated chlorophyll concentrations exceeded observed concentrations by ~2 mg m^{-3} and the spring bloom was more pronounced.

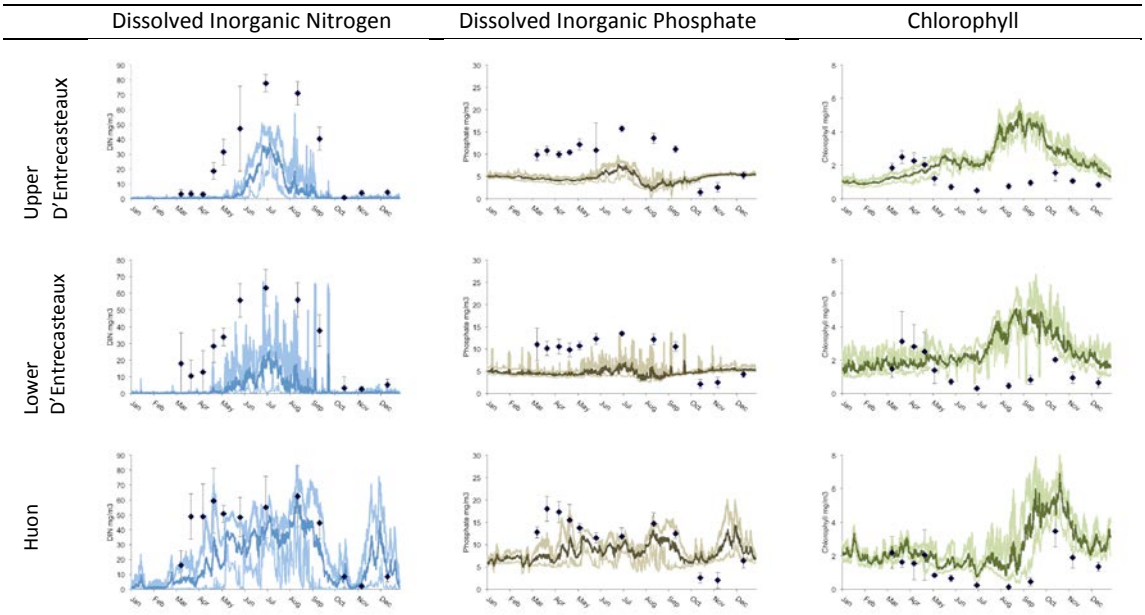

Figure 5-3: Summary of model calibration: comparison of simulated model results versus observations (2009) of dissolved inorganic nitrogen, dissolved inorganic phosphate and Chlorophyll concentrations

in DCHE. Black circles are observations with error bars (standard deviation); Dark line is model median and light lines show model range.

Simulated conditions in the south D'Entrecasteaux Channel were similar to those in the north of the channel. Simulated surface DIN and phosphorous were lower than observed in winter and chlorophyll concentrations were greater than observed in winter and spring. This pattern was consistent with an excess of stratification in winter and spring in the model, suggesting that the simulated water column was more stable than in reality, which facilitated excess phytoplankton growth. For the Huon Estuary, surface nutrients and chlorophyll concentrations were well reproduced by the model, although there was a slight tendency for the model to overestimate chlorophyll and underestimate DIN and phosphate in winter and spring.

Priority improvements to the model that could improve the skill include improved parameterisation of vertical mixing and seasonal stratification in the lower Derwent Estuary and D'Entrecasteaux Channel; resolution of variable wind-driven air-sea oxygen flux; and improved characterisation of point source and boundary nutrient, plankton and sediment concentrations. Additional observations of phytoplankton species composition, zooplankton grazing rates and sediment characteristics would also contribute to better precision in the calibration. Nonetheless, the results indicate the model is able to reproduce the dynamics in timing and magnitude and it is therefore fit for purpose.

5.2.5 Model scenarios

The DHD model was implemented with modified forcing from the fish farm loads and different arrangements of macroalgae farming to simulate scenarios used to quantify the increase in primary phytoplankton production due to finfish aquaculture and the capacity of IMTA to bioremediate this increased production. Each model simulation ran from September 2008 to August 2009.
The initial concentration of *M. pyrifera* was 100 $\mathrm{mg\ N\ m^{-3}}$ for both $\mathrm{N_f}$ and $\mathrm{N_s}$ as in Hadley et al. (2015.) The change in water column chlorophyll concentration $(\mathrm{mg\ Chl\ m^{-3}})$ over the top 10 m was used as a measure of the effect of finfish aquaculture and the bioremediation potential of macroalgae. According to ANZECC (2000) guidelines a concentration of 4 $\mathrm{mg\ Chl\ m^{-3}}$ or greater is categorized as 'poor' water quality in Australian estuaries (nb. 5 in Qld).

Increase in primary phytoplankton production due to finfish aquaculture

In this scenario the model was forced with three values of finfish loads:

- 'no' loading from the finfish farms.
- 'Low' loading at 2008 – 2009 inputs (table 1.)

- 'High' loading at 10 x 'low' loads.

Those scenarios allowed a comparison of phytoplankton production under increasing finfish loads. The titles 'high' and 'low' for finfish loads are used to distinguish the two cases and not as a classification of each quantity.

Quantifying bioremediation potential of macroalgae based IMTA.

In those scenarios macroalgae (*Macrocystis pyrifera)* farms are simulated to test IMTA implementation strategies.

- *Macrocystis pyrifera* grown everywhere: Macroalgae is initialised in all pelagic cells to establish where best to place the farms under 'high' and 'low' loads.
- *Macrocystis pyrifera* grown in single cells next to finfish farms to simulate macroalgae based IMTA; algae is cultivated at a depth of 1-4m for both 'high' and 'low' finfish loads.
- Optimisation of IMTA: The last scenarios are aimed at assessing optimisation strategies. Cultivation period was increased to 2 years, with identical environmental forcing for both years. Macroalgae farm area was doubled. Finally a simple harvesting scheme was introduced with 50% biomass removed at the end of spring. Combinations of these three strategies were run for 'low' and 'high' loads to look at the impact on IMTA results.

5.3 Results

5.3.1 Influence of finfish aquaculture on water quality

Chlorophyll concentration (top 10m) in the absence of finfish aquaculture was comparatively constant in the DCHE for each season (Row 1 Figure 5-4). At 'low' aquaculture load chlorophyll concentration is highest in spring, particularly in the lower D'Entrecasteaux (Row 2 Figure 5-4). Chlorophyll concentration decreases in summer and again in autumn retaining the same spatial distribution. For 'high' aquaculture loads, chlorophyll concentration levels have increased substantially across the DCHE in spring with concentrations above 8 $\mathrm{mg\,Chl\,m^{-3}}$ observed. The highest concentrations appear to be in the side bays in the D'Entrecasteaux Channel. In summer and autumn this chlorophyll concentration decreases substantially and resembles closely the concentration levels and spatial patterns observed for these seasons at 'low' forcing. The areas that show highest chlorophyll concentrations in summer (under both loads) do not appear to match with those regions with the highest density of salmon farms.

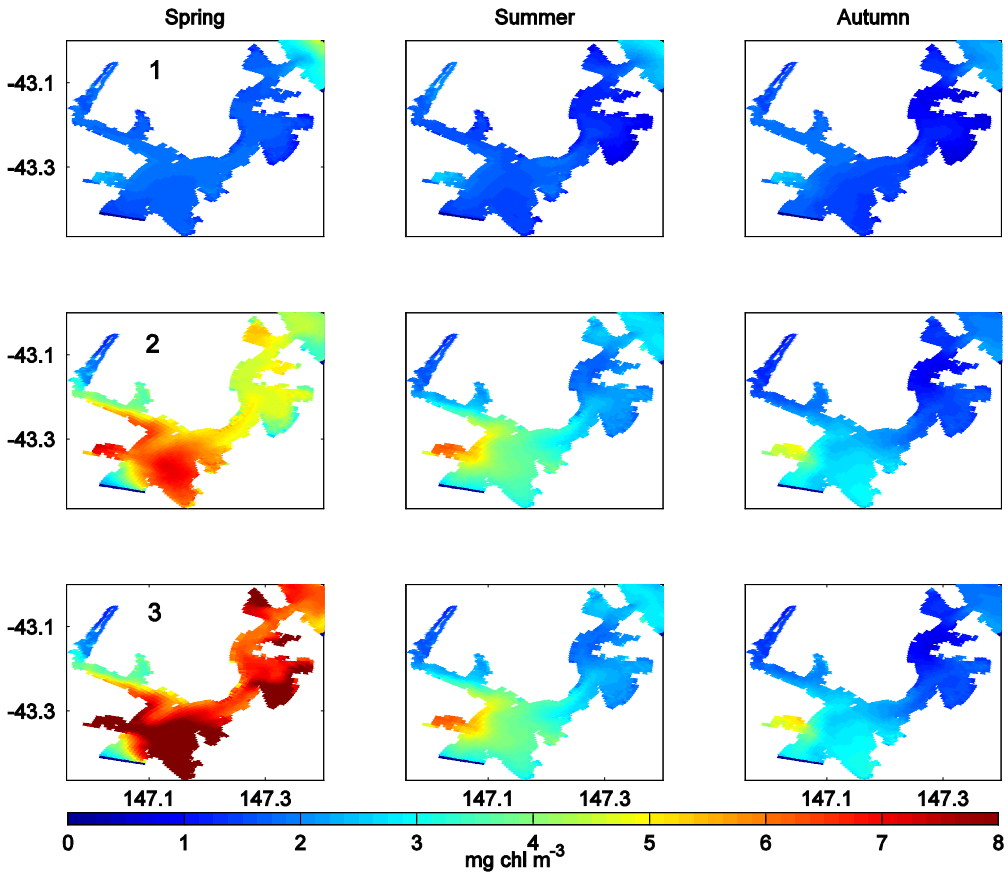

Figure 5-4: Average seasonal chlorophyll concentration (mg chl m^{-3}; top 10m) of the D'Entrecasteaux Channel and Huon Estuary with no finfish aquaculture (1); finfish aquaculture at 'low' loads (2); finfish aquaculture at 'high' loading (3) for 3 seasons: spring; summer; and autumn.

5.3.2 Implementation of M. pyrifera based IMTA

5.3.2.1 Site of greatest M. pyrifera growth

For *Macrocystis pyrifera* grown in all pelagic cells the total N ($= N_s + N_f$) at the end of May (2009) was greatest around the sites of the finfish leases (bottom row Figure 5-5). The results shown are for macroalgae in the top 10m of the water column. Growth was found to be optimal at 4m depth around finfish leases. This result was consistent for both 'low' and 'high' aquaculture. Similarly, mean DIN concentration for the 9-month beginning in September 2008, was greatest (in the upper 10 m) at the finfish farm sites for both aquaculture loads (fig. 5 top row).

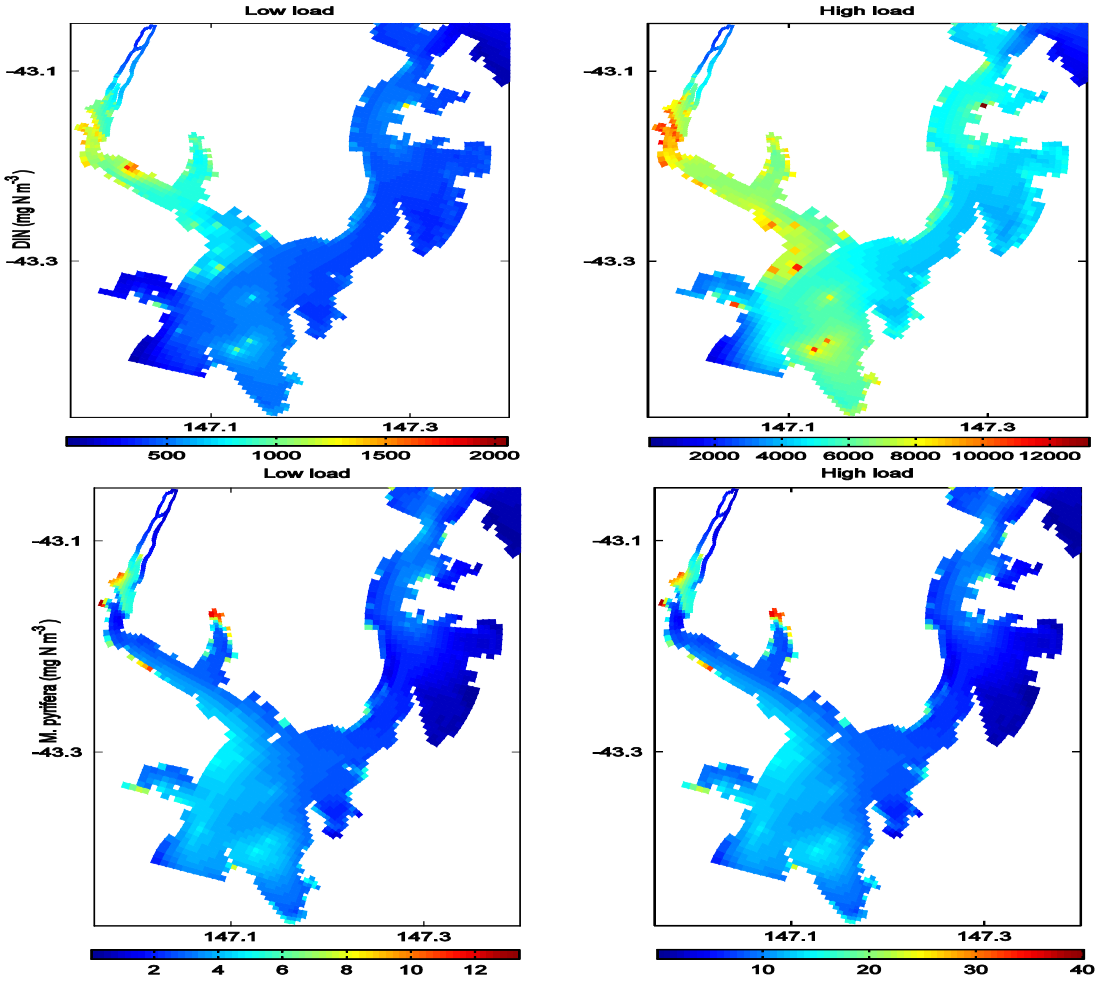

Figure 5-5: Average DIN (top 10m) from September – May for 'low' finfish loads (top left) and 'high' loads (top right). The bottom line shows the macroalgae concentration (top 10m) at the end of May for 'low' finfish loads (bottom left) and 'high' loads (bottom right). In this experiment macroalgae was initialized in all pelagic cells to see where it grew best.

5.3.2.2 IMTA at low finfish loads

The bioremediation achieved using IMTA was calculated as the percentage reduction in the overall increase in chlorophyll concentration brought about by finfish aquaculture. This meant firstly calculating the difference in chlorophyll concentration in the DCHE with and without finfish aquaculture and comparing those differences when IMTA was included. For these results *Macrocystis pyrifera* was cultivated for the scenarios outlined in section 5.2.5 and bioremediation results for spring, summer and autumn calculated for the four scenarios (Figure 5-6). Bioremediation was clearly highest in autumn with all four scenarios showing similar results. In this season bioremediation ranged between 15 – 20% in large areas of the D'Entrecasteaux and up to 30% in the lower Huon Estuary and some isolated areas if the upper D'Entrecasteaux. Summer was the least successful season for bioremediation with only the double farm size scenario showing visible bioremediation; 15% in a small area of densely populated farms in the lower D'Entrecasteaux which extends into the Huon. In spring all four scenarios showed

similar patterns of bioremediation. In this season bioremediation was highest in the area in the southwest of the D'Entrecasteaux and large bay on the eastern side of the upper D'Entrecasteaux. In these areas bioremediation ranged from 10-15%.

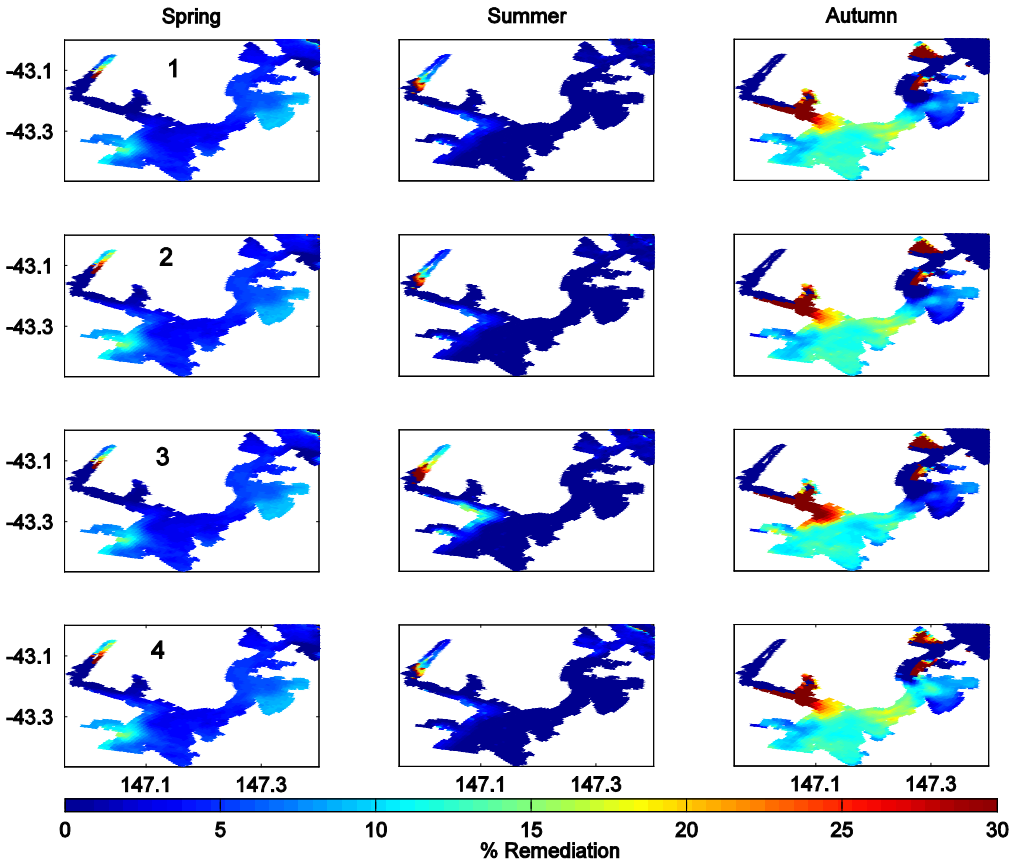

Figure 5-6: Seasonal reduction in water column chlorophyll concentration (top 10m) achieved using IMTA for 'low' finfish loads. Kelp and finfish farms were located in the same single grid cells (with an adjacent grid cell for double farm size scenario). Our four scenarios are shown in each row: the single grid cell farms in first year of cultivation (1); the single grid cell farms in second year of cultivation (2); double grid cell farms in first year of cultivation (3); harvesting scenario (4) . % Remediation was calculated by firstly finding the difference in chlorophyll concentration for the DCHE under 'low' loads with and without IMTA and then expressing this as a percentage of the increase in chlorophyll concentration due to finfish farming; DCHE with and without finfish farms.

5.3.2.3 IMTA at high finfish loads

The same method was used to calculate the bioremediation for 'high' aquaculture loads as that used for the 'low' forcing case. For each of the four scenarios: 1 year cultivation (1); 2 year cultivation (2) ; area doubling (3) and harvesting (4 Figure 5-7) there were similar patterns of bioremediation within the DCHE. Bioremediation was clearly highest in autumn with values ranging from 20 - 30% across most of the DCHE in an almost identical pattern across scenarios. In spring there was very little evidence of bioremediation at substantial levels; with perhaps the second year cultivation showing slightly higher bioremediation (this

scenario is identical in a modelling sense to harvesting for this season). In summer it was only the area doubling scenario that showed bioremediation; in an almost identical pattern (and intensity) seen in the low forcing scenario.

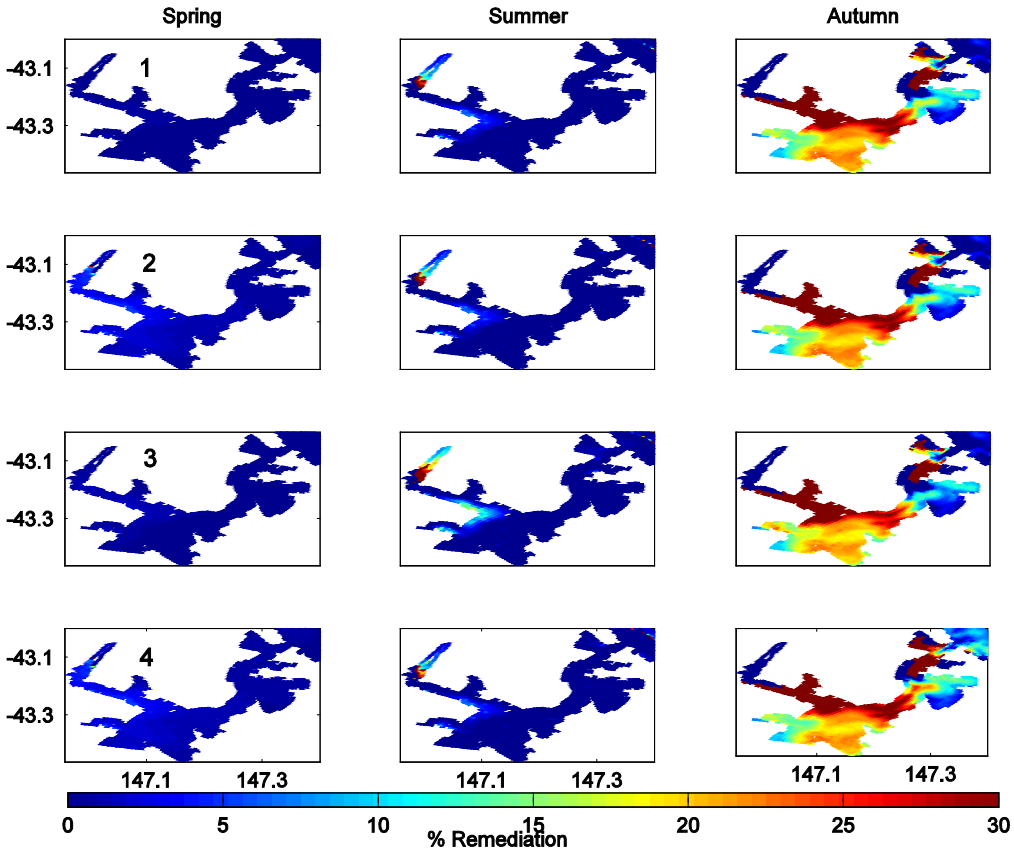

Figure 5-7: Seasonal reduction in water column chlorophyll concentration (top 10m) achieved using IMTA for 'high' finfish loads. Kelp and finfish farms were located in the same single grid cells (with an adjacent cell for double farm size scenario). % Remediation was calculated (same method as 'low' loads) for four IMTA implementations: the single grid cell farms in first year of cultivation (1); the single grid cell farms in second year of cultivation (2); double grid cell farms in first year of cultivation (3); harvesting scenario (4) .

5.3.3 Bioremediation of water quality and DIN

The % area of the Huon Estuary, upper and lower D'Entrecasteaux Channel that exceeded the ANZECC threshold for poor water quality (> 4 mg chl m^{-3}) was calculated for 'low' finfish loads. The % area was compared for the system without IMTA and for our 4 scenarios (Table 5-2). In spring, IMTA resulted in a slight increase in the % area over the ANZECC threshold for the Huon Estuary for all scenarios. In summer the area doubling resulted in a 25% reduction of this area compared to the

no IMTA case; all other scenarios resulted in a 5% decrease. In autumn there was no area above the threshold for any scenario (including no IMTA). For the lower D'Entrecasteaux the maximum reduction in this area (achieved by any scenario) was in the order of 1%. In the upper D'Entrecasteaux it was only in spring that this threshold was exceeded under the no IMTA scenario. All four scenarios resulted in a reduction of this area of approximately 4%.

Table 5-2: The % area of each region with a chlorophyll concentration > 4.0 $(\mathrm{mg\ m^{-3}})$ for 'low' aquaculture loads. The table offers a comparison of the change in in this area with and without IMTA. IMTA results are the first (SF1) and second (SF2) year of cultivation with farms in single grid cells, double farm size (DF) and Harvest scenarios.

% Area with chlorophyll > 4.0 $(\mathrm{mg\ m^{-3}})$ at low loads									
	Huon			Lower D'Entrecasteaux			Upper D'Entrecasteaux		
	Spr.	Sum.	Aut.	Spr.	Sum.	Aut.	Spr.	Sum.	Aut.
Scenario									
No IMTA	54.2	13.4	0	92.1	34.9	8.9	90.3	0	0
SF 1	56.0	12.8	0	90.8	34.7	8.6	86.4	0	0
DF	55.2	10.0	0	90.8	34.5	8.4	86.4	0	0
SF 2	54.5	12.8	0	90.8	34.7	8.6	86.6	0	0
Harvest	54.5	12.8	0	90.8	34.7	8.6	86.6	0	0

Bioremediation was also gauged by the percentage of the farm DIN loads removed by the farmed algae per region (Figure 5-8). The N removed was calculated from the maximum of total N $(N_s + N_f)$ for each site. This was done for the first year of cultivation for single and double farm sizes, under high and low loads. In general N remediation was higher under 'low' loads. DIN removal also displayed a linear increase with doubling of farm size. The lower D'Entrecasteaux recorded the highest removal rates per region at 12% (single farm) for low loads and 2% high loads, followed by the upper D'Entrecasteaux (8%, 1%) and the Huon Estuary (6%, 1%) . This result was consistent across the scenarios shown.

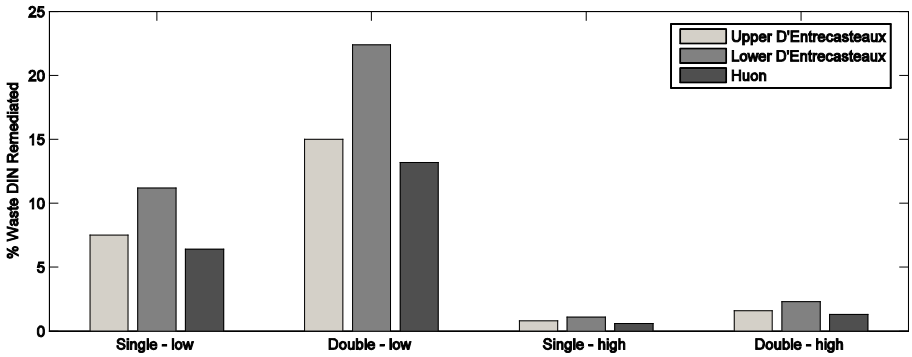

Figure 5-8: The % removal of DIN for each region: upper D'Entrecasteaux Channel; lower D'Entrecasteaux Channel and Huon Estuary under 'low' and 'high' loads for named scenarios. The

bars represent the total macroalgal N (fixed + stored) removed (maximum) as a percentage of the farm load for each region.

Macroalgae biomass (fixed N) plotted against time for one site in the upper D'Entrecasteaux showed saturation at both high and low loads (Figure 5-9). Biomass saturated in the first year of growth in February under both loads. The maximal biomass achieved was similar at both loads. In the second year biomass saturated mid-December under both loads, once again at similar values of fixed N. Interestingly at about March all biomass seemed to follow a similar trajectory until May indication similar values of fixed N were achieved irrespective of loading or peak biomass.

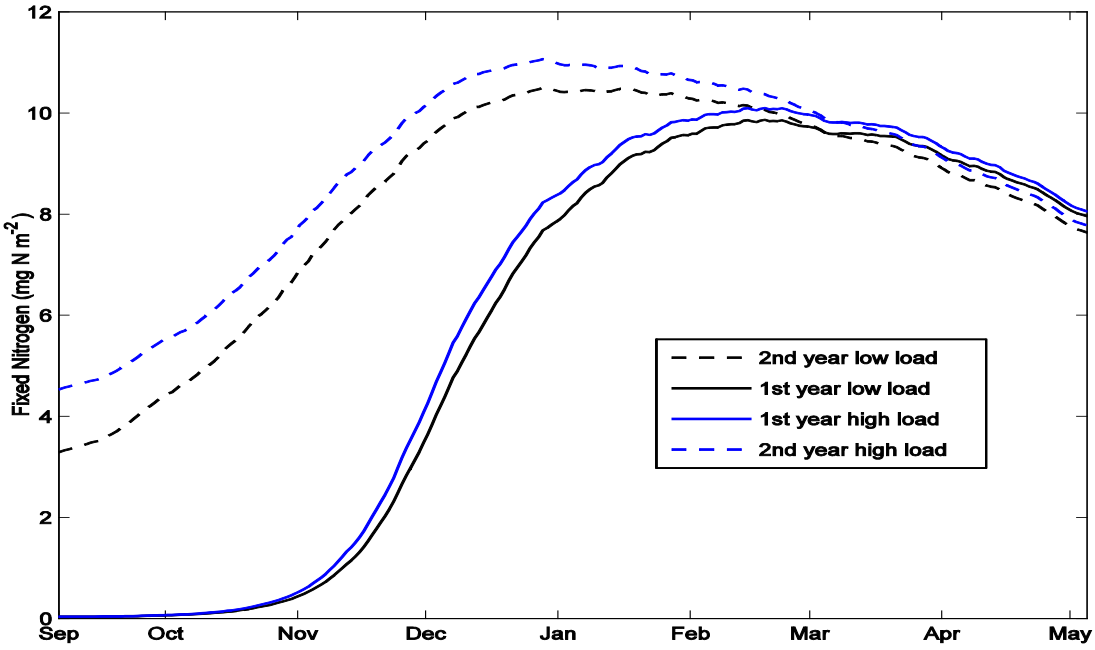

Figure 5-9: Macroalgal growth (fixed N) for a farm in the upper D'Entrecasteaux under 'low' (black) and 'high' (blue) aquaculture loads and for first (solid line) and second year (dashed line) of cultivation. The plots show biomass saturation under all scenarios with marginally higher growth under high loads.

5.4 Discussion

5.4.1 Phytoplankton Production under Increased Aquaculture Loads.

In this study the upper D'Entrecasteaux was shown to be an area of high phytoplankton production in spring under increasing aquaculture loads. This finding partly corroborates the earlier work of Wild-Allen et al. (2010). The southern section of the upper D'Entrecasteaux is relatively shallow (< 10m) with high residence times, and these two factors combined can drive high phytoplankton production rates (Cloern et al. 2001.) In the upper D'Entrecasteaux there are only 4 finfish farms operational it is most likely that the inflowing water, from the Huon Estuary and lower D'Entrecasteaux Channel was driving production in that region in spring. Rapid

dispersal at the source can result in aquaculture waste accumulating at distances not easily associated with the farms (Tsagaraki et al. 2011), therefore an increase in phytoplankton production due to the waste may be attributed to local farms when it is really driven from those further afield. The increased production died off in the upper D'Entrecasteaux in summer and autumn mirroring in line with the decrease seen in the lower D'Entrecasteaux and Huon. This is once again most likely due to impact in the upper D'Entrecasteaux being driven from production in the lower regions.

In an environmental monitoring program review (Ross and Macleod 2013), it was identified that the Huon Estuary showed elevated ammonia in both bottom and surface waters consistent with a system response to increased input of nutrients for 2009-10. However the review also acknowledged that lack of data from earlier years precluded a fully quantitative assessment. The report also found there was no identified increase in phytoplankton production, although once again data to perform a comprehensive analysis was lacking. The model results showed primary production was enhanced in this region by finfish aquaculture in spring and summer however this increase was comparable for both loads.

The results in the Huon Estuary may be due to a combination of factors. In 2009, the finfish farms in the Huon were operational mainly in spring with the majority slowing or stopping operation in summer and autumn. Secondly, water flow into the Huon Estuary was at depth from the ocean boundary at the lower D'Entrecasteaux (Herzfeld et al. 2010). These two factors combined make it reasonable to conclude that the farms contained within the Huon Estuary and not those in D'Entrecasteaux Channel will drive the increase in phytoplankton production in this region. However, it is difficult to solely attribute the lack of primary production in autumn to a slowing in finfish aquaculture output. The Huon Estuary is generally high in light attenuating CDOM (Clementson et al. 2004), which can reduce production particularly in autumn when seasonal irradiance is lower. It is likely that high CDOM ultimately means production in this region is ultimately light limited. This is consistent with the observations of increased ammonium but not phytoplankton observed by Ross and Macleod (2013).

In the lower D'Entrecasteaux, chlorophyll production is not centered around the areas containing the finfish farms, as loading increased it is observably highest in the side bays. The intensity of production was seasonally driven which was in general the case for the whole DCHE. The high production in spring, which lowers in summer, and further again in autumn is a response to factors such as changes in the light and mixed layer depth regulating autotrophic growth. Interestingly in summer and autumn the production is very similar for both aquaculture loads. For the lower D'Entrecasteaux there did not appear to be much influence on primary production from the farms within the upper D'Entrecasteaux and Huon Estuary. The relative short-term fate of the DIN released by finfish farms is variable and dependent on

farm site, depth of release and prevailing currents. In the longer term scenarios the DIN will follow the pattern outlined in previous hydrodynamic studies of the region. Herzfeld et al. (2010) described the hydrodynamics for the D'Entrecasteaux Channel and Huon Estuary region using the SHOC model. Deep water flows into the system from the ocean boundary of the lower D'Entrecasteaux, moving up to form the salt-wedge in the Huon Estuary and back out along the northern shore and then largely north into the upper D'Entrecasteaux with only a small portion flowing south once outside the Huon Estuary. The upper D'Entrecasteaux is not well connected (Herzfeld et al. 2010) to the other regions and tracers released there will stay in this region. Those released in the Huon and lower D'Entrecasteaux will disperse throughout the whole region. For this reason the Huon and lower D'Entrecasteaux are described as well connected. This pattern of residual circulation will largely determine the long term fate of farm released tracers; however, local effects driven by the strength and timing of the release of farm waste should be observed in the short term at least.

There were only two aquaculture loads considered in this study. The 'low' load was used, as it is representative of the actual forcing used in within the region in 2008-2009. The 'high' load was a purely theoretical case that needed to be distinguished from 'low' forcing and so an order of magnitude increase was deemed appropriate. Varying loads between the values used could see a range of impacts on primary production. For example elevation in ammonia may result in no discernible rise in production of phytoplankton because of a tight coupling with zooplankton, as has been observed around finfish farms in the oligotrophic Mediterranean (Pitta et al. 2009.) If the loading were high enough then this coupling may break resulting in a phytoplankton bloom. In general a high input of ammonium has the potential to switch the system from nitrogen to phosphorous limited however as the farms output phosphorous in inorganic form and in N:P ratios higher than the Redfield ratio this would be unlikely. Ammonia could however rise to toxic levels or result in oxygen draw down. Although there are a range of mechanisms that may mask phytoplankton increases, in general the model suggests that the increase in phytoplankton primary production is linked to aquaculture loading in spring in particular. However, the fact that there is no increase between high and low loads in the DCHE in summer and autumn means something is limiting production in these two seasons. This is most likely light due to high CDOM and restricted river flow causing stratification.

The effect of finfish aquaculture on phytoplankton production may change if the location of finfish farms were altered within the DCHE. Placing sites in areas of high currents may result in DIN being washed away. This in turn could result in higher production in other parts of the estuary as advection breaks the nutrient phytoplankton coupling (Arhonditsis et al. 2007). In this study we have not examined the effect of the spatial arrangement of farms on the spatial pattern of primary production within the region. However, it seems clear from the results that phytoplankton primary production is dispersed through the region not concentrated around finfish farms. It is also clear that DIN was being advected away from the

sites, promoting phytoplankton production away from the source. In a large system like the one presented here it may be that siting aquaculture in regions that are well flushed will reduce local impacts associated with DIN but the system wide result may be unchanged. Consequently, siting finfish production in well-flushed areas where DIN effects may be dispersed but still contribute to the overall nutrient pool of the system should be considered in conjunction with the potential to better contain those nutrients and seek to remove them with IMTA. However, production in summer and autumn is limited by factors not related to farm siting.

5.4.2 *Bioremediation* from *IMTA*

5.4.2.1 Reduction in chlorophyll

The results conclusively showed the capacity of IMTA to bioremediate the excess water column chlorophyll resulting from finfish aquaculture and that this capacity reduced in spring in summer, but increased in autumn as finfish loading increased. There is most likely a limit to the extent to which IMTA can keep primary production below safe levels such as those outlined in ANZECC. Although IMTA produced some bioremediation at 'high' loads, particularly in autumn, in general the increase in water chlorophyll concentration was too high in places at this load to be effectively reduced to an acceptable level. There was some evidence as to how the IMTA could be optimised using simple implementation strategies and how IMTA could be targeted to a specific season. The results provide a way of testing further empirical studies into IMTA. Monitoring of the chlorophyll concentration should be focused in the regions identified under current loads i.e. those areas of the upper and lower D'Entrecasteaux identified in summer or in lower D'Entrecasteaux and Huon (in general) in autumn. Empirical studies could implement harvesting and vary cultivation period and farm area to examine the effect on bioremediation.

Calculation of the reduction in the area exceeding the ANZECC levels was only performed for the 'low' aquaculture loads because the 'high' forcing simulation resulted in excessive chlorophyll concentrations. The 'low' finfish load used in this study calculated from real data contained in industry reports and was representative of 2008-2009 levels in the DCHE. Since 2009 regulations have been in place limiting finfish aquaculture in the DCHE based on the amount of N they can release (Ross and Macleod 2012). The 'low' load was approximately equivalent to the total allowable N for aquaculture. Given that loading will not exceed this level under current regulations, the results were encouraging as IMTA reduced some areas to below the ANZECC threshold. A major caveat on this result was obviously the increase seen in the impacted area in spring in the Huon. IMTA may have slowed phytoplankton growth initially delaying it till later in spring where it was able to grow even quicker; due to lower flow or higher PAR. The mechanism for this increase may be complex but needs further investigation.

The reduction in area was poor in the lower D'Entrecasteaux however this was the region with highest production and therefore greatest amount of area over the ANZECC guidelines. It was also the area with the highest %bioremediation, once again it is the metric use to quantify bioremediation success that comes under scrutiny. If an absolute measure like ANZECC is used then the IMTA results are poor in the lower D'Entrecasteaux however if the relative measure of the percentage reduction in increased chlorophyll is used, IMTA is more successful. An important point to mention is that placing macroalgae farms in in the upper D'Entrecasteaux may not be necessary if the purpose of IMTA is reducing phytoplankton production resulting from finfish aquaculture. If finfish farms outside this region drive the increase then IMTA within the region may not be necessary. This could potentially reduce costs associated with IMTA of implementation by 20% in this instance.

5.4.2.2 Remediation of finfish released N

The %N removed varied with region and IMTA implementation strategy and reduced with finfish load. IMTA is more often quantified in terms of N removal (Ren et al. 2012; Abreu et al. 2009; Carmona et al. 2006) than reduction in primary production. However, nitrogen output from a finfish farm does not necessarily drive higher production in an estuary (Pitta et al. 2009; Cloern et al. 2001). Production rates depend on complex interactions between a host of factors such as flushing rates, stratification and plankton community structure. IMTA is also used to grow macroalgae sustainably with large biomass with which to supply a new market (FAO 2009; Troell et al. 2009). Therefore high N removal is important.

We calculated the N remediation by the ratio of macroalgal N (fixed + stored) to finfish load. This was better calculated per region than at individual farms. It was difficult to gauge how much growth at each farm was influenced from N from farms other than the one adjacent to the macroalgae. However, if the macroalgae were benefitting from N sourced from another finfish farm further away and if that farm were no longer operational, it may affect the outcome of IMTA. This could impact on empirical studies conducted to test the results of this study. If one finfish lease stops operation anywhere in the DCHE then this should not affect the overall N remediation in the Huon Estuary for example. In any case N remediation was reasonably similar across the three regions. The decrease in N remediation with finfish loading is for similar reasons as the corresponding decrease in chlorophyll remediation; the N loading was too high.

Other investigations into IMTA that specifically return the percentage removal of N from finfish waste, have shown this amount can vary significantly dependent on the individual experiment. Broch et al. (2013) in a modeling approach found their algae remove 0.34% of salmon waste N. That small figure was attributed to a mismatch in finfish and macroalgae production cycles. These results show that any mismatch can be reduced particularly through extending cultivation period in conjunction with an efficient harvesting scheme. This would allow for the right

balance between sufficient biomass and growth rate. A simplified application of the IMTA model used in this study showed *Macrocystis pyrifera* is capable of removing 70% of farm N under moderate flow (Hadley et al. 2015); however this was in the absence of competition from phytoplankton. What we can conclude is that the removal rates of N can be increased through implementation strategy and knowledge of the system in general.

5.4.3 Cultivation period

Cultivation period had a negative effect on N removal under both 'low' and 'high' aquaculture loads. In effect growing macroalgae over two environmentally identical years was analogous to running two repeat IMTA experiments with different stocking densities (initial biomass.) Plots of biomass versus time for one of the sites demonstrated growth reached a maximum in each year under both loads. Biomass once established enables high removal rates in the underlying IMTA model (Hadley et al 2015.) Another comparable modelling study also identified initial biomass of macroalgae as having a major impact on macroalgae's ability to compete with phytoplankton for nutrients under high nutrient loads, and highlighted how self-shading and depleting nutrients acted in tandem with biomass (Bartleson et al. 2005). However, if biomass is too high then growth saturates and strategies such as harvesting become important. In our study the results showed that biomass is saturating at similar levels under both aquaculture loads, whereby the year of cultivation changes the time of season the biomass reaches a maximum. The similar maximum achieved at both loads means there is a limit to how much DIN IMTA can remove. The process must therefore be optimized by harvesting or increasing farm size.

Under 'low' aquaculture loads the increased cultivation period should allow the biomass to establish so that IMTA was more efficient in spring of the second year for phytoplankton reduction and most likely N removal (although not calculated) however growth rates should reduce in summer onwards. For both 'high' and 'low' loads the higher biomass in spring resulted in slightly greater chlorophyll reduction. However the saturation in growth must be addressed for optimal bioremediation by harvesting.

5.4.4 Farm Area

Increasing farm area had the largest effect on the bioremediation of both primary production and N but this is perhaps the least favorable strategy due to the limited availability of suitable areas for farming. Actual area is cited as one of the key factors limiting inshore aquaculture development worldwide (FAO 2009), increasing farm area may not be possible or desirable. The grid used in the DCHE made each macroalgae farm about 16 hectares. Although this is a large area other factors such as available space, bioremediation potential and market demand would drive management decisions around farm size. An experimental study by Abreu et al.

(2009) shows that 0.36 ha of macroalgae could remove 1.8 tN of finfish output which in this study would put farm areas anywhere between 1.8 to 56 hectares given finfish loads used in this study; assuming 100% removal of N. However, it is not just a matter of extrapolating the results from small-scale experiments to determine the farm area needed to remediate a larger input. In this study the %N remediated approximately doubled with a doubling of farm area. However, not all the N in the system adds to primary production, a large proportion is eventually flushed out of the system. A better approach is to determine the impact of N loading on primary production and then optimise macroalgae farms to remediate this impact.

5.4.5 Harvesting

Harvesting in spring promoted an increased reduction of phytoplankton production in autumn in the upper D'Entrecasteaux an effect seen at both loads. This is seen when results for second year scenario are compared to the harvesting scenario. Hadley et al. (2015) showed that harvesting has the potential to increase biomass return by 15-fold in comparison to harvesting only at the end of the season. Once biomass is established to the extent it can adequately remove DIN then harvesting reverses the limiting effects related to high biomass such as self-shading. An optimal harvesting scheme should aim to keep macroalgae biomass at steady state where it is matched to the N output of a finfish farm. This matching process keeps growth rates high, otherwise the macroalgae biomass eventually slows then saturates growth, fills the reserves using a small proportion for cellular functions and the rest is lost to the system. Harvesting in general enables a steady supply of macroalgae to the market. This required rate of supply will also inform the harvesting scheme used. In this investigation a large establishment period was used because this was found to be optimal (Hadley et al. 2015); however, there was only one harvest performed as model runs are lengthy and the overall purpose was to demonstrate the contribution harvesting makes to the process. The reason why the effect from harvesting is seen in autumn and not summer maybe due to the amount of biomass removed i.e. 50%

5.4.6 Other considerations and future work

In the dynamic plots shown in the results for the individual farm the maximum biomass under 'high' loads was 17.1 $\mathrm{kg\ m^{-2}}$ in the first year assuming dry weight is 10% of wet weight. Other studies have had this amount vary from 11 – 22 kg m^{-2} wet weight (9 months) (Buschmann et al. 2011) to 66 kg m^{-2} (Westemeier et al. 2011) (5 months) for *Macrocystis pyrifera* grown in IMTA environments. The biomass returned is therefore reasonable; however, farm size was large and this can have other implications such as the impact on simulated dissolved oxygen.

We have not considered oxygen depletion in this investigation. In the case of large biomass of macroalgae, respiration at night could result in lower oxygen levels near the finfish cages, resulting in adverse effects on the fish. The EMS model solves for dissolved oxygen as a ratio of biomass but diurnal respiration has not been modeled explicitly. In general the DCHE is not low in dissolved oxygen but IMTA represents a significant perturbation to the system. Future work should include oxygen dynamics associated with diurnal growth and respiration of the macroalgae.

5.4.7 *Concluding Remarks*

The results of this modelling exercise suggest that we can achieve up to ~30% reduction in the increase in chlorophyll concentration resulting from 'low' intensity finfish aquaculture, by growing giant kelp (*Macrocystis pyrifera*) in conjunction with finfish leases; this remediation was up to ~ 40% for 'high' intensity aquaculture. The removal of N and reduction of chlorophyll can be incrementally improved by a series of optimisation strategies. Understanding the system dynamics allowed us to better assess the local and system wide impact of finfish aquaculture farming and more fully evaluate the bioremediation strategies. The results suggest that growing macroalgae next to the aquaculture cages provides the best bioremediation outcome under the current farm site distribution; however, under 'high' finfish loads there existed a band of potential sites centered on the farm leases. We also conclude that implementation strategies based on initial biomass, harvesting and farm area could be used to improve spatial and temporal control over aquaculture driven increases in phytoplankton production. Further investigation of the growth potential for specific macroalgae in this system would be valuable to further inform the modelling process.

5.5 Appendix 5-A – Biogeochemical model equations and parameters

For each layer and grid location the time evolution of each model substance (**Y**) is the sum of conservative advection, diffusion and sinking processes (φ**Y**) and non-conservative biogeochemical rate processes (**βY**):

$$\partial Y/\partial t = -\varphi Y + \beta Y \qquad (1)$$

where $\varphi Y = (u\Delta Y + \Delta_H K_H \Delta Y) - (\partial/\partial z)K_Z(\partial Y/\partial z) + (\partial w_S Y/\partial z)$
and $\Delta = (\partial/\partial x) + (\partial/\partial y) + (\partial/\partial z)$; $\Delta_H = (\partial/\partial x) + (\partial/\partial y)$

[Here u is the velocity vector; K_H and K_z are the horizontal and vertical diffusion coefficients and w_S is the settling velocity.]

Table 5-A1: Non-conservative β terms for each biogeochemical model state variable (some at Redfield 106C:16N:1P or Atkinson ratio 550C:30N:1P)

Symbol	State Variable (Ratio)	Processes	β term
Nitrogen (mg N m^{-3})			
B_1	Small phytoplankton (R)	net growth, grazing, mortality	$\beta_{B1} = (\mu_{B1} - m_B)B_1 - g_1$
B_2	Large phytoplankton (R)	net growth, grazing, mortality	$\beta_{B2} = (\mu_{B2} - m_B)B_2 - g_2\phi_2 / r_{enc}$
B_3	Dinoflagellates (-)	net growth, grazing, mortality	$\beta_{B3} = (\mu_{B3} - m_B)B_3 - g_2\phi_3 / r_{enc}$
B_4	Microphytobenthos (R)	growth, grazing, mortality	$\beta_{B4} = (\mu_{B4} - m_{B4}B_4)B_4 - g_2\phi_4 / r_{enc}$
N_s	Stored N (*M. pyrifera*) (-)	Net uptake, fixation, loss	$\beta_{Ns} = (u_{NsN1} + u_{NsN2})Q_{\min} / N_f - g_{ma}N_s - d_M N_s$

N_f	Fixed N (*M. pyrifera*) (A)	Net fixation, mortality	$\beta_{Nf} = g_{ma}N_s - d_M N_f$
M	Macroalgae (A)	net growth, mortality	$\beta_M = (\mu_M - m_M)M$
S	Seagrass (A)	net growth, mortality	$\beta_S = (\mu_S - m_S)S$
Z_1	Small zooplankton (R)	growth, mortality	$\beta_{Z1} = g_1 e - m_{Z1}Z_1^2$
Z_2	Large zooplankton (R)	growth, mortality	$\beta_{Z2} = g_2 e - m_{Z2}Z_2^2$
N_1	Nitrate (-)	uptake, nitrification(wc+sed), denitrification(sed)	$\beta_{N1} = -(\mu_{B1}B_1 + \mu_{B2}B_2 + \mu_{B3}B_3 + \mu_{B4}B_4 + \mu_S S + \mu_M M)N_1/(N_1+N_2)$ $- u_{NsN1}Q_{\min}/N_f + r_N N_2 O/(K_O + O)$ $+ (1 - K_{OD}/(K_{OD}+O))r_{Nsed}O^2 N_2/(K_O^2 + O^2)$
N_2	Ammonium (-)	uptake, mortality, defecation, remineralisation, nitrification(wc+sed)	$\beta_{N2} = -(\mu_{B1}B_1 + \mu_{B2}B_2 + \mu_{B3}B_3 + \mu_{B4}B_4 + \mu_S S + \mu_M M)N_2/(N_1+N_2)$ $- u_{NsN2}Q_{\min}/N_f + d_M N_s + (1-\gamma)(m_{Z1}Z_1^2 + m_{Z2}Z_2^2) + (g_1+g_2)(1-e-\varsigma)$ $+ r_L(D_1+D_2)(1-\xi-\vartheta) + r_R D_3(1-\vartheta_3) + r_D N_3 - r_N N_2 O/(K_O+O) - r_{Nsed}O^2 N_2/(K_O^2+O^2)$
N_3	Dissolved organic N (-)	remineralisation	$\beta_{N3} = \vartheta r_L(D_1+D_2) + \vartheta_3 r_R D_3 - r_D N_3$
D_1	Pelagic labile detritus (R)	mortality, defecation, remineralisation	$\beta_{D1} = m_B(B_1+B_2+B_3) + d_M N_f + m_{B4}B_4^2 + \gamma(m_{Z1}Z_1^2 + m_{Z2}Z_2^2) + \varsigma(g_1+g_2)(1-e) - r_L D_1$
D_2	Benthic labile detritus (A)	mortality, remineralisation	$\beta_{D2} = m_S S + m_M M - r_L D_2$
D_3	Refractory detrital N (-)	remineralisation	$\beta_{D2} = \xi r_L(D_1+D_2) - r_R D_3$
Phosphorous (mg P m^{-3})			
P_1	Dissolved inorganic P (-)	uptake, mortality, defecation, remineralisation, desorption	$\beta_{P1} = -((\mu_{B1}B_1 + \mu_{B2}B_2 + \mu_{B3}B_3 + \mu_{B4}B_4)R_{WP} + (\mu_S S + \mu_M M)A_{WP})$ $+ (1-\gamma)(m_{Z1}Z_1^2 + m_{Z2}Z_2^2)R_{WP} + (g_1+g_2)(1-e-\varsigma)R_{WP}$ $+ r_L(D_1 R_{WP} + D_2 A_{WP})(1-\xi-\vartheta) + r_R E_1(1-\vartheta_3) + r_D P_2 + d_2 + d_3$
P_2	Dissolved organic P (-)	remineralisation	$\beta_{P2} = \vartheta r_L(D_1 R_{WP} + D_2 A_{WP}) + \vartheta_3 r_R E_1 - r_D P_2 + d_2 + d_3$
E_1	Refractory detrital P (-)	remineralisation	$\beta_{E1} = \xi r_L(D_1 R_{WP} + D_2 A_{WP}) - r_R E_1$

E_2	Unflocculated particulate inorganic P (-)	desorption, flocculation, immobilization	$\beta_{E2} = -d_2 - r_F E_2$ $\beta_{E2} = -d_2 - r_F E_2 - r_I E_2$ sediment
E_3	Flocculated particulate inorganic P (-)	desorption, flocculation, immobilization	$\beta_{E3} = -d_3 + r_F E_2$ $\beta_{E3} = -d_3 + r_I E_2 - r_I E_3$ sediment
E_4	Immobilized particulate inorganic P (-)	immobilization	$\beta_{E3} = r_4 E_2 + r_{E4} E_3$
Carbon (mg C m^{-3})			
B_{3C}	Dinoflagellates (-)	growth, grazing, mortality	$\beta_{B3C} = (\mu_{B3C} - g - m_B) B_{3C} - g_2 \phi B_{3C} / r_{enc} B_3$
C_1	Dissolved inorganic C (-)	uptake, mortality, defecation, remineralisation	$\beta_{C1} = -((\mu_{B1} B_1 + \mu_{B2} B_2 + \mu_{B4} B_4) R_{WC} + \mu_{B3C} B_{3C} + (\mu_S S + \mu_M M) A_{WC})$ $+ (B_{3C} - B_3 R_{WC}) m_B + (1-\gamma)(m_{Z1} Z_1^2 + m_{Z2} Z_2^2) R_{WC}$ $+ (1 - e - \varsigma)((g_1 + (g_2 / r_{enc})(\phi_2 + \phi_4)) R_{WC} + g_2 \phi_3 B_{3C} / r_{enc} B_3)$ $+ r_L (D_1 R_{WC} + D_2 A_{WC})(1 - \xi - \vartheta) + r_R F_1 (1 - \vartheta_3) + r_D C_2$
C_2	Dissolved organic C (-)	remineralisation	$\beta_{C2} = \vartheta r_L (D_1 R_{WC} + D_2 A_{WC}) + \vartheta_3 r_R F_1 - r_D C_2$
F_1	Refractory detrital C (-)	remineralisation	$\beta_{F1} = \xi r_L (D_1 R_{WC} + D_2 A_{WC}) - r_R F_1$
Oxygen (mg O m^{-3})			
O	Dissolved oxygen (-)	growth, mortality, defecation, remineralisation	$\beta_{P1} = ((\mu_{B1} B_1 + \mu_{B2} B_2 + \mu_{B3} B_3 + \mu_{B4} B_4) R_{WO} + (\mu_S S + \mu_M M) A_{WO})$ $+ ((1-\gamma)(m_{Z1} Z_1^2 + m_{Z2} Z_2^2) R_{WO}) O / (K_{OA} + O)$ $+ ((1 - e - \varsigma)((g_1 + (g_2 / r_{enc})(\phi_2 + \phi_4)) R_{WO} + R_{WO} g_2 \phi_3 B_{3C} / R_{WC} r_{enc} B_3)) O / (K_{OA} + O)$ $- (r_L (D_1 R_{WC} + D_2 A_{WO})(1 - \xi - \vartheta) + (r_R D_3 (1 - \vartheta_3) + r_D N_3) R_{WO}) O / (K_{OA} + O)$
Mineral Suspended Solids (kg TSS m^{-3})			
T_1	Unflocculated solids (-)	flocculation, burial	$\beta_{T1} = -r_F T_1$ $\beta_{T1} = -(r_F + r_b) T_1$ for sediment

T_2	Flocculated solids (-)	flocculation, burial	$\beta_{T2} = +r_F T_1$ $\beta_{T2} = r_F T_1 - r_b T_2$	for sediment

Table 5-A2: Rate processes included in the state variable equations.

Symbol	Process	Equation
$u_{NB1,2,3,4}$	Maximum phytoplankton uptake of N (mg N $s^{-1}cell^{-1}$)	$u_{NB} = \psi(\varepsilon_{N1} N_1 + \varepsilon_{N2} N_2)$
$u_{PB1,2,3,4}$	Maximum phytoplankton uptake of P (mg P $s^{-1}cell^{-1}$)	$u_{PB} = \psi \varepsilon_{P1} P_1$
$u_{IB1,2,3,4}$	Maximum supply of light to phytoplankton portion respired (E $s^{-1}cell^{-1}$)	$u_{IB} = I_{av} k_a m_N - r\mu_B^{\max} m_{IB}$
u_{IB4}	Maximum supply of light to benthic algae (E $s^{-1}cell^{-1}$)	$u_{IB4} = \left(I_{botS} m_{NB}\left(1 - e^{-k_{a4} B4 dz}\right)/ B_4 dz\right) - r\mu_B^{\max} m_{IB}$
u_{NM}	Maximum macroalgae uptake of N (mg N $s^{-1}m^{-2}$)	$u_{NM} = (\varepsilon_{N1} N_1 + \varepsilon_{N2} N_2)/\delta$
u_{PM}	Maximum macroalgae uptake of P (mg P $s^{-1}m^{-2}$)	$u_{PM} = \varepsilon_{P1} P_1/\delta$
u_{IM}	Maximum supply of light to macroalgae (E $s^{-1}m^{-2}$)	$u_{IB} = I_{bot}\left(1 - e^{-k_M M}\right) - r\mu_M^{\max} m_{IM}$
u_{NS}	Maximum seagrass uptake of N (mg N $s^{-1}m^{-2}$)	$u_{NS} = S\mu_S^{\max}(N_1 + N_2)/K_N$
u_{PS}	Maximum seagrass uptake of P (mg P $s^{-1}m^{-2}$)	$u_{PS} = S\mu_S^{\max} P_1/K_P$

u_{IS}	Maximum supply of light to seagrass (E $s^{-1}m^{-2}$)	$u_{IS} = I_{botM}\left(1-e^{-k_S S}\right) - r\mu_S^{\max} m_{IS}$
μ	Autotroph growth (d^{-1})	$\mu = \mu^{\max} R_N R_P R_I$ found in a look-up table of solutions to 3 simultaneous equations equating uptake and growth (to avoid explicitly modelling relative resources R_N R_P R_I for each autotroph): $u_N\left(1-R_N\right) = \mu_{\max} R_N R_P R_I m_N$ $u_P\left(1-R_P\right) = \mu_{\max} R_N R_P R_I m_P$ $u_I\left(1-R_I\right) = \mu_{\max} R_N R_P R_I m_I$
l_I	Light limitation for *M. pyrifera* (-)	$\frac{e}{k*h}\left(e^{-\frac{I_z e^{-kh}}{I_s}} - e^{-\frac{I_z}{I_s}}\right)$
l_T	Temperature limitation for *M. pyrifera* (-)	$\frac{1}{1+\exp[-\varsigma_p(T-T_p)]}$
l_Q	Nutrient limitation for *M. pyrifera* (-)	$g\frac{Q-Q_{min}}{Q-k_c}$
Q	Internal quotient of N For *M. pyrifera* (mg N g^{-1} dw)	$Q_{min}(1 + N_s N_f^{-1})$
h	Height of *M. pyrifera* (m)	$\max((0.00174N_f/\text{num\_fronds})^{1.047}, 1)$
g_1	Small zooplankton grazing (mg N s^{-1}) (cell P cell Z^{-1} s^{-1}) (cell P cell Z^{-1} s^{-1})	$g_1 = \left(\min\left\{r_{ing}, r_{enc}\right\}\right)\left(Z_1 / Z_{1m}\right)\left(B_1 / B_{1m}\right)$ where: $r_{ing} = \mu_{Z1}^{\max} e\left(Z_{1m} / B_{1m}\right)$ $r_{enc} = \left(B_1 / B_{1m}\right)\left(\phi_{diff\,1} + \phi_{rmot1} + \phi_{shear1}\right)$
g_2	Large zooplankton grazing (mg N s^{-1}) (cell P cell Z^{-1} s^{-1}) (cell P cell Z^{-1} s^{-1})	$g_2 = \left(\min\left\{r_{ing}, r_{enc}\right\}\right)\left(Z_2 / Z_{2m}\right)\left(\left(B_2 / B_{2m}\right) + \left(B_3 / B_{3m}\right) + \left(B_4 / B_{4m}\right)\right)$ where: $r_{ing} = \mu_{Z2}^{\max} e\left(\left(Z_2 / B_{2m}\right) + \left(Z_2 / B_{3m}\right) + \left(Z_2 / B_{4m}\right)\right)$ $r_{enc} = \left(B_2 / B_{2m}\right)\left(\phi_{diff\,2} + \phi_{rmot2} + \phi_{shear2}\right) + \left(B_3 / B_{3m}\right)\left(\phi_{diff\,3} + \phi_{rmot3} + \phi_{shear3}\right) + \left(B_4 / B_{4m}\right)\left(\phi_{diff\,4} + \phi_{rmot4} + \phi_{shear4}\right)$
ϕ_{diff}	Diffusive encounter rate ($m^3 s^{-1}$cell Z^{-1})	$\phi_{diff} = \left(2BB.T / 3\sigma\upsilon_K\right)\left(2 + r_B / r_Z + r_Z / r_B\right)$

ϕ_{rmot}	Relative motion encounter rate (m^3s^{-1}cell Z^{-1})	$\phi_{rmot} = \pi(r_B + r_Z)^2\left(-w_S^2/\left(3U_P^2/3U_Z + U_Z\right) + \left(U_P^2/3U_Z + U_Z\right)\right)$
ϕ_{shear}	Fluid shear encounter rate (m^3s^{-1}cell Z^{-1})	$\phi_{shear} = 1.3\left(K_Z/\nu_K\right)^{0.5}\left(r_B + r_Z\right)^3$
r_F	Flocculation rate (s^{-1})	$r_F = r_{F10}$ for SS > 10 psu $r_F = r_{F10}(SS - 6)/4$ for 6 < SS < 10 psu
$d_{2,3}$	Desorption of P (mg P $m^{-3}s^{-1}$)	$d_2 = pT_2p_{ak}\left(E_2/T_2p_{ak} - P_1O/\left(K_{PA} + O\right)\right)$ $d_3 = p_aT_2p_{ak}\left(E_3/T_2p_{ak} - P_1O/\left(K_{PA} + O\right)\right)$

Table 5-A3: Derived model variables.

Symbol	Derived Variable	Equation
X	Phytoplankton chlorophyll (mg Chl m^{-3})	$X = \left(B_1 + B_2 + B_3 + B_4\right)Q_{XN}$
Kd	Attenuation coefficient (m^{-1})	$Kd = k_w + k_{fw}(35 - SS)/35 + k_{a1}B_1 + k_{a2}B_2 + k_{a3}B_3 + k_{a4}B_4$ $+ k_{dt}\left(D_1 + D_2 + D_3\right) + k_nN_3 + k_t\left(T_1 + T_2\right) + k_mM$
I_{av}	Layer mean PAR (E m^{-2} s^{-1})	$I_{av} = \left(Q_{QW}/AV\right)\left(I_{top} - I_{bot}\right)/Kd.dz$ where $I_{bot} = I_{top}e^{-Kd.dz}$
I_{botM}	PAR below macroalgae (E m^{-2} s^{-1})	$I_{botM} = \left(Q_{QW}/AV\right)I_{bot}e^{-k_MM}$
I_{botS}	PAR below seagrass (E m^{-2} s^{-1})	$I_{botS} = \left(Q_{QW}/AV\right)I_{botM}e^{-k_SS}$
I_{botB4}	PAR below microphytobenthos (E m^{-2} s^{-1})	$I_{botB4} = \left(Q_{QW}/AV\right)I_{botS}e^{-k_{a4}B_4dz}$

Table 5-A4: DHD Biogeochemical Model Equations and Parameters.

Symbol	Autotroph Parameters	Large Phyto-plankton B_2	Small Phyto-plankton B_1	Dino flagellates B_3	Micro-phyto-benthos B_4	Sea Grass S	Epiphytic M
r_B	Radius (m)	1.0E-5	2.5E-6	1.0E-5	1.0E-5	N/A	N/A
μ_{max}	Max growth rate (d^{-1})	1.5	1.25	0.4	1.5	0.8	0.1
r	Respired fraction of μ_{max} (-)	0.025	0.025	0.025	0.025	0.025	0.025
k	Specific absorption cross section ($m^2 mg\ N^{-1}$)	0.0018	0.0024	0.0013	0.0018	1.0E-5	0.003
m_B	Mortality term (d^{-1})	0.14	0.05	0.07	0.001 ($d^{-1}(mgN\ m^{-3})^{-1}$)	0.00275	0.01
K_N	Half saturation constant for N uptake in sediment (mg N m^{-3})	N/A	N/A	N/A	N/A	15.0	N/A
K_P	Half saturation constant for P uptake in sediment (mg P m^{-3})	N/A	N/A	N/A	N/A	15.0	N/A

Symbol	Zooplankton Parameters	Large Zoo-plankton Z_2	Small Zoo-plankton Z_1	Symbol	Optical Parameters	Value
r_Z	Radius (m)	$5.0E^{-4}$	$12.5E^{-6}$	k_w	Background attenuation of sea water	0.1
e	Growth efficiency (-)	0.38	0.38	k_{fw}	CDOM attenuation coefficient of fresh water (m^{-1})	4.4
μ_{max}	Maximum growth rate at 15˚C (d^{-1})	0.1	3.0	k_{dt}	Detrital specific attenuation coefficient (m^{-1})	0.0038
U_Z	Swimming velocity (m)	$1.5E^{-3}$	$2.0E^{-4}$	k_t	TSS specific attenuation	30

					coefficient ($m^{-1}kg^{-1}\ m^{-3}$)	
ζ	Fraction of growth inefficiency lost to detritus (-)	0.5	0.5	k_n	Dissolved organic nitrogen specific attenuation coefficient ($m^{-1}mgN^{-1}m^{-3}$)	0.0009
m_Z	Mortality (quadratic) rate ($d^{-1}(mgN\ m^{-3})^{-1}$)	0.002	0.02			
γ	Fraction of mortality lost to detritus (-)	0.5	0.5			

Symbol	**Detritus & Remineralisation Parameters**	**Value**	**Symbol**	***M. pyrifera* Parameters**	**Value**
r_L	Pelagic labile detritus breakdown rate (d^{-1})	0.1			
r_R	Refractory detritus breakdown rate (d^{-1})	0.0036	g_{mp}	Maximum growth rate (d^{-1})	0.2
r_D	Dissolved organic matter breakdown rate (d^{-1})	0.00176	V_{NH_4}	Maximum uptake rate (NH_4) $(mg\ N\ gdw^{-1}d^{-1})$	8.0
ϑ_L	Fraction of labile detritus converted to DOM (-)	0.01	V_{NO_3}	Maximum uptake rate (NO_3) $(mg\ N\ gdw^{-1}d^{-1})$	10.3
ξ	Fraction of labile detritus converted to refractory detritus (-)	0.19	K_{NH_4}	Half saturation constant (NH_4) $(mg\ N\ m^{-3})$	74.2
ϑ_R	Fraction of refractory detritus converted to DOM (-)	0.01	K_{NO_3}	Half saturation constant (NO_3) $(mg\ N\ m^{-3})$	182.0

r_N	Maximum water column nitrification rate (d^{-1})	0.1	Q_{max}	Maximum internal nitrogen (mg N gdw^{-1})	25.0
r_{Nsed}	Maximum sediment nitrification rate (d^{-1})	20	d_m	Mortality Rate (d^{-1})	0.003
K_O	O2 half saturation rate for nitrification (mg O m^{-3})	500	g_{mp}	Maximum growth rate (d^{-1})	0.2
K_{OD}	O2 half saturation rate for denitrification (mg O m^{-3})	10000	V_{NH_4}	Maximum uptake rate (NH_4) (mg N $gdw^{-1}d^{-1}$)	8.0
K_{OA}	O2 half saturation rate for aerobic respiration (mg O m^{-3})	500	V_{NO_3}	Maximum uptake rate (NO_3) (mg N $gdw^{-1}d^{-1}$)	10.3

Symbol	*M. pyrifera* Parameters	Value
Q_{min}	Minimum internal nitrogen (mg N gdw^{-1})	7.0
Q_{min}		
K_c	Half growth constant (mg N gdw^{-1})	6.0
T_0	Optimal Temperature (°C)	12.0
T_r	Range of Optimal Temperature (°C)	1.0
I_S	Saturation irradiance (E $m^{-2}s^{-1}$)	0.000134
a_{cs}	Nitrogen Specific Shading (m^2 mg N^{-1})	0.001
Num_fronds	Number of Fronds (-)	7.0

CHAPTER 6
GENERAL DISCUSSION AND CONCLUSIONS

6.1 Future of IMTA

The world's population is predicted to increase by 1.7 billion to 9 billion people by 2050. The adoption globally of a more westernized diet, particularly in China and India, combined with reduction in agricultural land due to urbanization, soil erosion and desertification, could increase demand for food by as much as 50% (Farsund et al. 2015). Fish provide a major source of protein in the human diet, particularly in the poorest nations. Global fish supplies are predicted to reach 181 million tonnes by 2030 with 60% being supplied by aquaculture (Lem et al. 2014). With over half of current aquaculture by weight provided by mariculture (Kapetsky 2013), this sector will increasingly be called upon to meet global demand. Most mariculture is practiced in the coastal region because of the relatively calm conditions and ready access to shore-based infrastructure and markets. However, space in these areas is limited because of production requirements such as depth, exposure and oxygenation, and social considerations such as use of the coastal ocean for other purposes such as recreational and cultural activity (FAO 2013).

Offshore aquaculture is largely exempt from the problems associated with coastal systems (Troell et al. 2009) but comes with its own issues such as harsher hydrodynamic conditions posing significant engineering issues and increased transport costs for workers and products. However, the issues for both inshore and offshore aquaculture are being revisited with the possibility of large-scale expansion of the industry globally. Further development of inshore aquaculture would, in general, present a more viable proposition if the problems associated with limitations on available area and waste disposal can be resolved. IMTA in particular addresses the issue of waste management in coastal aquaculture, whilst enabling higher yields of macroalgae biomass in both in and off shore regions. One problem with offshore aquaculture is that wave action and wind stress tend to restrict production to shellfish and finfish. Current research suggests that farming only 5% of the offshore aquaculture locations that are suitable for macroalgae could substantially increase global mariculture output (FAO 2013). Presently the primary motivation for IMTA tends to be bioremediation, however if large-scale algal production in the offshore region was feasible then the motivation behind IMTA may switch to food security.

Farm implementation is currently seen as the key issue in providing efficient IMTA (FAO 2009). However, it has been suggested that this approach suffers from a lack of investigation into the underpinning science (Buschmann et al. 2009; FAO 2009). Current studies into IMTA are focused on implementation issues such as

stocking density, farm size and cultivation depth (Abreu et al. 2009; Buschmann et al. 2008; Ren et al. 2012). This study sought to clarify the potential for IMTA to bioremediate the effects of nutrification from finfish aquaculture in coastal areas and identify the gaps in knowledge where a better understanding and/or more empirical data is necessary. The way forward for IMTA is to recognize that the environmental and economic value of each species needs to be established. In fact much of the success of IMTA in the future will be linked to ensuring that government and other stakeholders support the approach and that commercialization is not impeded. For IMTA to be successful with macroalgal culture as a key component, then an existing market for macroalgae should exist beforehand (Buschmann et al. 2009; FAO 2009).

In Australia aquaculture is increasing, with plans for the salmon industry in particular to produce 100 thousand tonnes by 2015 (FRDC 2015). Farmers of other aquaculture species can also see the potential, and it is likely that yellowtail kingfish, bluefin tuna and several other minor species will benefit from the technological advances and market development associated with the expansion of salmon aquaculture. Alongside this expansion it is anticipated that there will be an increasing focus on the sustainability of the aquaculture industry as a whole. A governmental report by Winberg et al. (2011) into the use of IMTA for sustainable aquaculture in Australia highlighted the need for cultivation of macroalgal species that offer development of products at the high-end of the market. Research has been undertaken (and is currently underway) that shows species should be cultivated for a broad range of purposes, over and beyond purely bioremediation. For example, some algal species have been cultivated for pharmaceutical purposes (i.e. chemicals for the treatment of cancer), and others for food or nutraceutical products. Research facilities worldwide, such as those provided by SARDI in south Australia, are investigating the potential for biofuels from macroalgae. However, it is a competitive marketplace and, given the significant supply of macroalgae products from Asia, if IMTA in Australia is looking to produce commercial products then high-end commodities are more likely to succeed (Troell et al. 2009).

6.2 General model behavior and IMTA

In a nutrient replete environment with plentiful access to light, like that found in near-field IMTA, high growth rates should both be predicted by a growth model as well as observed in the field. In a near field scenario it is reasonable to assume that vertical distribution of the cultured algae would control access to nutrients emanating from finfish cages and that larger, more complex structured species, such as kelp, with high growth rates should outcompete similarly fast growing but physically smaller species. It is conceivable that aquaculture technology may make it possible to grow smaller species like *Ulva lactuca* at multiple depths in a vertical distribution, preferably in a way that maximizes the nutrient stripping potential of this high growth rate species. In this case, the costs associated with this technology would need to be offset either by a significant bioremediation gain or market

potential for this species. The important thing is that biomass is clearly the limiting factor both in stripping nutrients and also in satisfying market demand (Troell et al. 2009).

While macroalgal biomass is initially the limiting factor for nitrogen removal, eventually growth will be saturated as the system switches to one limited by light or nutrients. Nutrient limited growth means the biomass has reached a size where the nutrients taken up are only enough to satiate basic cellular functioning and do not allow for growth. However, this does not mean nitrogen uptake by the macroalgae is matched to the output from the finfish cages. In light imitation, growth stops because light is being extinguished by the macroalgae canopy and is therefore not reaching the lower parts of the plant where nutrient levels would allow growth. In both nutrient and light limitation it is important to understand firstly the growth dynamics including the source of limitation and then implement appropriate management strategies. For light limitation, harvesting would be an appropriate strategy whereas for nutrient limitation issues such as stocking density and farm size should be investigated. One ideal scenario for macroalgae based IMTA would be to hold a crop at steady state through an optimal harvesting scheme which removes biomass at a rate consistent with the output of DIN from the finfish aquaculture operation. This may require a long-term crop being used as a nutrient sink. If the crop were to be kept over several years then the effect of algal age on growth and mortality would need further investigation. The maximal growth rate of *M. pyrifera* slows as it ages (Wheeler and North 1980), and age related senescence has been shown to be a major cause of frond loss in natural communities (Rodriguez et al. 2013). In general, an understanding of the process by which age impacts on growth of kelp is potentially important for the optimisation of IMTA. Whilst this study has not explicitly modeled age related growth, chapter 3 does consider maximum growth rate, number of fronds and mortality as stochastic processes. This approach offered insight into how modeling these as time-varying processes affects the model results, but it is not the same as modelling underlying processes of age dependent growth/mortality.

The formulation used in the macroalgae model had internal nitrogen in two forms, *viz*. as an internal reserve or fixed in the cellular structure. There are other formulations where growth is dependent on internal reserves of carbon as well as nitrogen (Broch et al. 2013), and these allow for a variable C/N ratio of biomass. Empirical studies have shown that macroalgae species can change their C/N ratio depending on availability of ambient DIN. *Ulva rigida* for example shows a higher uptake of N after periods of N starvation, which lowers its C/N ratio compared to periods of constant N supply (Corso and Neill 1991.) As a result of both feeding and physiological cycles, DIN output from salmon cages may be supplied in pulses, resulting in comparable periodic fluctuations in ambient concentrations. The formulation used in this study assumes that macroalgae growth is more important on timescales of days rather than hours or minutes, which are important in other species such as phytoplankton. Furthermore in the 3D BGC model the Atkinson ratio

of carbon: nitrogen: phosphorous (C:N:P) is used for macrophytes. The IMTA model was developed in the knowledge that it would be applied within the Environmental Modelling Suite (EMS) framework and therefore observed the Atkinson ratio.

Dissolved oxygen is another variable not formally accounted for in the underlying IMTA model. Dissolved oxygen (DO) is represented in the 3D models as a constant ratio of macroalgae growth. However, oxygen is a vital component for finfish aquaculture and if DO concentration is too low then this can result in mortality in fish stocks. Macroalgae based IMTA could potentially lower DO through the process of dark respiration, which can occur when light is low. This occurs most commonly at night but also when canopies become dense thus extinguishing light to lower regions of the macroalgae frond (Tait and Schiel 2013). Macroalgae respiration has the potential to create locally hypoxic conditions dependent on biomass (Flint et al. 2012), so again an appropriate harvesting schedule is a critical consideration. Macroalgae also has the potential to lower DO through mineralisation whereby organic material lost by the macroalgae is broken down by bacteria, resulting in oxygen draw down (Sundback et al. 1990). Currently in the D'Entrecasteaux Channel and Huon Estuary, dissolved oxygen is not thought to be limiting (Herzfeld et al 2010; Wild-Allen et al 2010.) However, given that macroalgae based IMTA could potentially be implemented in farms several hectares in area, dissolved oxygen would need to be more thoroughly investigated, particularly given the farms' proximity to salmon cages.

Chapter 2 compared the bioremediation potential of three candidate species for IMTA under a range of environmental conditions known to affect growth rates. A key feature for successful IMTA is that any cultured species needs to have an existing demand / market. The giant kelp, *Macrocystis pyrifera,* is a valued species in the coastal context but in large parts of the D'Entrecasteaux Channel and Huon Estuary it has almost vanished (Johnson et al. 2011). The re-introduction of this species even in a farming context would preserve its presence in this region; potentially encouraging further research into its decline in order to optimise cultivation. Consequently, cultivating this species would provide not just nutrient reduction benefits but also conservation benefits. *M. pyrifera* also has the added benefit that it can be used for production of biofuels, alginates and abalone food. For offshore IMTA strong kelps, designed to withstand increased currents would potentially be more valuable than small filamentous algae. However, species such as *Ulva sp*. and *Porphyra sp*. have also been shown to possess the anti-cancer properties (Winberg et al., 2009). Most algae will have a range of potential markets, however these may not be static and consequently it is important to continue to revise expectations.

6.3 Improving Models with Empirical Data

Model validation forms an essential part of any modelling study. Traditional methods involve comparison between observations and model output through skill

metrics, which assess performance (Stow et al. 2009). Correlation and instantaneous relationships both establish confidence in the model and provide for interpretation of the results. The Bayesian method used in this study provides another dimension, enabling model learning based on observations (Parslow et al. 2012). This is essential given the uncertainty surrounding the actual value of parameters. The ability to determine the best parameter set relative to all available parameters is an important result and allows for more realistic model output in general. If the observations were taken from the D'Entrecasteaux Channel and Huon Estuary, a parameter set for this region could be determined which would give further confidence in the results. This would enable general transferability of the model using a set of robust parameters that could be used to return accurate results for a range of physical settings.

The Bayesian method used in this study also provides a robust analysis of model uncertainty. Ensemble runs involving perturbations of all parameters simultaneously are an improvement on individual parameter perturbations, which are currently favoured for determining model sensitivity. This approach also provides a method of reducing uncertainty in a way that incorporates prior understanding of the underlying processes. New metrics such as Kullback-Leibler divergence, and visualization methods such as the parallel coordinate plots allow an interpretation of the reduction in uncertainty. Uncertainty in the underlying IMTA model was show to be quite large and in general BGC process models can encompass a large solution space, so any reduction in this space is helpful. However the new model must be physically realizable and not represent a shift in the process model unrepresentative of the actual system.

In Parslow et al. (2012) the authors described how different observations may improve the modelling results for their NPZD model. In the present study the observed variables were macroalgal height and weight. Observations of these variables reduced uncertainty but did not necessarily provide more information on parameter values. If observations of total internal nitrogen of macroalgae were also included in the experimental process, this may provide additional information with which to constrain parameter values. It is possible to set up synthetic data sets reflecting observations of different variables to assess how each variable (individually and in combination) constrains the model output and contributes to parameter learning. This provides a method to determine which variables should best be observed in an actual field experiment in order to improve model results and inform parameter values; potentially also reducing the overall cost of conducting monitoring experiments.

6.4 Generalised spatio-temporal resolution of IMTA

The effectiveness of IMTA (as a solution to the negative impacts of DIN loading from finfish aquaculture) was determined by first defining the property of the estuary that is being impacted. Focusing on phytoplankton production and aligning this with the ANZECC guidelines for 'good' water quality in terms of

chlorophyll concentration provided an excellent metric for quantifying the success of the approach. ANZECC guidelines stipulate the concentration should not exceed the threshold value for three readings taken within the period of a month (ANZECC 2000). These guidelines recognize the spatio-temporal variability inherent in natural production particularly in estuaries. An important outcome of a modelling study such as this is to aid in the development of risk appropriate monitoring programs that are 'capable' of detecting farm impacts. Having demonstrated the importance that hydrodynamic forcing plays in driving primary production from the aquaculture output, it would be advisable to monitor chlorophyll in those areas where naturally high production occurs. If monthly or seasonal means are considered then farms placed in areas of high natural primary production are likely to have more of an accumulated effect on primary production, and so monitoring around these farms is encouraged. Monitoring around farms placed in areas of low natural production may also provide important information. If for example, primary production remained low near a salmon cage then the reasons why may be important when determining the impacts of aquaculture

The simulation described in chapter 4 showed how the hydrodynamics of an estuary can drive internal variations in primary production, and how these might vary as a result of increased loading from finfish aquaculture. Whilst the estuarine hydrodynamics described for the test estuary may not be typical of all estuaries other studies have similarly identified a ROFI as having a major impact on the spatio-temporal variability in primary production within an estuary (Fujiwara 2003; Herzfeld et al. 2010)). In terms of this investigation it was important to show how a proper understanding of estuarine production, and in particular the underlying processes, is essential in successful implementation of IMTA.

The non-linear jump in phytoplankton production as aquaculture loads were increased implied there was a critical loading at which phytoplankton escape grazing. Algal blooms in general are common phenomena although not directly attributable to finfish aquaculture. That the algal bloom occurred was not the interesting point, rather that it was sustained for a period of three months. Typically blooms peak and then dissipate as the background N is used up by the phytoplankton. This study highlighted what is possible when N is being constantly re-supplied. A sustained autumn bloom resulting from an incremental increase in forcing is only one of many possibilities that could arise from an increase in the intensity of finfish aquaculture. The phytoplankton-zooplankton interaction was reasonably simple in this formulation, involving 2 functional groups (large and small) of each. Different community structures may produce other spatial patterns of production. However, this result does highlight what could potentially occur if aquaculture is unregulated. Conversely this study did not include a feedback mechanism that acts to reduce finfish production as water quality declined, such as might occur with a reduction in dissolved oxygen resulting in stock loss. It is possible that this kind of inhibitory mechanism is realistic and would act to suppress the rise in primary production we observed in the model.

6.5 IMTA in the D'Entrecasteaux Channel and Huon Estuary

Chapter 5 provided a quantification of the potential for IMTA to support sustainable aquaculture in the D'Entrecasteaux Channel and Huon Estuary, building on the work of the previous three chapters. It should be noted that this was a theoretical study and in the absence of data from actual macroalgae based IMTA experiments we can only speculate on the implications of the results. However, the study did provide a robust analysis of the underlying process model, including output, in simplified applications (Chapters 2 and 3). Furthermore the 3D model used in chapter 5 has been applied in numerous case studies (Herzfeld et al. 2010; Wild-Allen et al. 2010; Skerrat et al. 2013) and a validation of model output showed it performed well when compared with observations in the region. It is mainly for these reasons the results should be treated with some confidence. Furthermore, chapter 5 offers scenario based analyses, i.e. scenarios are compared for their bioremediation potential to provide information about potential implementations of IMTA in the region. While the model would benefit from empirical experiments on IMTA in the region, the overall conclusions from the scenarios nonetheless appear to be well founded.

Based on the enrichment experiments conducted in chapter 5 there should be an observable increase in phytoplankton production as aquaculture intensity increases. Empirical studies from the D'Entrecasteaux Channel and Huon Estuary have shown no increase in phytoplankton production, despite a significant increase in salmon aquaculture, although ammonia levels have been detected at elevated levels consistent with this increase (Ross and Macleod 2012). Studies like those of Pitta et al (2012) showing the role of zooplankton in grazing down aquaculture driven increases in phytoplankton in oligotrophic waters, offers one explanation of empirical observations. In general though, the absence of data comparing this region with previous years, particularly on decadal time-scales make it difficult to fully contextualize the observations.

The model results identified the upper D'Entrecasteaux as one area that showed increased phytoplankton production due to increased finfish aquaculture (consistent with Wild-Allen et al. 2010). The results also indicated that the rise in production in that region was primarily driven by finfish farms in the Huon and lower D'Entrecasteaux. A monitoring program based in the upper D'Entrecastaux would therefore capture the impacts of finfish aquaculture without being sensitive to individual farm outputs. If for instance an individual lease in the Huon stopped production then this might be detected in the upper D'Entrecasteaux and the impact would be easily attributed to the production in that farm; however, it would not in all likelihood be registered as a major change. Conversely several different monitoring sites in the Huon may register the change in production of the lease totally differently or not at all depending on their location. The major point is that a

monitoring program in the Huon or lower D'Entrecasteaux would require a greater understanding of local impacts on primary production by each lease whereas the upper D'Entrecasteaux captures the general impact of salmon aquaculture on primary production and monitoring may require less sophistication.

The modelling indicated that siting macroalgae farms surrounding the finfish aquaculture leases was the most effective management strategy. This result stems from the fact that DIN was consistently highest around the salmon leases. Given that DIN drove biomass growth of giant kelp, which in turn drove removal of DIN, placing macroalgae farms next to leases seems the best course if removing DIN is the ultimate aim of IMTA. Of course high biomass was not restricted to sites near the leases, particularly under high finfish loads. In the event that growing macroalgae was not permitted near salmon leases then other areas may allow reasonable bioremediation. Siting salmon aquaculture in locations that do not contribute to the system wide phytoplankton production is another consideration. This would restrict production from farms to local regions. If these locations do not affect areas in the system with high environmental importance such as reefs or seagrass meadows, then they might be acceptable. More environmentally valuable areas or areas sensitive to DIN increases could also be directly protected by IMTA, with farms placed near these regions to buffer them from excess DIN.

One attractive quality of aquaculture from a planning perspective is it provides control over species production (FAO 2009). This is true of macroalgae farming where harvesting, choice of species, length of cultivation period all enable control over production rates. However these strategies need to be investigated properly. Harvesting too early or frequently could potentially result in lower bioremediation than non-harvesting. Similarly, increasing macroalgae farm area when farm loading is low would result in greater cost for no significant return in N removal. In fact dead macroalgae sporelings, resulting from lack of nutrients, would only serve to increase total N in the region. The key is optimisation of IMTA by the choice and implementation of farming strategy. Establishing an optimal harvesting regime that both satisfies market demand and retains high growth rates would be an ideal strategy. Given that this study showed macroalgal biomass was closely tied to the output from the salmon farms, it would be sensible that both industries (algae and salmon) be closely aligned in terms of development strategies, particularly if the overall goal is bioremediation as both parties would have an interest in the outcome. If the overall goal were to supply the market with macroalgae then the salmon farmer may have no interest in the result.

6.6 General conclusions and the next step

Simulated near field macroalgae based IMTA showed that for a temperate estuary there were a range of species specific conclusions that can be drawn. Notably, giant kelps such as *M. pyrifera* attain higher rates of nutrient removal than smaller faster growing species, due to their capacity to grow through a range of

depths in the water column and thus provide a much larger absolute biomass of tissue for nutrient uptake. Increasing flow rate had an overall neutral effect on *M. pyrifera* uptake when averaged over a nine month period. For the smaller species examined the results varied. Increasing flow rate increased nutrient uptake for *U. lactuca* but decreased uptake for *Porphyra umbilicalis* over the same period. Varying cultivation depth from 0-5 m had no effect on total N removed by *U. lactuca* or *P. umbilicalis*, whereas *M. pyrifera* removed less N at 1 m and more at 3 m. Harvesting *M. pyrifera* had the potential to increase total N removal by up to 15 fold, depending on the strategy used, with the most effective schemes being those that allowed a three month establishment phase.

In general the data assimilation method used here demonstrated large variance in model output as a result of uncertainty in the underlying parameterisation. However, we showed that this uncertainty in state variables, both observed and unobserved, can be greatly reduced through conditioning on sparse data. Furthermore the process allowed for learning in the parameter space, enabling greater confidence in the model for future runs, and also allowed for a more realistic model processes.

3D simulation of an estuary showed that effective placement of macroalgae farms is dependent on the primary production cycle and spatial distribution of primary production within the estuary. Placement of macroalgae farms is important, for example because some sites can produce a high biomass of kelp but still have only minimal impact on reducing finfish aquaculture derived chlorophyll concentration. In contrast, if placed judiciously, macroalgae farms can biomitigate the potential impacts of finfish aquaculture. The simulation of IMTA in the D'Entrecasteaux Channel and Huon Estuary showed that phytoplankton production driven by finfish aquaculture can be reduced by up to 80% and 20% under high and low finfish loads respectively, and that the control and capacity of IMTA can be greatly enhanced by controlling harvesting and initial biomass. However the study also investigated the limits of IMTA and showed that macroalgae growth saturates over a 2-year growing cycle in the D'Entrecasteaux Channel and Huon Estuary; under low and high loads. However, an effective harvesting scheme in particular will maintain high growth rates and increase the capacity of IMTA. The study also showed that the bioremediation capacity of IMTA measured as both a decrease in chlorophyll concentration and DIN removal, will decrease with increasing aquaculture loads. This is a reminder that IMTA should not be viewed as panacea but rather as component of sustainable aquaculture.

In future work it is suggested that experimental trials of macroalgal culture based IMTA be set up at different sites in the region to obtain realistic growth rates under a range of environmental conditions. It is also suggested work be undertaken on monitoring long term macroalgal respiration and growth rates under differing nutrient concentrations. These data would help to refine the models and underpin more accurate predictions of both the nutrient removal potential and associated

impacts of IMTA. The ultimate aim of future research would be to lay the ground work for a farm scale trial of IMTA in the region.

CHAPTER 7
REFERENCE LIST

Abreu MH, Varela DA, Henríquez L, Villarroel A, Yarish C, Sousa-Pinto I, Buschmann AH (2009) Traditional vs. Integrated Multi-Trophic Aquaculture of Gracilaria chilensis C. J. Bird, J. McLachlan & E. C. Oliveira: Productivity and physiological performance. Aquaculture 293: 211-220

ACCESS (2014) http://www.bom.gov.au/nwp/doc/access/NWPData.shtml

Al-Hafedh YS, Alam A, Buschmann AH (2014) Bioremediation potential, growth and biomass yield of the green seaweed, *Ulva lactuca* in an integrated marine aquaculture system at the Red Sea coast of Saudi Arabia at different stocking densities and effluent flow rates. Reviews in Aquaculture DOI: 10.1111/raq.12060

Aldridge JN, Trimmer M (2009) Modelling the distribution and growth of 'problem' green seaweed in the Medway estuary, UK. Hydrobiologia 629:107-122

Anderson DM, Glibert PM, Burkholder JM (2002) Harmful Algal Blooms and Eutrophication: Nutrient Sources, Composition, and Consequences. Estuaries 25(4b): 704-726

Andrieu C, Doucet A, Holenstein R (2010) Particle Markov chain Monte Carlo methods. Journal of the Royal Statistical Society, Series B 72:269–302

ANZECC. (2000). Australian and New Zealand Water Quality Guidelines for Fresh and Marine Sources. Canberra

Arhonditsis GB, Stow CA, Paerl HW, Valdes-Weaver LM, Steinberg LJ, Reckhow KH (2007) Delineation of the role of nutrient dynamics and hydrologic forcing on phytoplankton patterns along a freshwater–marine continuum. Ecol Mod 208:230-246

Bartleson RD, Kemp MW, Stevenson CJ (2005) Use of a simulation model to examine effects of nutrient loading and grazing on *Potamogeton perfoliatus* L. communities in microcosms. Ecol Mod 185:483-512

Bonsdorff E, Blomqvist EM, Mattila J, Norrko A (1997) Coastal Eutrophication: Causes, Consequences and Perspectives in the Archipelago Areas of the Northern Baltic Sea. Estuar Coast Shelf S 44:63-72

Bostock J, McAndrew B, Richards R, Jauncey K, Telfer T, Lorenzen K, Little D, Ross L, Handisyde N, Gatward I and Corner R (2010) Aquaculture global status and trends. Phil Trans R Soc 365: 2897-2912

Brigolin D, Pastres R, Nickell TD, Cromey CJ, Aguilera DR, Regnier P (2009) Modelling the impact of aquaculture on early diagenetic processes in sea loch sediments. Mar Ecol Prog Ser 388: 63-80

Broch OJ, Ellingsen IH, Forbord S, Wang X, Zsolt V, Alver MO, Skjermo J (2013) Modelling the cultivation and bioremediation potential of the kelp *Saccharina latissima* in close proximity to an exposed salmon farm in Norway. Aquacult Env Interact 4: 187-206

Bruhn A, Dahl J, Nielsen HB, Nikolaisen L, Rasmussen MB, Markager S, Jensen PD (2011). Bioenergy potential of *Ulva Lactuca*: Biomass yield, methane production and combustion. Bioresource Technol 102: 2595-2604

Buschmann AH, Varela DA, Hernandez-Gonzalez MC, Huovinen P (2008). Opportunities and challenges for the development of an integrated seaweed-based aquaculture activity in Chile: determining the physiological capabilities of Macrocystis and Gracilaria as biofilters. J Appl Phycol 20:571-577

Buschmann AH, Cabello F, Young K, Carvajal J, Varela DA, Henrıquez L (2009) Salmon aquaculture and coastal ecosystem health in Chile: Analysis of regulations, environmental impacts and bioremediation systems. Ocean Coast Manage 52: 243-249

Butler ECV (2006) The Tail of Two Rivers in Tasmania: The Derwent and Huon Estuaries. Hdb Env Chem 5:1-45

Carmona R, Kraemer GP, Yarish C (2006) Exploring Northeast American and Asian species of *Porphyra* for use in an integrated finfish–algal aquaculture system. Aquaculture 252:54-65

Chopin T, Yarish C, Wilkes R, Belyea E, Lu S, Mathieson A (1999) Developing *Porphyra/*Salmon integrated aquaculture for bioremediation and diversification of the aquaculture industry. J Appl Phycol 11:463-472

Clementson LA, Parslow JS, Turnbull AR, Bonham PI (2004) Properties of light absorption in a highly coloured estuarine system in south-east Australia which is prone to blooms of the toxic dinoflagellate *Gymnodinium catenatum*. Estuar Coast Shelf S 60:101-112

Cloern JE (2001) Our evolving conceptual model of the coastal eutrophication problem. Mar Ecol Prog Ser 210:223-253

Cloern JE, Foster SQ, Kleckner AE (2014) Phytoplankton primary production in

the world's estuarine-coastal ecosystems. Biogeosciences 11:2477-2501

Corzo A, Neill XF (1991) C/N ratio in response to nitrogen supply and light quality in *Ulva rigida C. Agardh* (Chlorophyta: Ulvophyceae). Sci Mar 55(2): 405-411

Crawford C, Swadling K, Thompson P, Clementson L, Schroeder T, Wild-Allen K (2009) Nutrient and Phytoplankton Data from Storm Bay to Support Sustainable Resource Planning. Project No. 2009/067 Final Report, IMAS Hobart Tasmania

Cressie N, Wikle CK (2011) Statistics for Spatio-Temporal Data. John Wiley & Sons Inc., Hoboken, New Jersey

Cromey CJ, Nickell TD, Black KD (2002) DEPOMOD—modelling the deposition an biological effects of waste solids from marine cage farms. Aquaculture 214(1-4):211-239.

CSIRO (2009) CSIRO Atlas Of Regional Seas (CARS), from http://www.marine.csiro.au/~dunn/cars2009/

CSIRO Huon Estuary Study Team (2000) Huon Estuary Study – Environmental research for integrated catchment management and aquaculture. Fisheries Research and Development Corporation. Project Number 96/284, June 2000. CSIRO Division of Marine Research. Marine Laboratories, Hobart 285p

Dugdale R, Wilkerson F, Parker A, Marchi A, Taberski K (2102). River flow and ammonium discharge determine spring phytoplankton blooms in an urbanized
estuary. Estuar Coast Shelf S 115:187-199

ElkhornSlough.org (2012). Elkhorn Slough Plants: Sea Lettuce, from http://www.elkhornslough.org/sloughlife/plants/sea_lettuce.htm

Eng CT, Paw JN, Guarin FY (1989) The environmental impact of aquaculture and the effects of pollution on coastal aquaculture development in Southeast Asia. Mar Pol Bull 20(7): 335-343

Enriquez S, Agusti S, Duarte CM (1994). Light Absorption by Marine Macrophytes. Oecologia 98:121-129

Everett JD, Baird ME, Suthers IM (2007) Nutrient and plankton dynamics in an intermittently closed/open lagoon, Smiths Lake, south-eastern Australia: An ecological model. Estuar Coast Shelf S 72:690-702

FAO (2009) Integrated mariculture a global review. Fisheries and Aquaculture Technical Paper. No. 529. Rome, FAO

FAO (2011) Fisheries and Aquaculture Technical Paper. No. 553. Rome, FAO. 181p

FAO (2013) A global assessment of offshore mariculture potential from a spatial perspective. Fisheries and Aquaculture Technical Paper. No. 549. Rome, FAO

FAO (2014) ftp://ftp.fao.org/fi/stat/Overviews/AquacultureStatistics2012.pdf.

Flint N, Pearson RG, Crossland MR (2012) Use of aquatic plants to create fluctuating hypoxia in an experimental environment. Mar Fresh Wat Res 63(4): 351-360.

Forrest B, Keeley N, Gillespie P, Hopkins G, Knight B, Govier D (2007) Review of ecological effects of finfish aquaculture: Final report. Prepared for the Ministry of Fisheries, NZ. In, Book Cawthron Report No. 1285. Cawthron Institute, Nelson

FRDC (2015) http://frdc.com.au/environment/Aquaculture/Pages/default.aspx

Fujiwara T (2003) Buoyancy-driven current during cooling periods in Ise Bay, Japan. J Geophys Res 108, No. C8

Gerard VA (1982) In situ Water Motion and Nutrient Uptake by the Giant Kelp *Macrocystis pyrifera*. Mar Biol 69:51-54

Glibert PM, Dugdale R, Wilkerson F, Parker AE, Alexander J, Antell E, Blaser S, Johnson A, Lee J, Lee T, Murasko S, Strong S (2014) Major – but rare – spring blooms in 2014 in San Francisco Bay Delta, California, a result of the long-term drought, increased residence time, and altered nutrient loads and forms. J Exp Mar Bio Ecol 460:8-18

Gutierrez A, Correa T, Munez V, Santibanez A, Marcos R, Caceres C, Buschmann A (2006) Farming of the giant kelp *Macrocystis pyrifera* in southern Chile for development of novel food products. J Appl Phycol 18:259-267.

Hafting JT (1999) Effect of tissue nitrogen and phosphorus quota on growth of *Porphyra yezoensis* blades in suspension cultures. Hydrobiologia 398/399:305-314.

Haines KC, Wheeler PA (1978) Ammonium and nitrate uptake by the marine macrophytes *Hypnea Musciformis* (Rhodophyta) and *Macrocystis Pyrifera* (Phaeophyta). J Phycol 14:319-324.

Hadley S, Wild-Allen K, Johnson CJ, Macleod CK (2015) Modeling macroalgae growth and nutrient dynamics for integrated multi-trophic aquaculture. J Appl Phycol 27:901-916

Hernandez I, Fernandez-Engo MA, Perez-Llorens JL, Vergara JJ (2005) Integrated outdoor culture of two estuarine macroalgae as biofilters for dissolved nutrients from Sparus aurata waste waters. J Appl Phycol 17:557-567

Hernández I, Martínez-Aragón JF, Tovar A, Pérez-Lloréns JL,Vergara JJ (2002) Biofiltering efficiency in removal of dissolved nutrients by three species of estuarine macroalgae cultivated with sea bass (*Dicentrarchus labrax*) waste waters 2. Ammonium. J Appl Phycol 14:375-384

Hernandez-Garcia E, Lopez C (2004) Sustained plankton blooms under open chaotic flows. Ecol Complexity 1(3):253-259.

Herzfeld M, Parslow J, Margvelashvili N, Andrewartha JR, Sakov P (2005a) Numerical Hydrodynamic Modelling of the Derwent Estuary. CSIRO Marine and Atmospheric Research, Derwent Estuary Program, Final Report, 91 pp

Herzfeld M (2006) An alternative coordinate system for solving finite difference ocean models. Ocean Modelling 14:174-196

Herzfeld M, Schmidt M, Griffies SM, Liang Z (2010a) Realistic test cases for limited area ocean modelling. Ocean Modelling 37(1):1-34.

Herzfeld M, Andrewartha J, Sakov P (2010) Modelling the physical oceanography of the D'Entrecasteaux Channel and the Huon Estuary, south-eastern Tasmania. Mar Fresh Water Res 61:568-586

Herzfeld M, Gillibrand P (2015) Active open boundary forcing using dual relaxation time-scales in downscaled ocean models. Ocean Modelling 89:71-83.

Holmer M, Black K, Duarte CM, Marba N, Karakassis I (2008) Aquaculture in the Ecosystem. Netherlands: Springer. Ebook

Howarth RW (1988) Nutrient limitation of net primary production in marine ecosystems. Annu Rev Ecol Syst 19:89–110.

Inselberg A (1998) Visual Data Mining with Parallel Coordinates. Comp Stats 13(1):47-63

Islam M (2005). Nitrogen and phosphorus budget in coastal and marine cage aquaculture and impacts of effluent loading on ecosystem: review and analysis towards model development. Mar Pol Bull 50: 48–61

Jiang ZJ, Fang JG, Mao YZ, Wang W (2010) Eutrophication assessment and bioremediation strategy in a marine fish cage culture area in Nansha Bay, China. J Appl Phycol 22:421-426

Johnson CR, Banks SC, Barrett NS, Cazassus F, Dunstan PK, Edgar GJ, Frusher SD, Gardner C, Haddon M, Helidoniotis F, Hill KL, Holbrook NJ, Hosie GW, Last PR, Ling SD, Melbourne-Thomas J, Miller K, Pecl, GT, Richardson AJ, Ridgway KR. Rintoul SR, Ritz DA, Ross DJ, Sanderson JC, Shepherd SA, Slotwinski A, Swadling KM, Taw N (2011) Climate change cascades: Shifts in oceanography, species' ranges and subtidal marine community dynamics in eastern Tasmania. J Exp Mar Biol Ecol 400:17-32

Jones E, Parslow J, Murray L (2010) A Bayesian approach to state and parameter estimation in a Phytoplankton-Zooplankton model. Australian Meteorological and Oceanographic Journal 59: 7-16.

Kapetsky JM, Aguilar-Manjarrez J, Jenness J (2013) A global assessment of potential for offshore mariculture development from a spatial perspective. FAO Fisheries and Aquaculture Technical Paper No. 549. Rome, FAO. 181 pp

Keeley NB, Forrest BM, Macleod CK (2013) Novel observations of benthic enrichment in contrasting flow regimes with implications for marine farm monitoring and management. Mar Pol Bull 66(1-2): 105-116

Keeley N, Forrest BM, Crawford C, Hopkins GA, MacLeod C (2014) Spatial and temporal dynamics in macrobenthos during recovery from salmon farm induced organic enrichment: when is recovery complete. Mar Pol Bull 80: 250-262

Kopczak CD, Zimmerman RC, Kremer JN (1991) Variation in nitrogen physiology and growth among geographically isolated populations of the giant kelp *Macrocystis Pyrifera* (Phaeophyta). J Phycol 27: 149-158

Kopczak CD (1994) Variability of nitrate uptake capacity in *Macrocystis Pyrifera* (Laminariales Phaeophyta) with nitrate and light availability. J Phycol 30:573-580

Lansberg JH (2002) The Effects of Harmful Algal Blooms on Aquatic Organisms. Reviews in Fisheries Science, 10(2): 113–390

Lee CS, Ang P Jr. (1991) A simple model for seaweed growth and optimal harvesting strategy. Ecol Model 55:67-74

Lem A, Bjorndal T, Lappo A (2014) Economic analysis of supply and demand for food up to 2030 – Special focus on fish and fishery products. FAO Fisheries and Aquaculture Circular No. 1089. Rome, FAO. 106 pp

Li P, Vu QD (2013) Identification of parameter correlations for parameter estimation in dynamic biological models. BMC Systems Biology 7:91

Limpert E, Stahel WA, Abbot M (2001) Lognormal Distributions across the Sciences: Keys and Clues. BioScience 51(5): 341-352

Lobban CS, Harrison PJ (1994) Seaweed Ecology and Physiology. Cambridge University Press, Cambridge

Macleod, C.K.; Crawford, C.; Moltschaniwskyj, N.A. (2004). Assessment of long term change in sediment condition after organic enrichment: Defining recovery. Mar Pol Bull 49: 79–88

Maier G, Glegg GA, Tappin AD, Worsfold PJ (2012) A high resolution temporal study of phytoplankton bloom dynamics in the eutrophic Taw Estuary (SW England). Sci Total Environ 434:228–239

Mann KH, Lazier JRN (1991) Dynamics of Marine Ecosystems: Biological-Physical Interactions inthe Oceans. Boston,MA: Blackwell Scientific Publications Inc

Margvelashvili, N., Herzfeld, M., Parslow, J., 2005. Numerical modelling of fine sediment and zinc transport in the Derwent Estuary. CSIRO Marine and Atmospheric Research, Derwent Estuary Program, Final Report, 51 pp.

Margvelashvili N (2008) Stretched Eulerian coordinate model of coastal sediment transport. Comput Geosci 35: 1167-1176

Markager S, Sand-Jensen K (1996) Implications of thallus thickness for growth-irradiance relationships of marine macroalgae. Eur J Phycol 31:79-87

MarLIN. (2012). Purple laver - Porphyra umbilicalis, from http://www.marlin.ac.uk/speciesinformation.php?speciesID=4194

Melbourne-Thomas J, Johnson CR, Fung T, Seymour MR, Chérubin LM, Arias-González JE and Fulton EA (2011) Regional-scale scenario modeling for coral reefs: a decision support tool to inform management of a complex system. Ecological Applications 21:1380-1398

Mente E, Martin JC, Tuck I, Kormas KA, Santos MB, Bailey N, Pierce GJ (2010) Mesoscale effects of aquaculture installations on benthic and epibenthic communities in four Scottish sea lochs. Aquat Living Resour 23:267-276

Mongin M, Baird ME (2014). The interacting effects of photosynthesis, calcification and water circulation on carbon chemistry variablility on a coral reef flat: a modelling study. Ecol Model 284:19-34

Murray LM (2013) Bayesian state-space modelling on high-performance hardware

using LibBi. arXiv:1306.3277 {stat.CO]

Muylaert K, Tackx M, Vyverman W (2005) Phytoplankton growth rates in the freshwater tidal reaches of the Schelde estuary (Belgium) estimated using a simple light-limited primary production model. Hydrobiologia 540:127-140

Neori A, Cohen I, Gordin H (1991) *Ulva lactuca* biofilters for marine fishpond effluents. II. Growth rate, yield and C:N ratio. Bot Mar 34:483–489

Nixon SW (1989) An extraordinary red tide and fish kill in Narragansett Bay, in Novel Phytoplankton Blooms, Causes and Impacts of Recurrent Brown Tides and Other Unusual Blooms, Coastal and Estuarine Stud. 35:429-447.

North WJ, Jackson GA, Manley SL (1986). *Macrocystis* and its environment, knowns and unknowns. Aquat Bot 26:9-26

Ott MW, Garrett C (1998) Frictional estuarine flow in Juan de Fuca Strait, with implications for secondary circulation. J Geophys Res 103, No. C8

Paerl HW, Valdes LM, Peierls BL, Adolf JE, Harding LW (2006) Anthropogenic and climatic influences on the eutrophication of large estuarine ecosystems. Limnol Oceanogr 51(1, part 2):448-462.

Parslow J, Herzfeld M, Hunter JR, Andrewartha JR, Sakov P, Waring J (2001) Mathematical Modelling of the Dispersal and Fate of CES Discharge from the Boyer Mill in the Upper Derwent Estuary. Final Report. CSIRO Marine Research, Hobart.

Parslow J, Cressie N, Campbell EP, Jones E, Murray L (2013) Bayesian learning and predictability in a stochastic nonlinear dynamical model. Ecological Applications 23: 679-698

Parsons KE (2012). State of the D'Entrecasteaux Channel and the lower Huon Estuary 2012. Report for the D'Entrecasteaux Channel Project, prepared by Ecomarine Consulting

Pedersen A, Kraemer G, Yarisha C (2004). The effects of temperature and nutrient concentrations on nitrate and phosphate uptake in different species of *Porphyra* from Long Island Sound (USA). J Exp Mar Biol Ecol 312:235-252

Phinney DA, Yentsch CS, Phinney DI (2004) Primary Productivity of Phytoplankton and Subtidal Microphytobenthos in Cobscook Bay, Maine. Ecosystem Modeling in Cobscook Bay, Maine: A Boreal, Macrotidal Estuary, Northeastern Naturalist 11 (special edition 2): 101-122

Pitta P, Tsapakis M, Apostolaki ET, Tsagaraki T, Holmer M, Karakassis I (2009)

'Ghost nutrients' from fish farms are transferred up the food web by phytoplankton grazers. Mar Ecol Prog Ser 374:1-6

Planque B, Lindstrom U, Subbey S (2014) Non-deterministic modelling of food-web dynamics. 10.1371/journal.pone.0108243

Ren JS, Stenton-Dozey J, Plew DR, Fang J, Gall M (2012) An ecosystem model for optimising production in integrated multitrophic aquaculture systems. Ecol Model 246:34–46

Robertson-Andersson DV, Potgieter M, Hansen J, Bolton JJ, Troell M, Anderson R, & Probyn T (2008) Integrated seaweed cultivation on an abalone farm in South Africa. J Appl Phycol 20:579–595

Rodriguez GE, Rassweiler A, Reed DC, Holbrook, SJ (2013) The importance of Progressive senescence in the biomass dynamics of giant kelp (*Macrocystis pyrifera*). Ecology 94:1848-1858

Ross DJ, Macleod CK (2012) Evaluation of broadscale environmental monitoring program (BEMP) data from 2009-2012. IMAS Technical Report 140pp

Rykiel EJ (1995) Testing of Ecological Models: The Meaning of Validation. Ecol Model 90:229-244

Sanderson JC, Cromey CJ, Dring MJ, Kelly MS (2008) Distribution of nutrients from seaweed cultivation around salmon cages at farm sites in northwest Scotland. Aquaculture 278: 60- 68

Sanderson JC, Di Benedetto R (1988) Tasmanian seaweeds for the edible market Department of Sea Fisheries Technical report. Marine Laboratories Department of Sea Fisheries, Hobart, Tasmania.

Silva C, Yanez E, Martin-Diaz ML, DelValls TA (2012) Assessing a bioremediation strategy in a shallow coastal system affected by a fish farm culture - Application of GIS and shellfish dynamic models in the San Pedro, SW Spain. Mar Pollut Bull 64:751-765

Simpson JH (1997) Physical processes in the ROFI regime. J Phys Proc 12:3-15

Skerratt J, Wild-Allen K, Rizwi F, Whitehead J, Coughanowr C (2013) Use of a high resolution 3D fully coupled hydrodynamic, sediment and biogeochemical model to understand estuarine nutrient dynamics under various water quality scenarios. Oce Coast Man 83: 52-66

Solidoro C, Pecenik G, Pastres R, Franco D, Dejak C (1997). Modelling macroalgae (*Ulva rigida*) in the Venice lagoon: Model structure identification and first parameters estimation. Ecol Model 94:191-206

Staurnes M, Kroglund F, Rosseland BO (1995) Water quality requirement of Atlantic salmon (salmon salar) in water undergoing acidification or liming in Norway. Water Air Soil Pollut 85: 347-352

Stow CA, Jolliff J, McGillicuddy Jr DJ, Doney SC, Allen JC, Friedrichs MAM, Rose KA, Wallhead P (2009) Skill assessment for coupled biological/physical models of marine systems. J Mar Syst 76: 4-15

Sundback K, Jonsson B, Nilsson P, Lindstrom I (1990) Impact of accumulating drifting macroalgae on a shallow-water sediment system: an experimental study. Mar Ecol Prog Ser 58:261-274

Tait LW, Schiel DR (2013) Impacts of Temperature on Primary Productivity and Respiration in Naturally Structured Macroalgal Assemblages. PLOS ONE DOI: 10.1371/journal.pone.0074413

Thompson PA, Bonham P, Wilcox S, Crawford C (2005) Baseline monitoring in D'Entrecasteaux Channel Technical report. CSIRO Marine and Atmospheric Research, Hobart, Tasmania

Thompson PA, Bonham PI, Swadling KM (2008) Phytoplankton blooms in the Huon Estuary, Tasmania: top-down or bottom up control. J Plank Res 30(7):735-753

Trancoso AR, Saraiva S, Fenandes L, Pina P, Leitao P, Neves R (2005) Modelling macroalgae using a 3D hydrodynamic-ecological model in a shallow, temperate estuary. Ecol Model 187:232-246

Troell M, Joyce A, Chopin C, Neori A, Buschmann AH, Fang J (2009) Ecological engineering in aquaculture — Potential for integrated multi-trophic aquaculture (IMTA) in marine offshore systems. Aquaculture 297: 1–9

Tsagaraki TM, Petihakis G, Tsiaras K, Triantafyllou, Tsapakis M, Korres G, Kakagiannis G, Frangoulis C, Karakassis I (2011) Beyond the cage: Ecosystem modelling for impact evaluation in aquaculture. Ecol Mod 222: 2512-2523

Utter BD, Denny MW (1996) Wave-induced forces on the giant kelp *Macrocystis Pyrifera (Agardh)*: Field test of a computational model. J Exp Biol 199:2645–2654

Wang X, Olsen LM, Reitan KI, Olsen Y (2012). Discharge of nutrient wastes from salmon farms: environmental effects, and potential for integrated multi-trophic aquaculture. Aquacul Env Interact 2:267-283

Westermeier R, Patiño DJ, Murúa P, Müller DG (2011) Macrocystis mariculture in Chile: growth performance of heterosis genotype constructs under field conditions. J Appl Phycol 23: 819-825

Wheeler WN (1980) Effect of boundary Layer transport on the fixation of carbon by the giant kelp *Macrocystis pyrifera*. Mar Biol 56:103-10

Wheeler PA, North WJ (1980) Effect of nitrogen supply on nitrogen content and growth rate of juvenile *Macrocystis Pyrifera* (Phaoephyta) sporophytes. J. Phycol 16: 577-582

Wheeler PA, North WJ (1981) Nitrogen Supply, Tissue Composition and Frond Growth Rates for *Macrocystis pyrifera* off the Coast of Southern California. Mar Bio 64: 59-69

Wikle CK, Milliff RF, Herbei R, Leeds WB (2013) Modern Statistical Methods in Oceanography: A Hierarchical Perspective. Stat Sci 28(4): 466-486

Wild-Allen K, Herzfeld M, Thompson P, Rosebrock U, Parslow J, Volkman J (2010) Applied coastal biogeochemical modelling to quantify the environmental impact of fish farm nutrients and inform managers. J Marine Syst 81:134-147

Wild-Allen K, Skerratt J, Whitehead J, Rizwi F, Parslow J (2013) Mechanisms driving estuarine water quality: A 3D biogeochemical model for informed management. Estuar Coast Shelf S 135:33-45

Wild-Allen K, Rayner M (2014) Continuous nutrient observations capture fine-scale estuarine variability simulated by a 3D biogeochemical model. Mar Chem 167: 135-149

Winberg PC, Skropeta D, Ullrich A (2011) Seaweed cultivation pilot trials – towards culture systems and marketable products. Australian Government Rural Industries Research and Development Corporation, RIRDC Publication No. 10/184. PRJ - 000162. Original report located here:rirdc.infoservices.com.auitems/10-184

Wolanski E (2007) Estuarine ecohydrology. New York, NY: Elsevier

Wu RSS (1995) The Environmental Impact of Marine Fish Culture: Towards a Sustainable Future. Mar Pol Bull 32(4-12): 159-166

Yokoyama H, Ishihi Y (2010) Bioindicator and biofilter function of *Ulva spp*. (Chlorophyta) for dissolved inorganic nitrogen discharged from a coastal fish farm — potential role in integrated multi-trophic aquaculture. Aquaculture 310:74-83

Yoshiyama K, Sharp JH (2006) Phytoplankton response to nutrient enrichment in an urbanized estuary: Apparent inhibition of primary production by overeutrophication. Limnol Oceanogr 51(1, part2): 424-434

Zhang J, Fang J, Wang W, Du M, Gao Y, Zhang M (2012) Growth and loss of mariculture kelp *Saccharina japonica* in Sungo Bay, China. Appl Phycol 24:1209–1216

Zimmerman RC, Kremer JN (1984) Episodic nutrient supply to a kelp forest ecosystem in Southern California. J Mar Res 42:591-604